Stefan Krause

Effects of microbial activity on marine carbonates

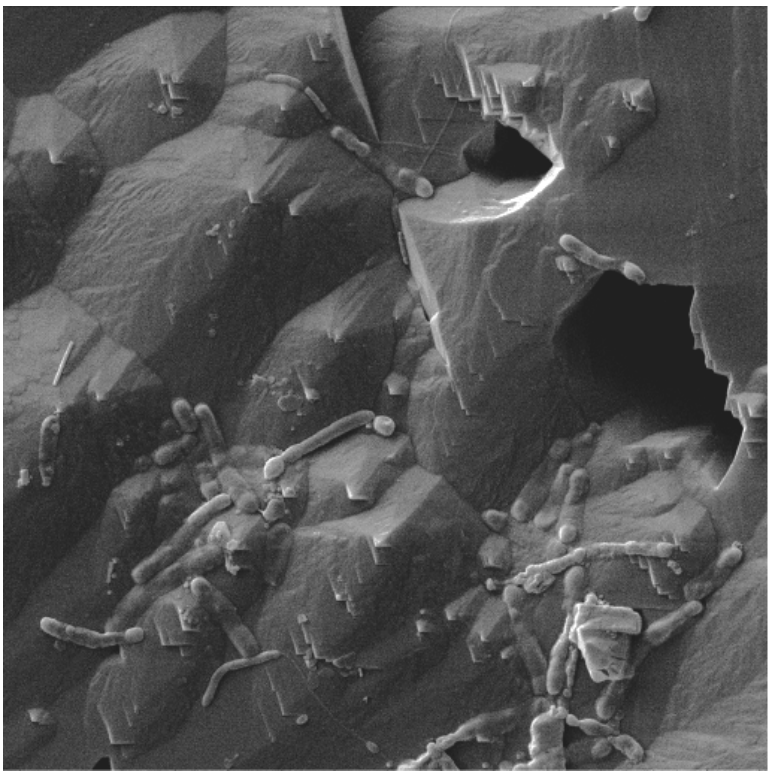

Effects of microbial activity on marine carbonates

Dissertation

Zur Erlangung des Doktorgrades in den Naturwissenschaften

- Dr. rer. nat. -

vorgelegt im Fachbereich Biologische Meereskunde der Christian-Albrechts-Universität zu Kiel

Stefan Krause

Kiel

März 2012

Hiermit erkläre ich, dass ich die vorliegende Doktorarbeit selbstständig und ohne unerlaubte Hilfen erstellt habe. Ferner habe ich weder diese noch eine ähnliche Arbeit an einer anderen Abteilung oder Hochschule im Rahmen eines Prüfungsverfahrens vorgelegt, veröffentlicht oder zur Veröffentlichung vorgelegt.

Kiel, den.....

Stefan Krause

1. Gutachterin: Prof. Dr. Tina Treude

2. Gutachter: Prof. Dr. Wolf-Christian Dullo

Weitere Prüfer:

Prof. Dr. Ulf Riebesell

Prof. Dr. Arne Körtzinger

Prof. Dr. Frank Melzner

Tag der Disputation: 12. April 2012

TABLE OF CONTENTS

Zusammenfassung

Kalziumkarbonate ($CaCO_3$) gehören zu den häufigsten Mineraliengruppen in marinen Sedimenten. Untersuchungen der letzten zwei Dekaden haben gezeigt, dass mikrobielle Aktivitäten einen maßgeblichen Einfluss auf Karbonate haben, was sowohl deren mikrobiell bedingte Bildung als auch Auflösung einschließt. Methan- und Sulfate-abhängige mikrobielle Prozesse beeinflussen die lokale Konzentrationen von Bikarbonationen (CO_3^{2-}) durch Veränderungen des pH Wertes und der Alkalinität. Zusätzlich zu den mikrobiellen Einflüssen auf die anorganische Chemie des Meerwassers wurden auch mikrobiell gebildete organische Komponenten entdeckt, welche die Reaktionskinetik von Karbonatmineralien beeinflussen können. Ein umfassendes Verständnis der Beziehungen zwischen Mikroben und Karbonaten ist essentiell für die Abschätzung des globalen Kohlenstoffkreislaufs und für das Verständnis von Gesteinsbildung. Dennoch sind die grundlegenden Mechanismen bis heute kaum untersucht. Die vorliegende Studie umfasst detaillierte Untersuchungen mikrobiell bedingter Präzipitation und Auflösung von Karbonatmineralien. Folgendes konnte gezeigt werden:

1. Biofilme, die von dem sulfatreduzierenden Bakterium *Desulfobulbus mediterranaeus* gebildet wurden, ermöglichten die Bildung von Magnesium Dolomit ($CaMg(CO_3)_2$). Die Präzipitation von Kristallen geschah ausschließlich innerhalb oder in räumlicher Nähe von extrazellulären polymeren Substanzen (EPS). Innerhalb der EPS wurden relativ mehr Kalzium (Ca) - als Magnesiumionen (Mg) angereichert, wodurch sich hier ein molares Mg/Ca von 0.8 ergab, wohingegen das umgebende Flüssigmedium ein Verhältnis von 4.7 aufwies. Die Analyse der Kalziumisotopie zeigte eine graduelle Verringerung von ^{44}Ca zwischen dem flüssigen Medium, dem Biofilm und den Dolomitkristallen. Dieses deutet darauf hin, dass bei der Sequestrierung von Ca-Ionen aus der Lösung in das Kristallgitter eine Zwei-Stufen-Fraktionierung stattfindet.
2. In Inkubationen von Kalzitpulver mit dem aerob methanotrophen Bakterium

trichosporium zeigte sich Kalzitauflösung, bedingt durch metabolisch aktive, inaktive und tote Zellen. Die höchsten Auflösungsraten von Kalzit wurden für die Versuchsansätzen mit aktiven und toten Zellen ermittelt. Die Ergebnisse der Studie zeigten, dass Kalzitauflösung sowohl durch die mikrobielle Bildung von Kohlendioxid, als auch durch das Einbringen organischer, intrazellulärer Substanzen und durch direkten Kontakt von Zellen mit Kristalloberflächen ausgelöst wurde. Langzeitinkubationen mit aktiven *M. trichosporium* Zellen zeigten starke Oberflächenerosionen an größeren Kalzitkristallen.

3. Inkubationsexperimente von Sediment-Seewasser Schlämmen (Slurries) aus Gebieten mit Methanaufstieg mit ^{14}C-Bikarbonat sowie ^{45}Ca zeigten, dass beide Radioisotope prinzipiell geeignet sind, Karbonatbildungsraten in natürlichen Sedimenten zu ermitteln. Der Vergleich zwischen sterilisierten und aktiven Slurries erlaubte eine Diskriminierung zwischen abiotischer und mikrobiell-bedingter Präzipitation. Die ermittelten Präzipitationsraten korrelierten mit der methanabhängigen mikrobiellen Aktivität in den Sediment slurries. Die Inkubationen mit ^{14}C erzielten generell geringer Präzipitationsraten, im Vergleich zu denen mit ^{45}Ca. Die Optimierung der Methode sollte deshalb Untersuchungen über die Wechselbeziehungen zwischen Ca-Ionen und den organischen Sedimentkomponenten beinhalten.
4. Der Kontinentalrand vor der costa-ricanischen Pazifikküste zeichnet sich durch die Advektion von methanangereichertem Fluid aus. Erste Ratenmessungen von anaerober Oxidation von Methan (AOM) und Sulfatreduktion in den Oberflächensedimenten zweier benachbarter Schlammhügel (Mound 11 und 12) zeigten, dass die Methanumsatzraten am Mound 11 um den Faktor 4.8 bis 6.3 höher waren als am Mound 12. Die Analyse der Zusammensetzung der stabilen Sauerstoff- und Kohlenstoffisotope in Karbonaten beider Gebiete zeigte für beide Elemente, im Vergleich zu Mound 12, eine höhere Anreicherung an schweren Isotopen an Mound 11. Die Ergebnisse der Studie bestätigen vorrausgegangene Untersuchungen, welche darauf hindeuten, dass an Mound 11 zur Zeit ein starker Fluss von Fluid aus einer tiefen Quelle stattfindet, während Mound 12 einen schwächerer Fluidfluss aus einer flacheren Quelle aufweist. Die Untersuchung zeigte, dass die Kombination aus Ratenmessungen

momentaner mikrobieller Aktivität und der Analyse von Karbonatarchiven eine sinnvolle Vorgehensweise ist, um zeitliche und räumliche Unterschiede im Fluss von methanangereicherten Fluiden an Methanaustrittsstellen einzugrenzen.

Zusammenfassend zeigten die genannten Studien, dass Mikroben die Stabilität mariner Karbonate nicht nur durch Veränderung der Wasserchemie, sondern auch durch die Bildung von extrazellulären polymeren Substanzen, Kontakt zwischen Zelle und Mineraloberfläche, oder der Freisetzung von intrazellulären organischen Komponenten beeinflussen.

Abstract

Calcium carbonates ($CaCO_3^{2-}$) belong to the most common mineral groups within the marine realm. Research efforts carried out over past two decades have shown that microbial activities largely determine the fate of carbonate minerals, including microbially mediated precipitation or dissolution. Methane- and sulfate-dependent microbial metabolic pathways influence local concentrations of carbonate (CO_3^{2-}) ions by causing changes in pH and alkalinity. In addition to changes in inorganic chemistry, microbial organic compounds have been identified to influence the kinetic conditions for carbonate minerals. Knowledge of the relationships between microbes and carbonates is essential for constraining global carbon cycling and for interpreting the rock record. However, some of the fundamental mechanisms remain elusive to date. The present study encompasses detailed investigations of microbial precipitation and dissolution of carbonate minerals and demonstrated the following:

1. Biofilms of the sulfate-reducing bacteria strain *Desulfobulbus mediterranaeus*, grown under modern anaerobic seawater chemistry, served as nucleation sites for magnesium-rich dolomite ($CaMg(CO_3)_2$). Crystals precipitated only within or in close proximity to extracellular polymeric substances (EPS). The EPS accumulated relatively more calcium (Ca) than magnesium (Mg) ions, resulting in a Mg/Ca ratio of 0.8, compared to 4.7 in the bulk liquid medium. Calcium isotopy investigations showed a gradual depletion of ^{44}Ca between bulk liquid medium, biofilm and dolomite crystals, indicating a two-step fractionation process involved in the sequestration of Ca^{2+} from the solution into the crystal lattice.
2. Incubation of calcite powder with the aerobic methanotrophic bacteria strain *Methylosinus trichosporium* showed calcite dissolution, facilitated by metabolically active, inactive and dead cells. Highest rates of calcite dissolution were observed in the presence of active and dead cells. The results suggest that calcite dissolution was mediated by microbial production of carbon dioxide,

release of organic acids and direct contact between cells and crystal surfaces. Long term incubations with active *M. trichosporium* cells showed strong surface erosion of large crystals.

3. Incubation experiments with sediment-seawater mixtures (slurries) from methane-seep environments using ^{14}C-bicarbonate and $^{45}Ca^{2+}$ showed that these radioisotopes are principally suitable to constrain calcification rates in natural sediments. Comparison of sterilized and active slurries allowed the discrimination between abiotic and microbially-mediated precipitation. Calcification rates correlated with methane-related microbial activity. Incubations with ^{14}C yielded generally lower calcification rates compared to ^{45}Ca incubations. Method refinement needs to include investigations of interaction between Ca^{2+} and organic sediment components.
4. The pacific continental margin offshore Costa Rica is characterized by methane-charged fluid advection. First direct rate determinations of anaerobic oxidation of methane (AOM) and sulfate reduction in the surface sediments of two neighboring mud mounds (Mound 11 and 12) showed methane turnover rates, one order of magnitude higher at Mound 11, compared to Mound 12. Analysis of stable oxygen and carbon isotope variations of authigenic carbonates from the two locations showed isotopically heavier values for Mound 11, compared to Mound 12. The results together support previous work suggesting that Mound 11 is currently supplied by strong fluid flow from a deep source, while Mound 12 is subjected to less intense advection of a shallow source fluid. The study demonstrated that the combination of microbial rate measurements in combination with carbonate archives is a suitable tool to constrain temporal and spatial variations of methane charged fluid flow at methane seeps.

In summary, the above studies demonstrated that microbes not only affect marine carbonate stability by changing the water chemistry, but also influence precipitation kinetics by production of extracellular polymeric substances, cell-mineral contact, and release of intracellular organic components.

Chapter 1

General introduction

1. Introduction

Minerals and rocks belong to the most elementary components of the Earth, with microbes interacting with them in numerous ways. The relationship between bacteria and the lithosphere ranges from microbially mediated formation of minerals to microbial utilization of rocks and minerals as a nutrient source or as a habitat. Therefore, microbial activities represent key processes shaping the Earth's crust.

The discipline of geomicrobiology addresses the interactions of microbial activity with geological and geochemical processes. Within this field, studies of microbial metabolism at and below the ocean floor are typically the focus of research, demonstrated by the rapidly growing interdisciplinary research efforts over the last two decades. This interest is attributed to an increasing anticipation that marine microbial communities represent key factors largely influencing the fate of minerals and global biogeochemical cycles of elements. So far, only a fraction of marine microbial organisms have been identified and it seems rather likely that numerous of unknown species survive performing chemical reactions that may either produce or consume rocks and minerals.

1.1. Microorganisms

A microorganism is, by definition, an organism that is unicellular or lives in a colony of cellular organisms. This particular group is taxonomically very diverse, including the three domains of eukaryotes, bacteria, and archaea (Fig. 1). The two domains of bacteria and archaea constitute the group of prokaryotes and differ from eukaryotes lacking a cell nucleus and the other membrane bound organelles. Bacteria and archaea are the most abundant and diverse group of organisms on Earth, present in virtually all terrestrial and marine environments, and accounting for approximately half of the biomass on Earth (Whitman *et al.*, 1998). Prokaryotes are characterized by an enormous genetic diversity, and consequentially numerous metabolic

pathways. The presented work focuses exclusively on bacteria and archaea and therefore, the terms 'microbe', 'microbial', or 'microorganism' are used hereafter to refer to the two prokaryotic domains only.

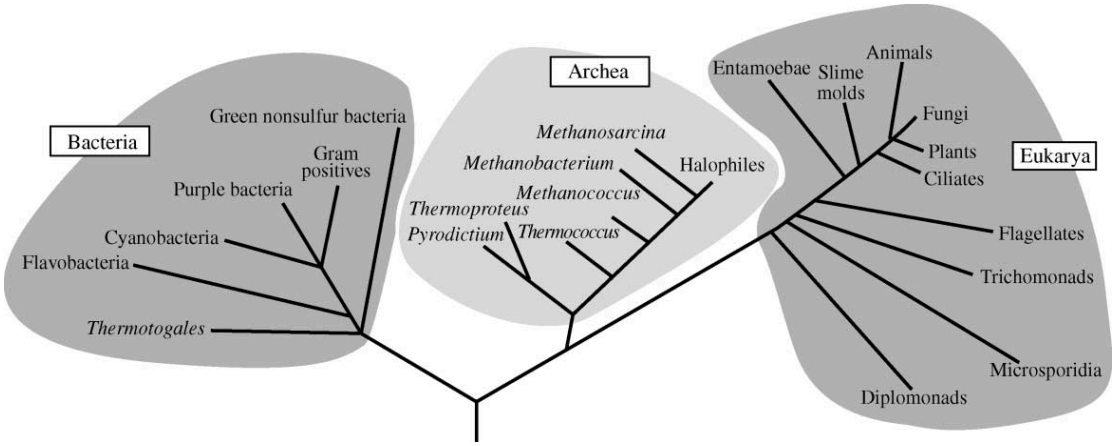

Figure 1. The „Tree of Life", source: (Raven et al., 1999).

Microorganisms play an outstanding role in Earth's geological processes, including the formation and decomposition of rocks and minerals. It is microbial metabolic activity largely driving the geo-biological cycle, thus affecting the pathways through which geochemical elements transfer between the different Earth system components.

1.2. Microbial biofilms

In addition to chemical reactions, carried out to acquire carbon, nutrients, and energy, also adaptations of microbes to environmental conditions have direct implications for the fate of minerals. In numerous environments, a common adaptation feature of microbial colonies on surfaces is the development of a biofilm (e.g. Costerton et al., 1995; Stoodley et al., 2002). In reference to the microbial community, a biofilm is defined as a group of cells that are attached to a biotic or abiotic substrate, enclosed in a gel matrix of extracellular polymeric substances (EPS) (Neu, 1996; Decho, 2000a). The reasons for biofilm formation might be manifold, including nutrient acquisition, protection against mechanical removal, and

environmental hazards (Bowden and Li, 1997; Jefferson, 2004; Simões et al., 2005). The biofilm matrix mainly consists of polysaccharides, and also proteins, nucleic acids, membrane lipids and fatty acids, secreted by the cells (Sutherland, 2001; Tsuneda et al., 2003), forming a complex three-dimensional structure (Fig 2. A, B). Biofilm EPS have been identified to influence the mineralization process, including inhibition, alteration and enhancement of mineral precipitation (Decho, 2010).

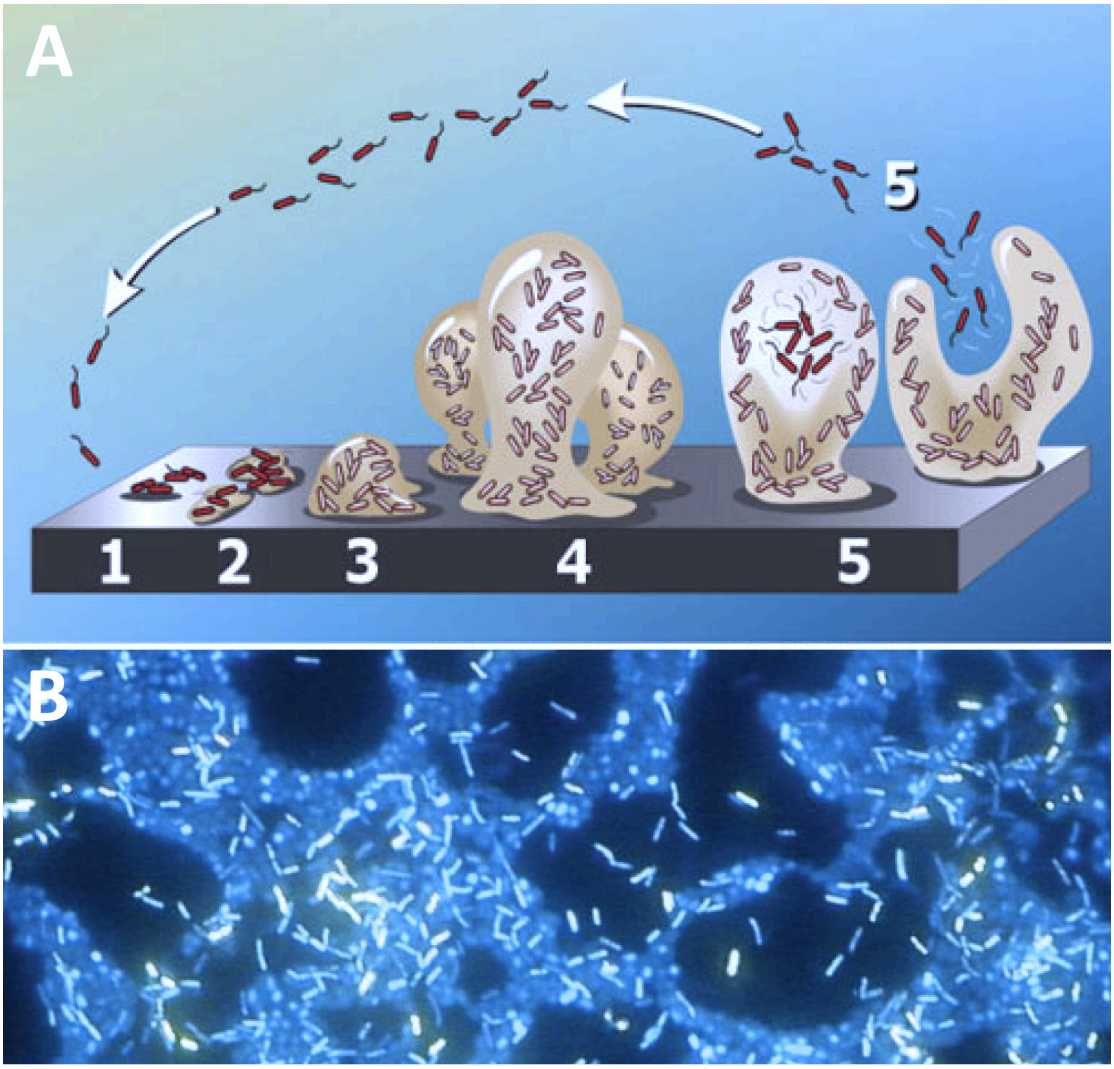

Figure 2. A. Stages of biofilm development including initial attachment (1), irreversible attachment (2), maturation (3-4) and finally dispersal (5) . Source: http://2011.igem.org/Team:Glasgow/Biofilm. **B.** Polymicrobial biofilm, stained with 4,6-diamidino-2-phenylindole (DAPI), source: Donlan (2002).

One potential mechanism affecting solubility of minerals is sorption of EPS macromolecules to crystal surfaces altering the kinetic prerequisites (Yang et al., 2008). Depending on the specific chemical composition of a biofilm, EPS might either derail (e.g. Kawaguchia and Decho, 2002; Gautret et al., 2004) or facilitate mineral precipitation (e.g. Decho, 2000; Sánchez-Román et al., 2008). Various EPS monomers effectively bind divalent cations, such as Ca^{2+} and Mg^{2+} (Flemming, 1995) with their functional groups. This binding capability leads to a considerable selective increase of ions, subsequently inducing mineral precipitation.

1.3. Biominerals

Biomineralization refers to processes in which organisms are involved in the formation of minerals. Most biominerals are calcium carbonates, silicates, iron oxides, and sulfides (Baeuerlein, 2000; Bazylinski, 2004). In order to define the genesis of minerals produced dependently on biological activity, clear definitions of the relevant processes are required. In this study, we therefore discriminate between the terms 'organomineral' and 'biomineral' based on Perry et al. (2007). According to their definition, 'organominerals' include mineral complexes formed in the presence of the byproducts of dead and decaying organisms. The term 'biomineral' generally refers to a mineral that was produced by living organisms (e.g. Weiner and Dove, 2003; Skinner and Jahren, 2003).

Two different modes of biomineral precipitation can be distinguished (Dupraz et. al., 2009): (1) biologically controlled mineral precipitation and (2) biologically induced mineral precipitation (Fig. 3).

1.3.1. Biologically controlled mineralization

Biologically controlled mineralization is a highly regulated process. This mode serves the function of specifically producing structural components, such as shells, skeletons, bones, teeth, etc. The molecular structure of nucleation sites are usually

genetically controlled to ensure defined mineral precipitation in terms of shape and mineral composition.

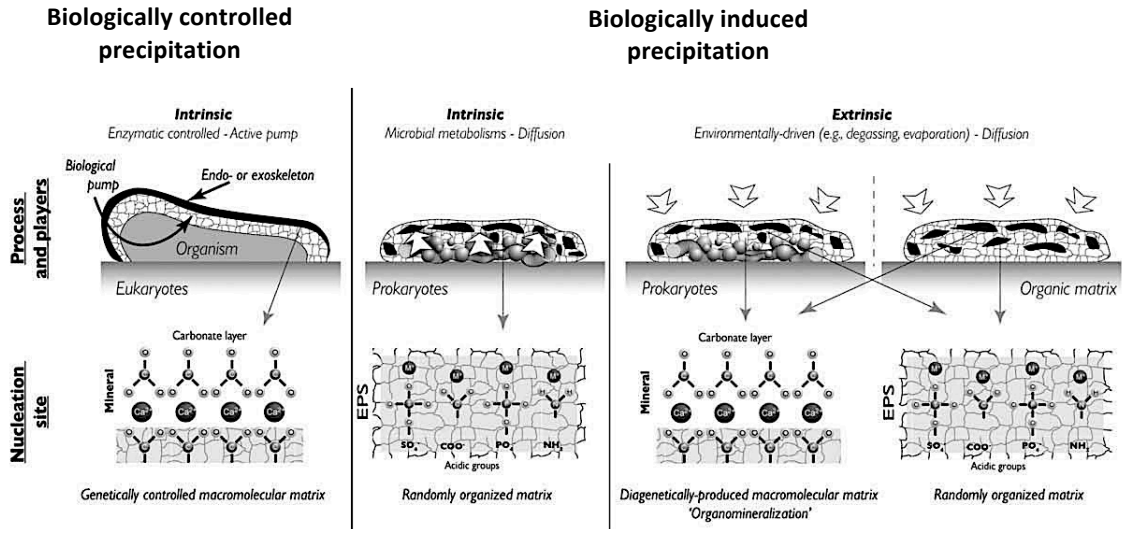

Figure 3. Classification of mineralization terms and processes showing the different types of mineralization for carbonate biomineralization. Modified after Dupraz et al. (2009).

Minerals produced under biological control are usually well defined in terms of structure and chemical composition. Additionally, a high level of spatial organization is encountered, including complex morphologies and controlled aggregations and textures. Minerals produced in biologically controlled environments also exhibit a preferential crystallographic orientation. Biologically controlled biomineralization is generally rare in the bacterial community. However, an example is the formation of intracellular magnetic crystals (mangnetosoma) in magnetotactic bacteria (Bazylinski and Frankel, 2004; Komeili, 2007) (Fig. 4), allowing movement in marine sediments in response to the environmental magnetic field (Blakemore, 1975).

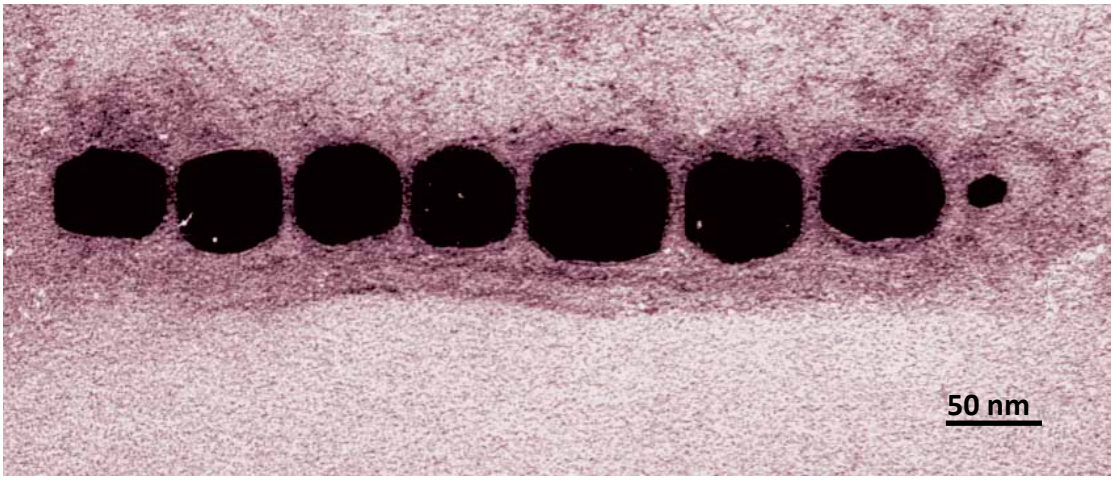

Figure 4. Transmission electron micrograph of a thin section of a magnetosome chain in a cell of the marine spirillum strain MV-4. Source: Bazylinski and Frankel (2004), Image courtesy of T. J. Beveridge.

1.3.2. Biologically induced mineralization

Formally, two processes known as biologically induced and biologically influenced mineralization were distinguished from each other as microbially or environmentally driven. However, as microbial activity and environmental conditions are intrinsically coupled, in this study the two processes will not be distinguished from each other and solely referred to as biologically induced mineralization, as suggested by Frankel and Bazylinski (2003), and Veis (2003) (Fig. 3).

Biologically induced mineralization is the result of biogeochemical processes largely defined by the environmental setting and the corresponding metabolic activity of organisms. Microbes interact in numerous ways with the surrounding environment, involving metabolic reactions and the mode of life (Fig. 5). A primary ecological role of microbes is the degradation of organic matter, a process known as re-mineralization, which is mandatory for element cycling. Microbial activity modifies spatial distribution of chemical components by liberation, production, transport, enrichment, and incorporation into biomass. The resulting alteration of geochemical properties as pH, redox potential, and gas concentrations may induce dissolution and also precipitation of various minerals. In numerous instances, inorganic minerals are precipitated as the result of metabolically produced ions, released into the adjacent environment (Greenfield, 1963; Vasconcelos et al., 1995).

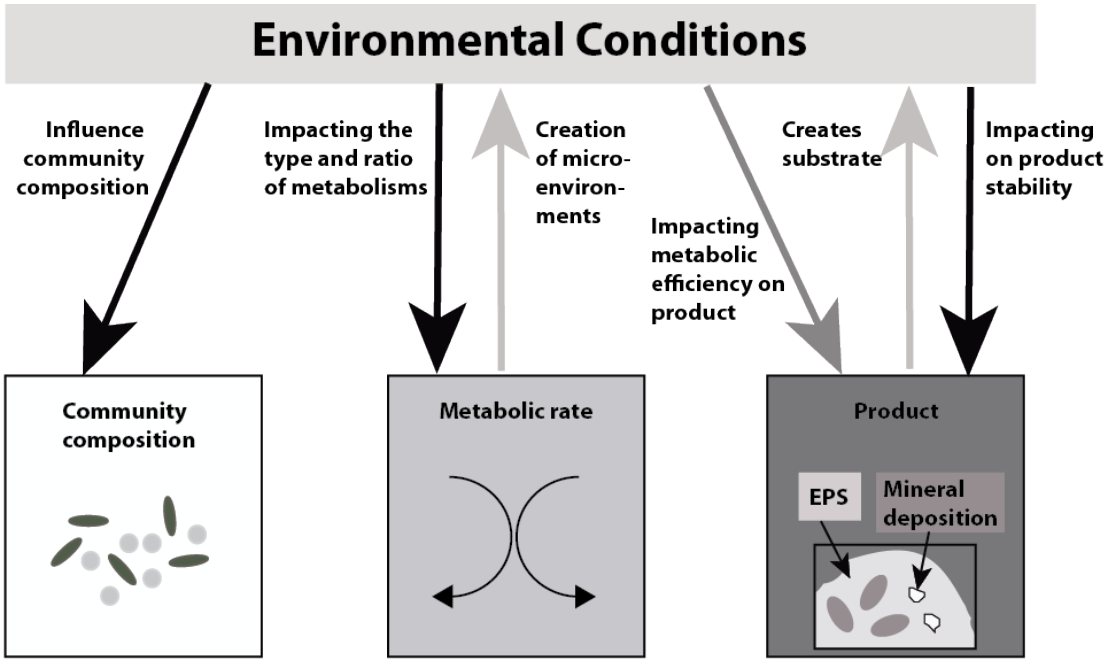

Figure 5. Relationship between environmental conditions and metabolic activity of microbial communities. Mineral precipitation is the result of interactions between microbial communities and environmental conditions. Microbial metabolic activity alters adjacent environmental conditions, mediating mineral precipitation. Modified after Dupraz et al. (2009).

Metabolic products are transported outside the cell passively via diffusion (e.g. inorganic carbonate ions) or actively via ion channels and excretion (Goodman, 2008). Continued supply of metabolic products to the environment surrounding the cell eventually may lead to supersaturation for one or several minerals, resulting in the subsequent precipitation and deposition of mineral particles. Thus, biologically induced mineralization is considered an unintended and uncontrolled consequence of metabolic activities (Frankel and Bazylinski, 2003). As there is no cellular control, precipitate size, shape, structure, chemical composition, and organization are generally heterogeneous and often poorly defined (Weiner and Dove, 2003).

1.4. Microbial mineral weathering

The process described as microbial mineral weathering refers to the generation of metabolic products and organic components that cause the dissolution of mineral

phases (Mailloux et al., 2009). Numerous studies have shown that microbes can substantially accelerate mineral solubility (e.g. Pokrovsky et al., 2009; Engel and Randall, 2011; Uroz et al., 2009), suggesting that microbial activity is a considerable factor for mineral diagenesis (Ehrlich, 1996).

A prominent mechanism responsible for mineral dissolution is acidification. In aquatic systems, mineral dissolution can be attributed to the presence of carbonic acid, resulting from microbial respiration (Soetaert et al., 2007), and nitric and nitrous acid, produced by nitrifying bacteria (Barker, 1997). Also, the release of organic acids largely contributes to mineral dissolution (Mailloux et al., 2009). Acidification is of prime relevance for silicate and carbonate minerals, as their dissolution is positively correlated with decreasing pH. In addition, cellular organic functional groups and chelating metabolites also induce mineral weathering via three simultaneously occurring mechanisms (Uroz et al., 2009). Organic acids and chelating molecules adhere to mineral surfaces and liberate nutrients from mineral phases by electron transfer. These compounds also break the oxygen links and chelate dissolved ions in carboxyl and hydroxyl groups.

Mineral dissolution can be an unintended reaction caused by microbial activity, not granting any benefit for the living organism. Although, largely irrelevant for cell metabolism, the microbial mediated release of ions into the water is of geological and chemical significance, affecting the global chemical cycles. In addition, intended mineral weathering as a strategy for nutrient and trace element acquisition, as well as an energy source, has been documented for numerous microbes (e.g. Shock, 2010; Pokrovsky et al., 2009; Edwards et al., 2005). Some taxa of microorganisms (referred to as euendoliths) are even known to bore holes into minerals (Fig. 6). The reasons for microbial boring are, to date, not fully understood. However, advantageous aspects for boring include availability of nutrients, avoidance of competition, protection from extreme environments and prevention of detachment.

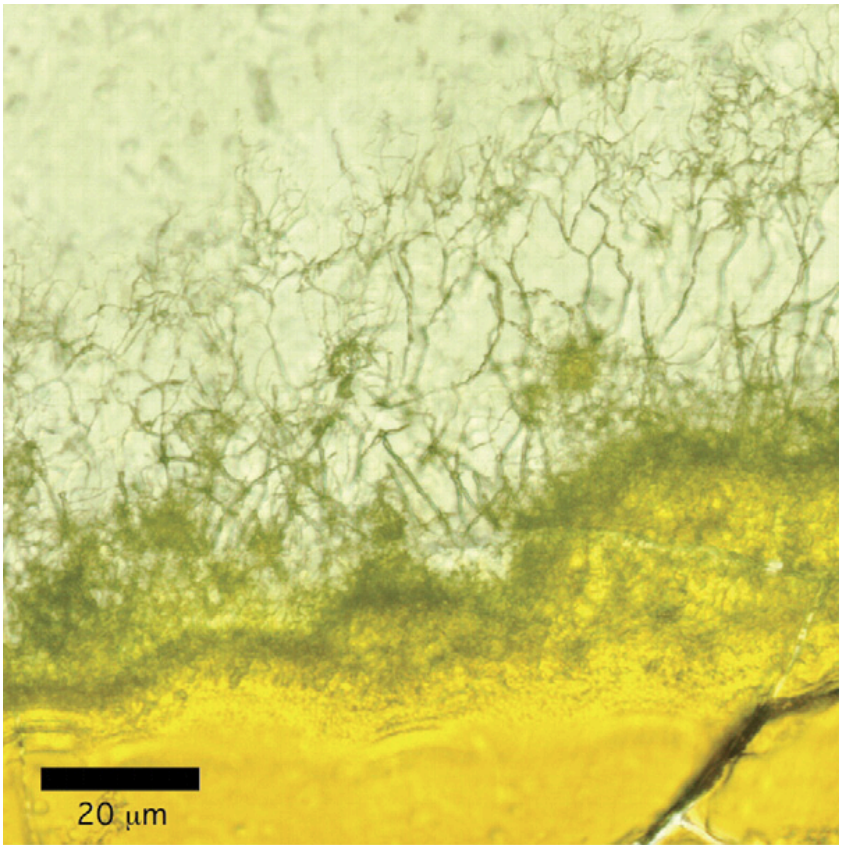

Figure 6. Microbial boring channels (green) in volcanic glass. Source: Cockell and Herrera (2008).

1.5. Marine carbonates

Among the minerals of marine origin, calcium carbonates ($CaCO_3^{2-}$) belong to the most common groups. Depositions carbonate minerals provide geological archives, allowing constraining paleo-environmental conditions. In addition, carbonates also have a regulatory function in global element cycling as they represent sinks and sources of carbon, depending on environmental pH and saturation conditions.

The initial formation of calcium carbonates in the ocean is almost exclusively facilitated by biological activity. Marine taxa including corals, molluscs, foraminifera, pteropods, and coccolithophores are long known to produce carbonate, mainly aragonite or calcite with varying quantities of magnesium. Fractions of shell fragments (carbonate oozes) deposited at the seafloor and partly lithified into limestone account for almost half the pelagic sediments the oceans (Hueneke and Mulder, 2010).

1.5.1. Pre-requisites for carbonate precipitation and dissolution under marine conditions

The fate of carbonate minerals in aquatic systems is largely depending on the carbonate system. In water, CO_2 does not simply dissolve, but also reacts with water to carbonic acid dissociating into bicarbonate (HCO_3^-) and carbonate (CO_3^{2-}) (Fig. 7).

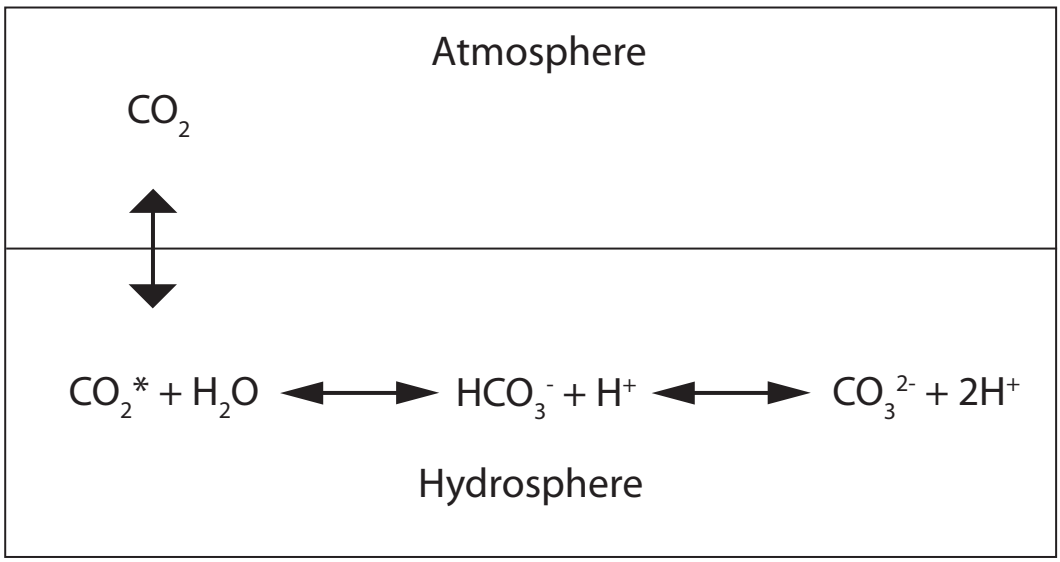

Figure 7. Illustration of the relation between atmospheric CO2 and the carbonate system in the hydrosphere. CO2* represents dissolved $CO_2$and H_2CO_3 (carbonic acid). Modified after Zeebe and Wolf-Gladow (2001).

The relationships between the carbonate system components are defined by the thermodynamic equilibrium constants K_1 and K_2.

$$CO_2(aq) + H_2O \overset{K_1}{\leftrightarrow} HCO_3^- + H^+ \overset{K_2}{\leftrightarrow} CO_3^{2-} + 2H^+ \quad (1)$$

The stoichiometric sum of the two dissolved carbonate bases, bicarbonate and carbonate, defines the carbonate alkalinity of a solution. At modern seawater conditions carbonate alkalinity (CA) accounts for approximately 96% of the total alkalinity (TA) (Drever, 1997).

According to Dickson (1981) the total alkalinity (TA) of seawater is defined by the concentrations of the following ions:

$$TA= [HCO_3^-] + 2[CO_3^{2-}] + [B(OH)_4^-] + [OH^-] + [HPO_4^{2-}] + 2[PO_4^{3-}] + [H_3SiO_4^-] + [NH_3] + [HS^-] - [H^+]_F - [HSO_4^-] - [HF] - [H_3PO_4] \quad (2)$$

$[H^+]_F$ is the free concentration of hydrogen ions.

For seawater the total alkalinity can be reasonably described by the abbreviated equation:

$$TA\approx [HCO_3^-] + 2[CO_3^{2-}] + [B(OH)_4^-] + [OH^-] - [H^+] \quad (3)$$

The dissolution or precipitation of carbonate is dependent on the saturation state (Ω), which is (for calcium carbonate) defined as:

$$\Omega = \frac{\{Ca^{2+}\}*\{CO_3^{2-}\}}{k_{sp}} \quad (4)$$

Where $\{Ca^{2+}\}$ and $\{CO_3^{2-}\}$ represent the activity of calcium and carbonate ions, and k_{sp} is the carbonate mineral specific thermodynamic solubility product constant. An Ω value < 1 indicates undersaturation, and thus mineral dissolution, while Ω > 1 is indicative for mineral precipitation at supersaturated conditions.

The surface water of the modern ocean is supersaturated by a factor 3 (aragonite) to 5 (calcite) with respect to calcium carbonate. In contrast to this observation, abiotic precipitation does not occur, because initial carbonate nucleation is kinetically unfavorable (Morse et al., 2003). Experiments have shown that carbonate crystal formation from seawater does not happen until the saturation state reaches ~20 - 25 (Morse and He, 1993).

1.5.2. Microbial influence on marine carbonates

The most important microbial metabolic pathways in the World's ocean affecting carbonate stability include:

Photosynthesis:

$$CO_2 + H_2O \rightarrow (CH_2O) + O_2 \quad (5)$$

Aerobic oxidation of methane

$$CH_4 + 2O_2 \rightarrow CO_2 + 2H_2O \quad (6)$$

Sulfate reduction (here with acetate):

$$SO_4^{2-} + CH_3COOH + 2H^+ \rightarrow HS^- + 2HCO_3^- + 3H^+ \quad (7)$$

Anaerobic oxidation of methane (AOM):

$$CH_4 + SO_4^{2-} \rightarrow HCO_3^- + HS^- + H_2O \quad (8)$$

Methanogenesis (carbon dioxide or acetate as terminal electron acceptors):

$$CO_2 + 4H_2 \rightarrow CH_4 + 2H_2O \quad (9)$$

$$CH_3COOH \rightarrow CH_4 + CO_2 \quad (10)$$

The microbial activities described above force re-equilibration of the carbonate system (Eqn. 1). Corresponding fluctuations in CO_3^{2-} ion concentration affect the saturation state (Ω) for carbonate (Eqn. 4), inducing either dissolution or precipitation. Considering the reaction pathways mentioned, microbial activity affects carbonate stability by two principal mechanisms, altering either the concentration of dissolved CO_2 or carbonate alkalinity. The microbial removal of CO_2 (Eqn. 5 & 9) induces a shift of the carbonates system, which is compensated by the removal of H^+ (Eqn. 1). The consequential increase in pH leads to an increase of

carbonate ions (CO_3^{2-}), while the alkalinity concentration is not affected. In the case of CO_2 production (Eqn. 6 & 10), re-equilibration of the carbonate system via the formation and dissociation of carbonic acid liberates H^+ ions. To reach equilibrium, protonation of carbonate ions is required, shifting the carbonate equilibrium towards bicarbonate ($HCO3^-$). Alternatively, microbial metabolic activity can result in the production of carbonate and bicarbonate ions (Eqn. 7 & 8), increasing carbonate alkalinity. Re-equilibration of the carbonate system under changing alkalinity does not affect solution pH.

1.5.3. Authigenic carbonates

The question if sedimentary bacteria possibly contributed to the formation of marine carbonate deposits has been discussed since the early 20th century (Drew, 1910). Subsequent investigations of microbial pathways, including production of metabolic products and the consequential change in carbonate saturation conditions indicated their direct influence on authigenic (generated where found) carbonate formation (e.g. Ritger et al., 1987; Bohrmann et al., 1998; Greinert et al., 2001).

In marine environments, authigenic carbonates are a common feature at cold vent locations (Fig. 8) where methane enriched- fluids rise from deeper sources towards the seafloor (e.g. Greinert et al., 2001; Bohrmann et al., 1998). Microbial anaerobic oxidation of methane (AOM) induces carbonate alkalinity increase (Boetius et al., 2000; Treude, 2003), resulting in carbonate precipitation in the case of supersaturation.

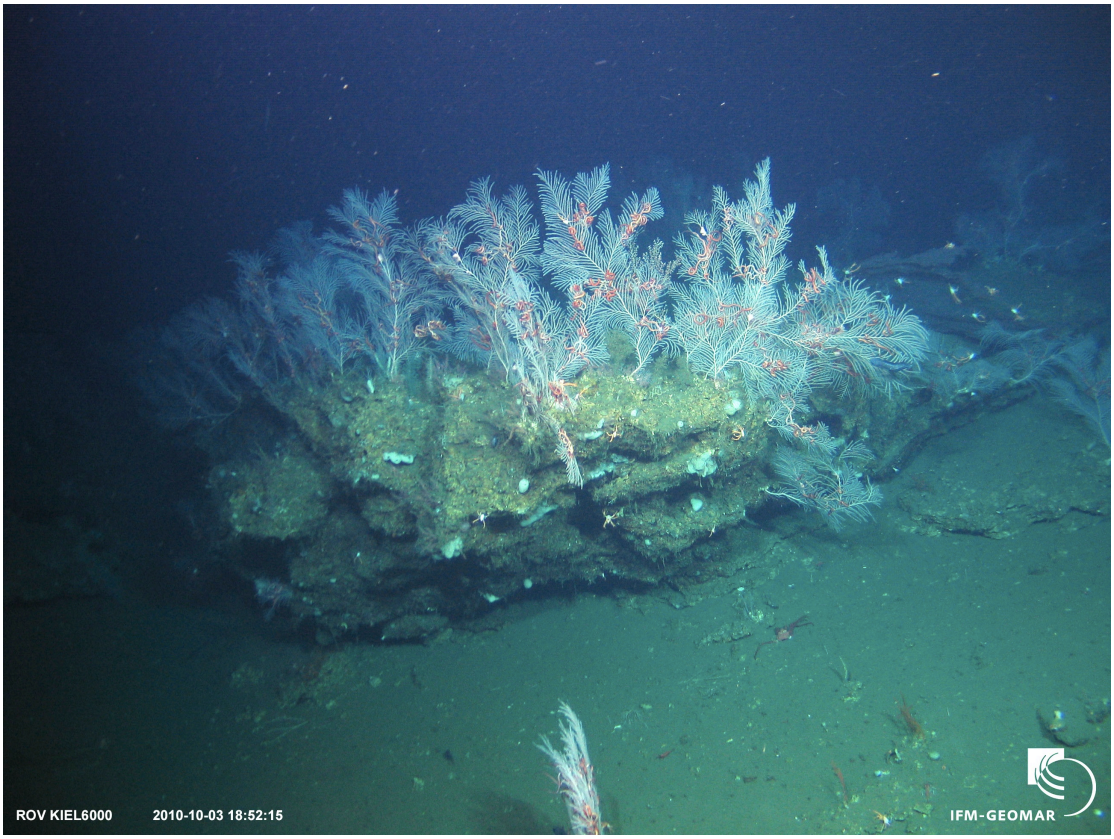

Figure 8. Authigenic carbonate block with sessile fauna at fluid venting site offshore Chile. Image courtesy of Helmholtz Center for Ocean Research GEOMAR, Kiel.

To date it is undoubted that metabolic activity of various bacterial groups, living in marine sediments, is intrinsically coupled to the fate of authigenic carbonates. Although, the knowledge of interactions between microbes and carbonates is growing rapidly, some of the fundamental mechanisms regarding formation, microbial influence on mineral chemistry, and pre-requisites for dissolution, remain enigmatic.

2. Objectives

The present study includes two objectives, of which the first one represents the main focus, whereas the second one is considered a supplement. The first objective is to constrain the relationship between marine microbial activity and the fate of carbonate minerals under laboratory conditions. The second objective includes the comparison of AOM activity and carbonate characteristics at locations, differing in advection of methane-charged fluid.

Laboratory experiments included detailed investigation of carbonate nucleation within a biofilm of a marine sulfate-reducing bacteria strain and carbonate dissolution as a direct consequence of carbon dioxide production by aerobic methanotrophic bacteria. In addition, a suitable method for direct measurements of calcification rates in natural sediment samples was developed. In these studies the main questions were:

- What is the influence of extracellular polymeric substances on carbonate mineralogy?
- Do extracellular polymeric substances alter the molar ratio of magnesium and calcium ions within the biofilm?
- Are biofilm components involved in fractionation of calcium isotopes?
- Does microbial aerobic methanotrophy enhance calcite dissolution?
- Does direct contact between microbial cells and mineral surfaces affect calcite stability?
- What is the influence of released intracellular components on calcite stability?
- Is the incubation of natural sediments with radioactive carbon and calcium tracers principally suitable to constrain calcification rates?

Environmental studies were carried out at an active continental margin, which is characterized by methane-charged fluid advection. Sediments of two neighboring mud mounds were investigated for methane-related microbial activity and stable isotope composition of authigenic carbonates. Main questions of this study were:

- What is the variability of AOM at different fluid seep locations?
- Do direct measurements of AOM activity support methane flux experiments and numerical modeling results of previous studies?
- Is the combined investigation of recent microbial activity and carbonate archives suitable for constraining fluid venting history?

3. Publications outline

Chapter 2 to 5 present the results of the present study “Effects of microbial activity on marine carbonates”. Each chapter is written in the form of a scientific manuscript, of which one is already accepted for publication (Chapter 2). The manuscripts of Chapter 3 and 5 are in preparation for submission. In the following I define my contributions to each manuscript.

1. Microbial nucleation of Mg-rich dolomite in exopolymeric substances (EPS) under anoxic modern seawater salinity: New insight into an old enigma

Stefan Krause, Volker Liebetrau, Stanislav Gorb, Mónica Sánchez-Román, Judith A. McKenzie, and Tina Treude, Geology (accepted)

This study was initiated by Tina Treude and Volker Liebetrau. Stefan Krause designed the experiments. Sample preparation, confocal laserscanning microscopy, and scanning electron microscopy was carried out by Stefan Krause with assistance of technical personnel. Stanislav Gorb carried out cryo-scanning electron microscopy imaging. Sample preparation for X-ray diffraction analysis (XRD) was carried out by Stefan Krause. Analysis of XRD spectra was carried by Mónica Sánchez-Román. Volker Liebetrau carried out sample preparation and calcium isotopy measurements with assistance from Stefan Krause. Stefan Krause wrote the manuscript with input from Tina Treude, Volker Liebetrau, Stanislav Gorb, Mónica Sánchez-Román, and Judith A. Mckenzie.

2. Enhanced calcite dissolution in the presence of aerobic methanotrophic bacteria

Stefan Krause, Giovanni Aloisi, Volker Liebetrau, and Tina Treude

Tina Treude and Volker Liebetrau initiated this study. The experiments were designed by Stefan Krause and Giovanni Aloisi. Stefan Krause carried out the sampling, counts of cell numbers, chemical analyses, and scanning electron microscopy imaging. Calculations were carried out by Stefan Krause and Giovanni Aloisi. Stefan Krause wrote the manuscript with input from Tina Treude, Giovanni Aloisi, and Volker Liebetrau.

3. A simple method for the quantification of microbially-induced calcification rates in marine sediment slurries using ^{14}C and ^{45}Ca radioisotopes

Stefan Krause and Tina Treude

This study was initiated by Tina Treude. Stefan Krause and Tina Treude designed the experiments. Stefan Krause was responsible for preparation of the experiments, sampling and measurements. Calculations were carried by Stefan Krause and Tina Treude. Stefan Krause wrote the manuscript with input from Tina Treude.

4. Fluid discharge characteristics of two neighboring mounds along the Pacific Costa Rican continental margin classified by direct measurements of microbial methane turnover and carbonate isotopic analyses

Stefan Krause, Philip Steeb, Christian Hensen, Tina Treude

This study was initiated by Tina Treude, Stefan Krause and Christian Hensen. Stefan Krause and Philip Steeb carried out all sampling procedures on-board. Stefan Krause prepared samples for $\delta^{18}O$ and $\delta^{13}C$ and XRD measurements and analyzed the XRD spectra for carbonate mineralogy. Philip Steeb calculated rates of anaerobic

oxidation of methane and sulfate reduction. Stefan Krause wrote the manuscript with inputs from Tina Treude and Philip Steeb.

4. References cited

Baeuerlein E. 2000. Biomineralization: From Biology to Biotechnology and Medical Application. Wiley-VCH, Weinheim, Germany. 294 p.

Barker, W.W., 1997, Biogeochemical weathering of silicate minerals: Geomicrobiology: Interactions between Microbes and Minerals,, p. 391-428.

Bazylinski, D.A., and Frankel, R.B., 2004, Magnetosome formation in prokaryotes.: Nature reviews. Microbiology, v. 2, no. 3, p. 217-30, doi: 10.1038/nrmicro842.

Blakemore, R., 1975, Magnetotactic Bacteria, Science, v. 190, no. 4212, p. 377-379.

Boetius, A., Ravenschlag, K., Schubert, C.J., Rickert, D., Widdel, F., Gieseke, A., Amann, R., Jorgensen, B.B., Witte, U., and Pfannkuche, O., 2000, A marine microbial consortium apparently mediating anaerobic oxidation of methane: Nature, v. 407, no. 6804, p. 623-626.

Bohrmann, G., Greinert, J., Suess, E., and Torres, M., 1998, Authigenic carbonates from the Cascadia subduction zone and their relation to gas hydrate stability: Geology, v. 26, no. 7, p. 647-650, doi: 10.1130/0091-7613(1998)026<0647:ACFTCS>2.3.CO;2.

Bowden, G.H., and Li, Y.H., 1997, Nutritional influences on biofilm development: Advances in Dental Research, v. 11, no. 1, p. 81-99.

Cockell, C.S., and Herrera, A., 2008, Why are some microorganisms boring?: Trends in microbiology, v. 16, no. 3, p. 101-6, doi: 10.1016/j.tim.2007.12.007.

Costerton, J.W., Lewandowski, Z., Caldwell, D.E., Korber, D.R., and Lappin-Scott, H.M., 1995, Microbial biofilms: Annual Review of Microbiology, v. 49, p. 711-745.

Decho, A.W., 2000, Microbial biofilms in intertidal systems : an overview: Continental Shelf Research, v. 20, p. 1257-1273.

Decho, A.W., 2010, Overview of biopolymer-induced mineralization: What goes on in biofilms?: Ecological Engineering, v. 36, no. 2, p. 137-144, doi: 10.1016/j.ecoleng.2009.01.003.

Dickson, A., 1981, An Exact Definition of Total Alkalinity and a Procedure for the Estimation of Alkalinity and Total Inorganic Carbon from Titration Data: Deep-Sea Research Part a-Oceanographic Research Papers, v. 28, no. 6, p. 609-623.

Donlan, R.M., 2002, Biofilms: microbial life on surfaces: Emerging infectious diseases, v. 8, no. 9, p. 881-90.

Drever, J.I., 1997, The Geochemistry of Natural Waters. Surface and Groundwater Environments, Prentice Hall, New York 436 pp.

Drew, G.H., 1910, On the precipitation of calcium carbonate in the sea by marine bacteria, and on the action of denitrifying bacteria in tropical and temperate seas: J. Marine Biol. Assoc., v. 9, p. 479-524.

Dupraz, C., Reid, R.P., Braissant, O., Decho, A.W., Norman, R.S., and Visscher, P.T., 2009, Processes of carbonate precipitation in modern microbial mats: Earth-Science Reviews, v. 96, no. 3, p. 141-162, doi: 10.1016/j.earscirev.2008.10.005.

Edwards, K., Bach, W., McCollom, T., 2005, Geomicrobiology in oceanography: microbe-mineral interactions at and below the seafloor, Trends in microbiology, v. 13, no. 9, p. 449-456.

Ehrlich, H.L., 1996, Geomicrobiology (Marcel Dekker, Ed.): New York.

Engel, A.S., and Randall, K.W., 2011, Experimental Evidence for Microbially Mediated Carbonate Dissolution from the Saline Water Zone of the Edwards Aquifer, Central Texas: Geomicrobiology Journal, v. 28, no. 4, p. 313-327, doi: 10.1080/01490451.2010.500197.

Flemming, H.C., 1995, Sorption sites in biofilms: Water Science and Technology, v. 32, no. 8, p. 27-33.

Frankel, R.B., and Bazylinski, D.A., 2003, Biologically induced mineralization by bacteria. Rev. Mineral Geochem., v. 54, p. 95-114.

Gautret, P., Camoin, G., Golubic, S., and Sprachta, S., 2004, Biochemical control of calcium carbonate precipitation in modern lagoonal microbialites, Tikehau atoll, French Polynesia: Journal of Sedimentary Research, v. 74, no. 4, p. 462-478.

Goodman, S.R., 2008, Medical cell biology, 3rd ed., London: Academic Press, p. 309.

Greenfield, L., 1963, Metabolism and concentration of calcium and magnesium and precipitation of calcium carbonate by a marine bacterium: Annals of the New York Academy of Sciences, v. 109, p. 23-45.

Greinert, J., Bohrmann, G., and Suess, E., 2001, Gas Hydrate-associated carbonates and methane-venting at Hydrate Ridge : Classification , distribution , and origin of authigenic lithologies, in Paull, C.K. and Dillon, W.P. eds., GEOPHYSICAL MONOGRAPH SERIES, AGU, Washington, D. C., p. 99-113.

Hueneke, H., and Mulder, T., 2010, Deep-sea sediments: Elsevier, Amsterdan, Oxford.

Jefferson, K.K., 2004, What drives bacteria to produce a biofilm?: FEMS microbiology letters, v. 236, no. 2, p. 163-73, doi: 10.1016/j.femsle.2004.06.005.

Kawaguchia, T., and Decho, A.W., 2002, Isolation and biochemical characterization of extracellular polymeric secretions (EPS) from modern soft marine stromatolites (Bahamas) and its inhibitory effect on caco3 precipitation: Preparative Biochemistry and Biotechnology, v. 32, no. 1, p. 51-63.

Mailloux, B.J., Alexandrova, E., Keimowitz, A.R., Wovkulich, K., Freyer, G. a, Herron, M., Stolz, J.F., Kenna, T.C., Pichler, T., Polizzotto, M.L., Dong, H., Bishop, M., and Knappett, P.S.K., 2009, Microbial mineral weathering for nutrient acquisition releases arsenic.: Applied and environmental microbiology, v. 75, no. 8, p. 2558-65, doi: 10.1128/AEM.02440-07.

Morse, J.W., Gledhill, D.K, Millero, F.J., 2003, CaCO3 precipitation kinetics in waters from the Great Bahama Bank: Implications for the relationship between Bank hydrochemistry and whitings, Geochimica et Cosmochimica Acta, v. 67, no. 15, p. 2819-2826.

Morse, J.W. and He, S., 1993, Influence of T, S and PCO2 on the pseudo-homogeneous precipitation of CaCO3 from seawater: implications for whiting formation, Marine Chemistry, v. 41, p. 291-297.

Neu, T.R., 1996, Significance of bacterial surface-active compounds in interaction of bacteria with interfaces: Microbiological Reviews, v. 60, p. 151-166.

Perry, R.S., Mcloughlin, N., Lynne, B.Y., Sephton, M. a., Oliver, J.D., Perry, C.C., Campbell, K., Engel, M.H., Farmer, J.D., and Brasier, M.D., 2007, Defining

biominerals and organominerals: Direct and indirect indicators of life: Sedimentary Geology, v. 201, no. 1-2, p. 157-179, doi: 10.1016/j.sedgeo.2007.05.014.

Pokrovsky, O.S., Shirokova, L.S., Benezeth, P., Schott, J., and Golubev, S.V., 2009, Effect of organic ligands and heterotrophic bacteria on wollastonite dissolution kinetics: American Journal of Science, v. 309, no. 8, p. 731-772, doi: 10.2475/08.2009.05.

Raven, J.A., Evert, R.F., and Eichhorn, S.E., 1999, Biology of the Plants: Worth Pub., New York.

Ritger, S., Carson, B., and Suess, E., 1987, Methane-derived authigenic carbonates formed by subduction-induced pore-water expulsion along the Oregon/Washington margin: Geological Society of America Bulletin, v. 98, p. 147-156.

Shock, E., 2010, Minerals as energy sources form microorganisms, Economic Geology, v. 104, no. 8, p. 1235-1248

Simões, M., Pereira, M.O., and Vieira, M.J., 2005, Effect of mechanical stress on biofilms challenged by different chemicals: Water Res., v. 39, no. 20, p. 5142-5152.

Skinner, H.C.W., and Jahren, A.H., 2003, Biomineralization, in Schlesinger, H.D. and Holland, Turekian, K.. eds., Treatise on Geochemistry, p. 117-184.

Soetaert, K., Hofmann, A.F., Middelburg, J.J., Meysman, F.J.R., and Greenwood, J., 2007, The effect of biogeochemical processes on pH (Reprinted from Marine Chemistry, vol 105, pg 30-51, 2007): Marine Chemistry, v. 106, no. 1-2, p. 380-401.

Stoodley, P., Sauer, K., Davies, D.G., and Costerton, J.W., 2002, Biofilms as complex differentiated communities: Annual Review of Microbiology, v. 56, p. 187-209.

Sutherland, I.W., 2001, Biofilm exopolysaccharides: a strong and sticky framework: Microbiology-Uk, v. 147, p. 3-9.

Sánchez-Román, M., Vasconcelos, C., Schmid, T., Dittrich, M., McKenzie, J.A., Zenobi, R., and Rivadeneyra, M.A., 2008, Aerobic microbial dolomite at the nanometer scale: Implications for the geologic record: Geology, v. 36, no. 11, p. 879-882, doi: 10.1130/g25013a.1.

Treude, T., Boetius, A., Knittel, K., Wallmann, K., Jørgensen, B.B., 2003, Marine Ecology Progress Series, v. 264, p. 1-14.

Tsuneda, S., Aikawa, H., Hayashi, H., Yuasa, A., and Hirata, A., 2003, Extracellular polymeric substances responsible for bacterial adhesion onto solid surface: FEMS Microbiology Letters, v. 223, no. 2, p. 287-292, doi: 10.1016/S0378-1097(03)00399-9.

Uroz, S., Calvaruso, C., Turpault, M.P., Sarniguet, a., de Boer, W., Leveau, J.H.J., and Frey-Klett, P., 2009, Efficient mineral weathering is a distinctive functional trait of the bacterial genus Collimonas: Soil Biology and Biochemistry, v. 41, no. 10, p. 2178-2186, doi: 10.1016/j.soilbio.2009.07.031.

Vasconcelos, C., McKenzie, J.A., Bernasconi, S., Grujic, D., and Tien, A.J., 1995, Microbial mediation as a possible mechanism for natural dolomite formation at low temperatures: Nature, v. 377.

Veis, A., 2003, Mineralization in Organic Matrix Frameworks: Reviews in Mineralogy and Geochemistry, v. 54, no. 1, p. 249-289, doi: 10.2113/0540249.

Weiner, S., and Dove, P.M., 2003, An Overview of Biomineralization Processes and the Problem of the Vital Effect: Reviews in Mineralogy and Geochemistry, v. 54, no. 1, p. 1-29, doi: 10.2113/0540001.

Whitman, W.., Coleman, D.C., and Wiebe, W.J., 1998, Prokaryotes: The unseen majority: PNAS, v. 95, no. 12, p. 6578-6583.

Yang, M., Stipp, S.L.S., and Harding, J., 2008, Biological Control on Calcite Crystallization by Polysaccharides: Crystal Growth & Design, v. 8, no. 11, p. 4066-4074, doi: 10.1021/cg800508t.

Zeebe, R. and Wolf-Gladrow, D., 2001, CO2 in Seawater: Equilibrium, Kinetics, Isotopes. Elsevier Oceanography Series, 65, Amsterdam, pp. 346.

Chapter 2

Microbial nucleation of Mg-rich dolomite in exopolymeric substances (EPS) under anoxic modern seawater salinity: New insight into an old enigma

Stefan Krause[1], Volker Liebetrau[1], Stanislav Gorb[2], Mónica Sánchez-Román[3], Judith A. McKenzie[4], and Tina Treude[1]

[1]Helmholtz Centre for Ocean Research Kiel (GEOMAR), Department of Marine Biogeochemistry, 24148 Kiel, Germany

[2]Christian-Albrechts-University of Kiel, Zoological Institute, 24098 Kiel, Germany

[3]Centro de Astrobiología (INTA-CSIC), 28850 Madrid, Spain

[4]ETH-Zürich, Geological Institute, 8092 Zürich, Switzerland

Accepted by Geology

ABSTRACT

Sulfate-reducing bacteria (SRB) are known to mediate dolomite formation under hypersaline conditions. Details of the crystal nucleation process are still poorly constrained. Our laboratory study demonstrates for the first time that *Desulfobulbus mediterraneus*, a marine sulfate-reducing bacterium, mediates primary precipitation of Mg-rich dolomite under anoxic conditions in media replicating modern seawater chemistry at low temperature (21 °C). Precipitation of crystals was associated with extracellular polymeric substances (EPS) in a monospecific biofilm, providing templates for nucleation by altering the molar Mg/Ca ratio. After initial nucleation of single nano-spherulites (~50 nm), growth was mediated by aggregation, resulting in spherulites of ~2–3 μm in diameter. Nucleation led to differences in Mg/Ca ratios and $\delta^{44/40}$Ca values between the organic material (i.e., biofilm including cells and EPS; 0.87 ± 0.01 [2 SD] and 0.48‰ ± 0.11 [2 SE], respectively), the crystals (1.02 ± 0.11 [2 SD] and <-0.08‰ ± 0.24 [2 SE], respectively), and the liquid bulk medium after mineral precipitation (4.53 ± 0.04 [2 SD] and 1.10‰ ± 0.24 [2 SE], respectively). These data indicate a two-step fractionation process involved in the sequestration of Ca from the solution into the crystal lattice of the mineral precipitated. Our results demonstrate the capability of EPS to overcome kinetic inhibition, fostering the formation of kinetically less favorable Mg-rich dolomite, and also question the applicability of Ca isotopy as a proxy for paleo-geochemistry of seawater.

INTRODUCTION

Dolomite [$CaMg(CO_3)_2$] constitutes a common carbonate mineral in sedimentary rock sequences, rarely found in modern marine environments (Arvidson and MacKenzie, 1999). Magnesium-rich dolomite is a rare form within the group of Ca-carbonates (McKenzie et al., 1990, Gunatilaka et al., 1987, Rosen et al., 1988; Warren, 1990), suggested to be the result of diagenetic alteration in hypersaline environments (Gunatilaka et al., 1987). Because abiotic precipitation of dolomite

under modern physico-chemical environmental conditions has not been demonstrated in the laboratory to date (Land, 1998; McKenzie, 1991), the process of primary marine dolomite formation remains poorly constrained. In contrast, microbially mediated dolomite formation by sulfate-reducing bacteria (SRB) has been observed as a significant ongoing biogeochemical process in the hypersaline Lagoa Vermelha, Brazil (Vasconcelos and McKenzie 1997; Vasconcelos et al., 1995). Based on these findings, Vasconcelos and McKenzie (1997) developed the microbial dolomite model, identifying consumption of organic matter by SRB as prerequisite of dolomite formation at Lagoa Vermelha. Extracellular polymeric substances (EPS) produced by SRB have been recognized as key factors influencing carbonate formation and mineralogy (Bontognali et al., 2008; Braissant et al., 2007; Dupraz et al., 2004), caused by high affinity to divalent cations, such as calcium (Ca^{2+}) and magnesium (Mg^{2+}) (Braissant et al., 2008; Perry et al., 2005). Supersaturation of the cation-binding sites and degradation of labile EPS compartments can locally increase the ion product of Ca^{2+} and Mg^{2+}, subsequently inducing precipitation of carbonate material (Dupraz et al., 2009).

Low-temperature laboratory dolomite formation by SRB has been reported for hypersaline conditions (van Lith et al., 2002; Vasconcelos et al., 1995; Warthmann et al., 2000), while evidence of dolomite precipitation by SRB at modern seawater salinity has not been experimentally observed. To date, dolomite formation at seawater salinity is only reported for aerobic bacteria (Sánchez-Román et al., 2011a, 2011b).

Under modern Earth's surface conditions, abiotic dolomite precipitation is thought to be inhibited by kinetic factors, such as the presence of sulfate ions (e.g., Morrow, 1982; Budd, 1997, Baker and Kastner, 1981) or the strong hydration shell of the Mg^{2+}-ion (Markham et al., 2002). Microbial activity has been observed to overcome these kinetic barriers (Sánchez-Román et al., 2008, 2009a, 2009b), but details of the involvement of microbes remain fragmentary. Here, we report for the first time Mg-rich dolomite precipitation in the EPS of the sulfate-reducing bacterium *Desulfobulbus mediterraneus* (Sass et al., 2002) grown in culture experiments under modern seawater conditions, with respect to salinity, Mg/Ca molar ratio and

temperature, and in the absence of oxygen. Biofilms (including cells of *D. mediterraneus* and EPS) and mineral precipitates were studied using different imaging, elemental, and isotopic analyses. We propose a possible mechanism for the nucleation and growth of non-stoichiometric dolomite crystals as a result of metabolic activity.

MATERIAL AND METHODS

Desulfobulbus mediterraneus was grown in culture experiments using an anaerobic synthetic medium with Mg^{2+} and Ca^{2+} adjusted to a molar ratio of 5, representing modern seawater conditions. After 3 and 14 days, the produced biofilm was collected for imaging by confocal laser scanning microscopy (CLSM), cryo-scanning electron microscopy (cryo-SEM), and conventional SEM. Electron microprobe (EMP) analysis, induction-coupled plasma (ICP) analysis of Mg/Ca ratio, X-ray diffraction (XRD), and isotopic analyses were carried out on samples incubated for 10 and 23 days. Calcium isotope ratios were measured in (1) the initial and final solution (i.e., before and after incubation with *D. mediterraneus*), (2) the biofilm bearing cells and EPS, and (3) purified crystal precipitates using thermal ionization mass spectrometry (TIMS). Cell-free medium served as controls. Medium composition, as well as detailed information about the experimental setup and techniques, is given in the GSA Data Repository.

EXPERIMENTAL RESULTS

Desulfobulbus mediterraneus unambiguously induced the nucleation of dolomite (Fig. 1; Table 1). No dolomite precipitation was observed in sterile controls. The refinement analysis of the crystal unit cell from the XRD scans revealed bacterial precipitates composed of ordered Mg-rich dolomite demonstrated by suprastructural ordering peaks (Table 1.). This finding is, to our knowledge, the first record of SRB involved in dolomite precipitation at Earth's surface temperature and

conditions resembling modern anoxic seawater. Over the course of the experiment (14 days), dolomite nanocrystals nucleated within the EPS and agglomerated to spheroidal crystals with a final diameter of ~2–3 µm (Fig. 2).

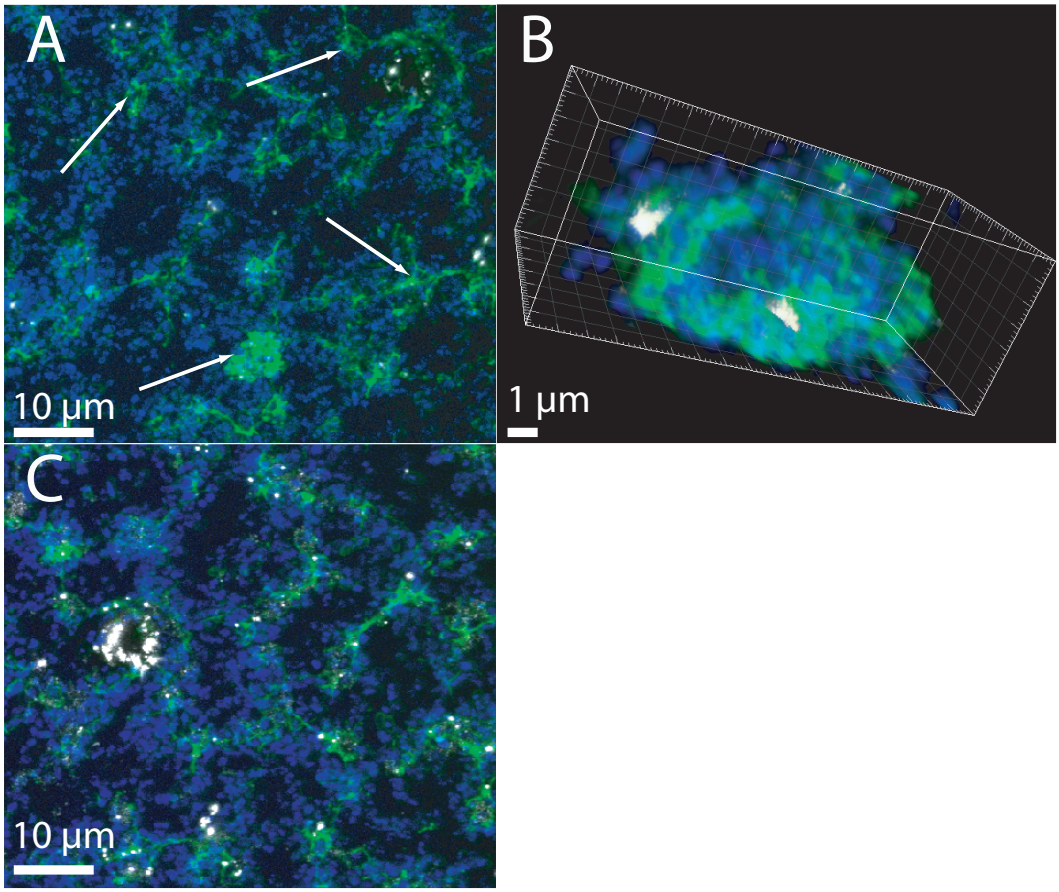

Figure 1. Confocal laser scanning microscopy (CLSM) images of *Desulfobulbus mediterraneus* biofilm growth stages. Extracellular polymeric substances (EPS) are depicted in green, bacterial cells in blue. White areas represent dolomite precipitates. A: In the early stage of biofilm formation (after 3 days), EPS are visible as streaky structures (white arrows). B: Close-up three-dimensional stack image of an early stage biofilm growth showing individual clusters of dolomite nanocrystals within the EPS matrix. C: After 14 days of biofilm growth, large amounts of EPS were produced by the bacteria. The precipitation and distribution of crystals are associated with EPS. Compared to the early stage of the biofilm growth, crystal quantity and size markedly increased.

Dolomite Nucleation and Crystal Morphology

Dolomite crystals precipitated exclusively within and /or adjacent to the EPS produced by *D. mediterraneus* (Fig. 1). Crystals changed during day 3 and 14 of incubation from nanometric to micron scale by aggregation of nanoparticles into

spherulites (Fig. DR1 in the Data Repository). Spherulites showed elevated Ca and Mg concentrations relative to adjacent cells. Using cryo-SEM, nano-crystalline particles with spheroidal morphology (~50–200 nm in diameter) were visible within the EPS (Figs. 1 and 2).

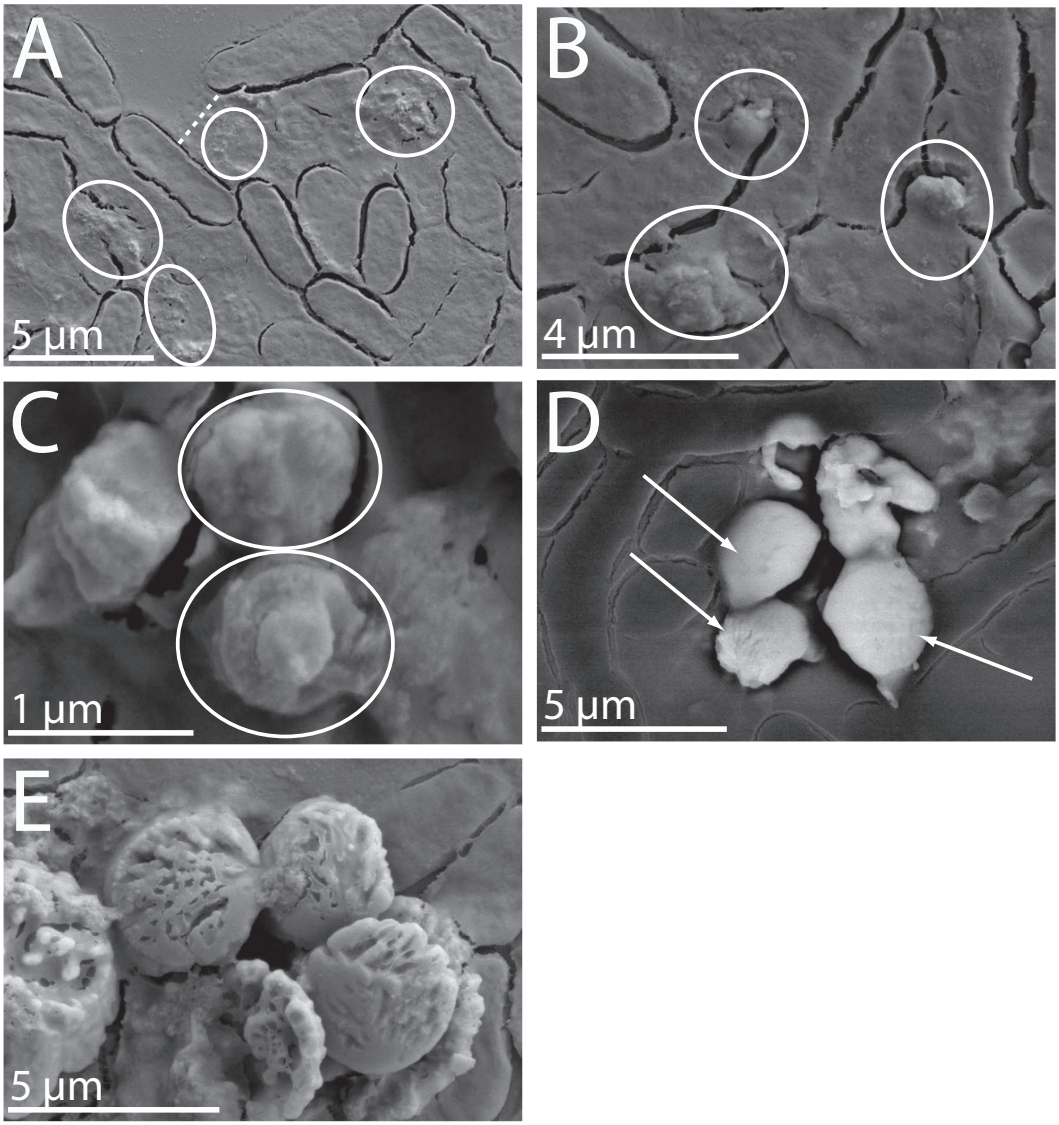

Figure 2. Cryo-scanning electron microscope images of dolomite crystals within the biofilm of *Desulfobulbus mediterraneus*. A: After 3 days of biofilm growth, nano-crystalline structures (bumps in white circles) were present within the extracellular polymeric substances (EPS) matrix. Dotted line marks the EPS boundary (top- outside, down- inside). B: After 14 days of growth, spheroidal crystals with grainy (B, C) or irregular surface structure (D, arrows) formed. Fractured crystals during sample preparation exhibited a porous inner structure (E).

Table 1. X-ray diffraction analysis of dolomite standard and experimental dolomite

Dolomite standard						Sample 1						Sample 2				
		Unit cell axes (Å)						Unit cell axes (Å)					Unit cell axes (Å)			
*hkl**	d_{hkl}†	a	b	c	Mineral§	*hkl**	d_{hkl}†	a	b	c	Mineral§	*hkl**	d_{hkl}†	a	b	c	Mineral§
101	4.024	4.808	4.808	16.055	$CaMg(CO_3)_2$ Stoichiom. dolomite	101	4.03	4.776	4.776	15.634	$Ca_{0.82}Mg_{1.18}(CO_3)_2$ Magnesian dolomite	101	3.985	4.776	4.776	15.547	$Ca_{0.8}Mg_{1.2}(CO_3)_2$ Magnesian dolomite
012	3.686				-	012	3.705				-	012	3.666				-
104	2.879				-	104	2.836				-	104	2.836				-
006	2.663				-	006	2.594				-	006	2.588				-
015	2.537				-	015	2.487				-	015	2.487				-
110	2.400				-	110	2.382				-	110	2.385				-
113	2.188				-	113	2.179				-	113	2.165				-
021	2.037				-	021	2.044				-	021	2.061				-

*Miller hkl indices denote planes orthogonal to the reciprocal crystal lattice vector.
The presence of superstructure reflections (hkl's of 015, 113, and 021) indicates an ordered dolomite (Reeder, 1983).
†Distance between adjacent planes in Å.
§Calculated by Unit cell refinement.

Electron microprobe crystal analysis revealed an average molar Mg/Ca ratio of 1.02 (±0.02, 2 SE), slightly higher with respect to stoichiometric dolomite (Mg/Ca = 1) **(**Table 2). This result was consistent with the XRD analyses.

Mg/Ca Ratio and Ca Isotopic Composition

Bulk medium liquid before and after incubation, grown biofilm, and purified crystals exhibited considerable differences in Mg/Ca ratios and $\delta^{44/40}$Ca (Table 2). Compared to medium after incubation, the biofilm showed a relative increase in Ca, resulting in a molar Mg/Ca ratio [0.87 ± 0.01(2 SD)] in the range of stoichiometric dolomite.

Table 2. Mg/Ca ratio and Ca isotopic composition

	Mg/Ca molar ratio*		$\delta^{44/40}$Ca*		
Initial medium	4.86	± 0.07	0.95	(n=6)	± 0.11§
Remaining medium	4.53	± 0.04	1.10	(n=6)	± 0.24
Bacteria+EPS	0.87	± 0.01	0.48	(n=6)	± 0.11§
Crystals§	1.02	± 0.02	0.05	(n=3)	± 0.24
Crystals blank corr.†			-0.08		± 0.24
Stoichiometric Dolomite	1				

*Variations expressed as 2nd standard error.
†δ 44/40Ca corrected for isotopic siganture of chemistry blank.
§2nd standard error < internal reproducibility, therefore 2nd standard error of internal reproducibility given.

The corresponding Ca isotope compositions showed a fractionation sequence from the isotopically heaviest bulk medium to the isotopically lightest purified dolomite crystals with a $\delta^{44/40}$Ca differing >1 ‰ (1.10 ± 0.24 [2 SE], n = 3; and 0.05 ± 0.24 [2 SE], n = 3, respectively). The degree of fractionation in the biofilm was intermediate between the bulk medium and the dolomite precipitates ($\delta^{44/40}$ Ca = 0.48 ± 0.11 [2 SE])], while its Mg/Ca molar ratio was close to 1.

DISCUSSION

Role of SRB Metabolism and EPS in Dolomite Nucleation

Since precipitation did not occur in sterile controls, Mg-rich dolomite formation can be attributed to the presence of *D. mediterraneus.* Dolomite precipitated exclusively in biofilm regions characterized by the presence of EPS. Previous studies demonstrated that EPS effectively binds $Ca^{2+}$and Mg^{2+}ions (Braissant et al., 2007). Labile fractions of EPS are subjected to rapid enzymatic degradation (Lens et al., 2003), releasing complexed cations. By increased Ca^{2+}, Mg^{2+}, and microbial CO_3^{2-} concentrations, the dolomite saturation state increases within the EPS matrix, relative to the bulk liquid, inducing dolomite formation. The kinetic constraints for dolomite nucleation include the high hydration energy of the Mg^{2+} (Lippmann, 1973). The chemical nature of EPS is thought to increase the solubility of Mg^{2+} by lowering the hydration energy for dolomite precipitation (Wright and Wacey, 2005). The analysis of the molar Mg/Ca ratio of the different compartments showed a shift from 4.53 in the bulk medium to 0.87 in the organic material, by which dolomite precipitation is favored at marine conditions (Burns et al., 2000). This discrepancy demonstrates that the EPS of *D. mediterraneus* has a direct influence on the Mg/Ca ratio in the vicinity of the biofilm, complexing relatively more Ca^{2+} than Mg^{2+}-ions. This phenomenon might be caused by the stronger hydration shell of the Mg^{2+}-ion (Markham et al., 2002).

In addition, we observed a sequential isotopic fractionation of >1‰ for Ca toward lighter isotopes from the liquid medium, via the biofilm, to the final dolomite

crystals. Natural dolomite with similar Ca isotope ratio relative to seawater has been reported for the Neoproterozoic dolomite in Namibia (-0.95‰) (Kasemann et al., 2005) and for Joulters Cay ooids (-0.76‰) (Steuber and Buhl, 2006). Considering the progressive depletion in Ca isotopic composition from the medium to the crystals, a two-step fractionation process can be hypothesized. The biofilm related fractionation provides a reservoir within the organic matter of a $\delta^{44/40}$Ca value smaller than the surrounding liquid. The dolomite within the EPS, which is forming from that reservoir, fractionates again in this direction, resulting in a dolomite depleted in ^{44}Ca relative to both, the biofilm and the surrounding fluid. Experimental inorganic calcite precipitation yields $\delta^{44/40}$Ca values of ~-0.5‰ (Tang et al., 2008), whereas fractionation in biogenic carbonates often results in $\delta^{44/40}$Ca depletion by ~1‰-1.2‰ (Böhm et al., 2006), matching the results of the present study (1.10 ± 0.24 [2 SE]).

Our findings suggest that the Ca isotopic composition of primary dolomite, and presumably also carbonate, might be strongly dependent on pre-fractionation by microbial activity, rather than fluid-dolomite fractionation. How to interpret the $\delta^{44/40}$Ca of dolomite thus requires refinement for the case of microbial mediation of dolomite precipitation. The observed fractionation processes also contribute to the understanding of discrepancies in $\delta^{44/40}$Ca signatures between potential precursors and dolomite as reported by Holmden (2009) for Ordovician deposits.

Microbial Influence on Natural Dolomite Formation

The results reported herein succinctly demonstrate that SRB form dolomite under conditions of modern marine salinity, expanding the microbial dolomite model (Vasconcelos and McKenzie, 1997) from spatially small, hypersaline environments to the global scale of the marine realm. Microbial sulfate reduction is present in nearly all marine sediments (Fenchel and Riedl, 1970; Jørgensen and Fenchel, 1974; Canfield, 1991), thus providing a potential explanation for the origin of large-scale dolomite deposits. According to the geological record, dolomite formations appear to have occurred in periods of low seawater oxygen levels (Burns et al., 2000). During these periods, aerobic processes were largely diminished in sediments

leaving more organic substrates for anaerobic degradation processes, of which sulfate reduction is dominant in marine systems (Jørgensen, 1982; Middelburg and Levin, 2009). In accordance with this hypothesis, dolomite formation has been reported from sediments of modern oxygen minimum zones in association with fascies

Mg-enriched dolomite is rare in the rock record (McKenzie et al., 1990, Gunatilaka et al., 1987, Rosen et al., 1988; Warren, 1990), and its formation is considered to be the result of the hydrological regime (Rosen et al., 1988) or diagenetic replacement (Gunatilaka et al., 1987) in hypersaline environments. In contrast, our study demonstrated microbially facilitated Mg-rich dolomite formation at normal salinity. Thus, Mg-dolomite formation for the Coorong area (South Australia) and the Al-Khiran region of Kuwait might require careful reconsideration including the possibility of microbial influence.

CONCLUSIONS

Our study demonstrates that microbially mediated low-temperature Mg-dolomite precipitation can occur in a solution replicating modern seawater salinity and Mg/Ca molar ratio. The results emphasize the role of EPS in providing nucleation sites by altering the molar Mg/Ca ratio in the vicinity of the biofilm. The potential of EPS to accumulate light Ca isotopes that creates a pre-fractionated reservoir, from which dolomite crystals precipitate, may have important implications for the reconstruction of palaeo-hydrological regimes of carbonate formation. Our findings provide clues to decipher the nucleation of dolomite in modern environments and better understand the geological record of dolomite.

ACKNOWLEDGEMENTS

This is a publication of the "The Future Ocean" Cluster of Excellence and the SFB-574: "Volatiles and Fluids in Subduction Zones" (contribution no. 231) at Kiel University, funded by the German Research Foundation (DFG). We thank A.G. Bittermann for her assistance with SEM and CLSM imaging, J. Ösert for assistance with cryo-SEM. We acknowledge M. Thöner for help with EMP analyses, J. Heinze and N. Augustin for XRD analysis, A. Kolevica and R. Surberg for ICP analyses and support for the TIMS analysis. C. Vasconcelos and F. Böhm are thanked for stimulating discussions on geological and isotopic aspects. The European Cooperation in Science and Technology supported this work with grants ECOST–ES0902-180410-000000 within the PERGAMON project

REFERENCES CITED

Arvidson, R.S., and MacKenzie, F.T., 1999, The dolomite problem: Control of precipitation kinetics by temperature and saturation state: American Journal of Science, v. 299, p. 257–288, doi:10.2475/ajs.299.4.257.

Baker, P.A., and Kastner, M., 1981, Constraints on the formation of sedimentary dolomite: Science, v. 213, p. 214–216, doi:10.1126/science.213.4504.214.

Böhm, F., Gussone, N., Eisenhauer, A., Dullo, W.-C., Reynaud, S., and Paytan, A., 2006, Calcium isotope fractionation in modern scleractinian corals: Geochemica et Cosmochemica Acta, v. 70, p. 4452–4462, doi:10.1016/j.gca.2006.06.1546.

Bontognali, T.R.R., Vasconcelos, C., Warthmann, R.J., Dupraz, C., Bernasconi, S.M., and McKenzie, J.A., 2008, Microbes produce nanobacteria-like structures, avoiding cell entombment: Geology, v. 36, p. 663–666, doi:10.1130/G24755A.1.

Braissant, O., Decho, A.W., Dupraz, C., Glunk, C., Przekop, K.M., and Visscher, P.T., 2007, Exopolymeric substances of sulfate-reducing bacteria: Interactions with

calcium at alkaline pH and implication for formation of carbonate minerals: Geobiology, v. 5, p. 401–411, doi:10.1111/j.1472-4669.2007.00117.x.

Braissant, O., Decho, A.W., Przekop, K.M., Gallagher, K.L., Glunk, C., Dupraz, C., and Visscher, P.T., 2008, Characteristics and turnover of exopolymeric substances in a hypersaline microbial mat: FEMS Microbiology Ecology, v. 67, p. 293-307, doi:10.1111/j.1574-6941.2008.00614.x.x

Budd, D.A., 1997, Cenozoic dolomites of carbonate islands: Their attributes and origin: Earth-Science Reviews, v. 42, p. 1–47, doi:10.1016/S0012-8252(96)00051-7.

Burns, S.J., Mckenzie, J.A., and Vasconcelos, C., 2000, Dolomite formation and biogeochemical cycles in the Phanerozoic: Sedimentology, v. 47, Suppl. 1, p. 49–61, doi:10.1046/j.1365-3091.2000.00004.x.

Canfield, D.E., 1991, Sulfate reduction in deep-sea sediments: American Journal of Science, v. 291, p. 177–188, doi:10.2475/ajs.291.2.177.

Dupraz, C., Visscher, P.T., Baumgartner, L.K., and Reid, R.P., 2004, Microbe-mineral interactions: Early carbonate precipitation in a hypersaline lake (Eleuthera Island, Bahamas): Sedimentology, v. 51, p. 745–765, doi:10.1111/j.1365-3091.2004.00649.x.

Dupraz, C., Reid, R.P., Braissant, O., Decho, A.W., Norman, R.S., and Visscher, P.T., 2009, Processes of carbonate precipitation in modern microbial mats: Earth-Science Reviews, v. 96, p. 141–162, doi:10.1016/j.earscirev.2008.10.005.

Fenchel, T.M., and Riedl, R.J., 1970, Sulfide System—A new biotic community underneath oxidized layer of marine sand bottoms: Marine Biology, v. 7, p. 255–268, doi:10.1007/BF00367496.

Gunatilaka, A., Saleh, A., Al-Temeemi, A., and Nassar, N., 1987, Calcium-poor dolomite from the sabkhas of Kuwait: Sedimentology, v. 34, p. 1006, doi:10.1111/j.1365-3091.1987.tb00589.x.

Holmden, C., 2009, Ca isotope study of Ordovician dolomite, limestone, and anhydrite in the Williston Basin: Implications for subsurface dolomitization and local Ca cycling: Chemical Geology, v. 268, p. 180–188, doi:10.1016/j.chemgeo.2009.08.009.

Jørgensen, B.B., and Fenchel, T., 1974, The sulfur cycle of a marine sediment model system: Marine Biology, v. 24, p. 189–201, doi:10.1007/BF00391893.

Jørgensen, B.B., 1982, Mineralization of organic matter in the sea bed—The role of sulphate reduction: Nature, v. 296, p. 643–645, doi:10.1038/296643a0.

Kasemann, S.A., Hawkesworth, C.J., Prave, A.R., Fallick, A.E., and Pearson, P.N., 2005, Boron and calcium isotope composition in Neoproterozoic carbonate rocks from Namibia: Evidence for extreme environmental change: Earth and Planetary Science Letters, v. 231, p. 73–86, doi:10.1016/j.epsl.2004.12.006.

Land, L.S., 1998, Failure to precipitate dolomite at 25 degrees C from dilute solution despite 1000-fold oversaturation after 32 years: Aquatic Geochemistry, v. 4, p. 361–368, doi:10.1023/A:1009688315854.

Lens, P., O'Flaherty, V., Moran, A.P., Stoodley, P., and Mahony, T., 2003, Biofilms in Medicine, Industry and Environmental Biotechnology: London, IWA Publishing.

Lippmann, F., 1973, Sedimentary Carbonate Minerals: New York, Springer-Verlag.

Markham, G.D., Glusker, J.P., and Bock, C.W., 2002, The arrangement of first- and second-sphere water molecules in divalent magnesium complexes: Results from molecular orbital and density functional theory and from structural crystallography: The Journal of Physical Chemistry B, v. 106, no. 19, p. 5118–5134, doi:10.1021/jp020078x.

McKenzie, J.A., 1991, Controversies in modern geology: Evolution of geological theories in sedimentology, Earth history, and tectonics, *in* Müller, D.W., et al., eds., The dolomite problem: An outstanding controversy: London, Academic Press, p. 37–54.

McKenzie, J.A., Isern, A., Karpoff, A.M., and Swart, P.K., 1990, Basal dolomitic sediments, Tyrrhenian Sea, ODP Leg 107: Proceedings of the Ocean Drilling Program, Initial Reports, v. 107, p. 999–1006.

Middelburg, J.J., and Levin, L.A., 2009, Coastal hypoxia and sediment biogeochemistry: Biogeosciences, v. 6, p. 1273–1293, doi:10.5194/bg-6-1273-2009.

Morrow, D.W., 1982, Diagenesis 1. Dolomite – Part 1: The Chemistry of Dolomitization and Dolomite Precipitation: Geoscience Canada, v. 9, p. 5–13.

Perry, T.D., Klepac-Ceraj, V., Zhang, X.V., McNamara, C.J., Polz, M.F., Martin, S.T., Berke, N., and Mitchell, R., 2005, Binding of harvested bacterial exopolymers to the surface of calcite: Environmental Science & Technology, v. 39, p. 8770–8775, doi:10.1021/es0508368.

Rosen, M.R., Miser, D.E., and Warren, J.K., 1988, Sedimentology, mineralogy and isotopic analysis of Pellet Lake, Coorong region, South Australia: Sedimentology, v. 35, p. 105–122, doi:10.1111/j.1365-3091.1988.tb00907.x.

Sánchez-Román, M., Vasconcelos, C., Schmid, T., Dittich, M., McKenzie, J.A., Zenobi, R., and Rivadeneyra, M.A., 2008, Aerobic microbial dolomite at the nanometer scale: Implications for the geologic record: Geology, v. 36, p. 879–882, doi:10.1130/G25013A.1.

Sánchez-Román, M., Vasconcelos, C., Warthmann, R., and Rivadeneyra, A., M., and McKenzie, J.A., 2009a, Microbial dolomite precipitation under aerobic conditions: Results from Brejo do Espinho Lagoon (Brazil) and culture experiments.: International Association of Sedimentologists, Special Publication, p. 167–178.

Sánchez-Román, M., McKenzie, J.A., de Luca Rebello Wagner, A., Rivadeneyra, M.A., and Vasconcelos, C., 2009b, Presence of sulfate does not inhibit low-temperature dolomite precipitation: Earth and Planetary Science Letters, v. 285, p. 131–139, doi:10.1016/j.epsl.2009.06.003.

Sánchez-Román, M., Romanek, C.S., Fernández-Remolar, D., Sánchez-Navas, A., McKenzie, J.A., Amils Pibernat, R., and Vasconcelos, C., 2011a, Aerobic biomineralization of Mg-rich carbonates: Implications for natural environments: Chemical Geology, v. 281, p. 143–150, doi:10.1016/j.chemgeo.2010.11.020.

Sánchez-Román, M., McKenzie, J.A., Wagener, R., A., de Luca, A., Romanek, C.S., Sánchez-Navas, A., and Vasconcelos, C., 2011b, Experimentally determined biomediated Sr partition coefficient for dolomite: Significance and implication for natural dolomite: Geochimica et Cosmochimica Acta, v. 75, p. 887–904, doi:10.1016/j.gca.2010.11.015.

Sass, A., Rutters, H., Cypionka, H., and Sass, H., 2002, *Desulfobulbus mediterraneus* sp nov., a sulfate-reducing bacterium growing on mono- and disaccharides: Archives of Microbiology, v. 177, p. 468–474, doi:10.1007/s00203-002-0415-5.

Steuber, T., and Buhl, D., 2006, Calcium-isotope fractionation in selected modern and ancient marine carbonates: Geochimica et Cosmochimica Acta, v. 70, p. 5507–5521, doi:10.1016/j.gca.2006.08.028.

Tang, J., Dietzel, M., Böhm, F., Köhler, S.J., and Eisenhauer, A., 2008, Sr^{2+}/Ca^{2+} and $^{44}Ca/^{40}Ca$ fractionation during inorganic calcite formation: II. Ca isotopes: Geochimica et Cosmochimica Acta, v. 72, p. 3733–3745, doi:10.1016/j.gca.2008.05.033.

van Lith, Y., Vasconcelos, C., Warthmann, R., Martins, J.C.F., and McKenzie, J.A., 2002, Bacterial sulfate reduction and salinity: Two controls on dolomite precipitation in Lagoa Vermelha and Brejo do Espinho (Brazil): Hydrobiologia, v. 485, p. 35–49, doi:10.1023/A:1021323425591.

Vasconcelos, C., and McKenzie, J.A., 1997, Microbial mediation of modern dolomite precipitation and diagenesis under anoxic conditions (Lagoa Vermelha, Rio de Janeiro, Brazil): Journal of Sedimentary Research, v. 67, p. 378–390.

Vasconcelos, C., McKenzie, J.A., Bernasconi, S., Grujic, D., and Tien, A.J., 1995, Microbial mediation as a possible mechanism for natural dolomite formation at low temperatures: Nature, v. 377, p. 220–222, doi:10.1038/377220a0.

Warren, J.K., 1990, Sedimentology and mineralogy of dolomitic Coorong lakes, South Australia: Journal of Sedimentary Petrology, v. 60, p. 843–858.

Warthmann, R., van Lith, Y., Vasconcelos, C., McKenzie, J.A., and Karpoff, A.M., 2000, Bacterially induced dolomite precipitation in anoxic culture experiments: Geology, v. 28, p. 1091–1094, doi:10.1130/0091-7613(2000)28<1091:BIDPIA>2.0.CO;2.

Wright, D.T., and Wacey, D., 2005, Precipitation of dolomite using sulphate-reducing bacteria from the Coorong Region, South Australia: Significance and implications: Sedimentology, v. 52, p. 987–1008, doi:10.1111/j.1365-3091.2005.00732.x.

DATA REPOSITORY

Microbial nucleation of Mg-rich dolomite in exopolymeric substances (EPS) under anoxic modern seawater salinity: New insight into an old enigma

Microorganism

Desulfobulbus mediterraneus strain 86FS1 is a gram-negative, chemoorganotrophic and strictly anaerobic bacterium (Sass et al., 2002). Growth temperature ranges from 10 to 30°C with an optimum at 25°C. The strain was isolated from deep-sea sediment (1268 m water depth, bottom water temperature 15°C) off the NE Spanish coast (Sass et al., 2002).

Culture medium

The experiments were conducted using an anoxic synthetic seawater medium (Medium 196, German Collection of Microorganisms and Cell Cultures) using Na-lactate as organic substrate. The concentration of magnesium and calcium were adjusted to 15.2 and 3 mmol l^{-1}, representing a modern seawater Mg/Ca molar ratio of 5. Medium headspace was gassed with 90% N_2, 10% CO_2 to remove oxygen. 200 µl resazurin solution was added as an indicator for oxygen contamination. After sterilizing under 90% N_2, 10% CO_2 atmosphere at 121°C for 20 minutes, the pH was adjusted to 7.4 with 0.1 M NaOH. pH was measured using a Schott Lab 850 pH meter, which was calibrated using NIST standards for pH 4.01, 6.87 and 9.18. The medium was transferred anaerobically into 50 ml serum vials with 90% N_2, 10% CO_2

headspace. The medium was kept in the dark until further use. Light microscopy observations did not show precipitation of carbonate material after several weeks.

Medium pH, alkalinity and sulfide concentration

During the 14 day incubation period pH changed from 7.4 to 7.8. Corresponding total alkalinity was measured by sample aliquot titration with 0.01 molar HCl and methyl red/methylene blue indicator under N_2 ventilation in a vessel after Pavlova. IAPSO standard seawater was used for calibration. During 14 day incubations total alkalinity changed from 59 to 80 mEq. Total sulfide concentration was determined photometrically at a wavelength of 480 nm (Cord-Ruwisch, 1985). Sulfide concentrations increased from 1.2 to 8 mmol l^{-1} during 14 day incubations. The initial and final carbonate alkalinity was calculated with the following formula (1):

$$[CA] = [TA] - [HS^-] - [OH^-] + [H^+] \quad (1)$$

Calculations were performed according to Zeebe and Gladrow (2001).

Growing biofilms on glass slides

3 ml of active *D. mediterraneus* culture was inoculated into a vial containing 50 ml of sterile, anoxic medium 196. The vial was transferred into a glove box and opened under 90% N_2, 10% CO_2 atmosphere. A sterilized microscopy glass slide was placed on the opening of the vial and fixed with tape. Subsequently, the vial was turned upside and stored in the dark. According to the resazurin indicator samples remained anoxic during the entire experiment. After 3 and 14 days glass slides were carefully removed. The apparent biofilm was rinsed carefully in 1x phosphate buffered saline (PBS), and excess liquid was removed. Control experiments with sterile medium did not show precipitates.

Confocal laser scanning microscopy (CLSM)

D. mediterraneus biofilms growth on glass slides were investigated with CLSM the same day the anoxic culture experiments were stopped. Lectin, a constituent of extracellular polymeric substances (EPS) was stained with wheat germ agglutinin (WGA) conjugated with ALEXA FUOR 488. To prepare a 1.0 mg/mL wheat germ agglutinin (WGA) conjugate stock solution 5.0 mg of lyophilized WGA conjugate were dissolved in 5.0 mL of PBS. The stock solution was diluted to 1.0 mg/mL by adding WGA conjugate working solution into Hank's balanced salt solution (HBSS). 100 µl of labeling solution was applied to each cover slip covering adhering cells. Samples were stained for 20 minutes at 20°C in the dark. Subsequently, excess solution was removed and biofilms were carefully washed twice with PBS. Excess liquid was removed, and cells were counterstained with freshly thawed 4',6-Diamidin-2-phenylindol (DAPI) working solution (1 µg ml^{-1}) for 15 minutes in the dark. Investigation of stained samples and control materials was carried out using a Leica TCS SP5. Wheat germ agglutinin (WGA) ALEXA FLUOR 488 was excitated by the 495 nm laser line and emission was detected at 519 nm. DAPI was excited at 358 and emission recorded at 461 nm. Both fluorescence signals were recorded using a sequential mode. The 488 nm laser line was also used for recording the reflected light channel (469 - 498 nm). Image analyses were carried out using Imaris software version 6.

Scanning electron microscopy (SEM)

SEM imaging of *D. mediterraneus* biofilms were carried out using a Zeiss supra 50 VP equipped with an energy dispersive X-ray spectrometer (EDAX). Sample preparation started with careful initial washing with PBS for 5 minutes. For fixation samples were immersed in 2.5% paraformaldehyde for 15 minutes. After washing in PBS, 2% osmium tetroxide in PBS was applied for 10 minutes. Samples were then carefully washed 3 times in purified water. Glass slides were then broken into smaller pieces and dried in a series of ethanol solutions. Subsequently, critical point drying removed remaining water. Biofilm bearing glass pieces were mounted on aluminum stubs using conductive carbon cement. Samples were stored in a desiccator

overnight. Before imaging, samples were sputter coated with an 8 nm gold layer. Images were obtained with secondary electron detector applying an accelerating voltage of 4 kV with a working distance of 8.2 mm. For EDX analysis the acceleration voltage was increased to 5.6 kV (Figure DR1).

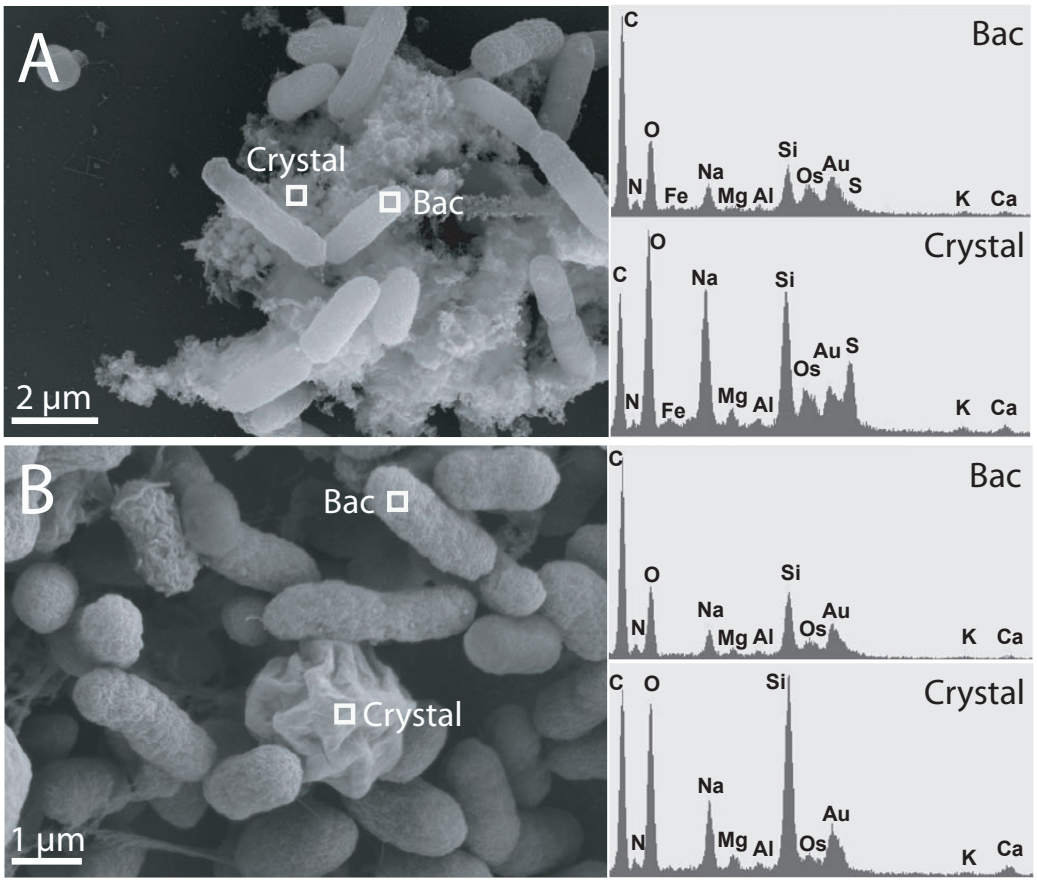

Figure DR1: Scanning electron microscopy images of Mg-rich dolomite in *D. mediterraneus* biofilm. A: Spheroidal dolomite nanocrystals (~50-200 nm) embedded in EPS were visible after 3 days of biofilm growth. B: After 14 days, larger crystals were observed within the biofilm. EDX spot analysis indicates the relative abundance of Mg and Ca in the crystals (Crystal) with respect to the bacterium (Cell). The prominent peak for silicon (Si) is caused by the glass slide the biofilm was grown on. Note: Due to dehydration during sample preparation the EPS was compressed and crystals might not be located in their original position.

Scanning Electron Microscopy with Cryogenic Preparation System (Cryo-SEM)

Cryo-SEM observations if *D. mediterraneus* biofilms were carried out with a Hitachi 4800s scanning electron microscope, equipped with a GARTAN GB cryo-unit.

Biofilms on glass slides were cut and mounted on aluminum stubs with double sided sticking tape. Cryo-fixation of the samples was carried out by immersing the stub carefully into liquid nitrogen. Samples were then introduced into the cooled SEM. Images were obtained using a secondary electron detector, operated at acceleration voltage of 5 kV and 13.7 mm working distance.

Electron microprobe analysis (EMP)

For EMP analyses, *D. mediterraneus* biofilms were grown on sterile glass slides for 10 days, as described above. Elemental analysis of the crystals in the biofilms was performed using a Jeol JXA-8200 WD/ED combined with a microanalyzer Superprobe. Prior to the analysis, samples were carefully washed 3 times in purified water and dried overnight. Before analyzing, samples were coated with a carbon layer of 10 nm thick. The Mg/Ca ratios of the crystal precipitates, listed in Table 2, represent the average value of 42 measurements of individual crystals within the biofilm.

X-ray diffraction analysis (XRD)

For mineralogy analysis of the crystal precipitates, 3 x 30 ml of active *D. mediterraneus* culture was inoculated into 3 x l sterile medium. Biofilm growth, pH, total alkalinity and sulfide concentration were monitored weekly. After 23 days, sulfide concentration exceeded 11 mmol l^{-1} and biofilm growth was stopped. The clear medium was carefully removed. The biofilm was resuspended with the last remaining 10 ml medium and transferred into a centrifuge tube. The suspension was centrifuged with 4500x g for 10 minutes at 4°C. The clear supernatant was discarded. The remaining pellet was resuspended in 50 ml of purified water with a pH of 8-9 to avoid dissolution of carbonate material. After resuspension, the sample was centrifuged again. The clear supernatant was discarded and replaced by 50 ml of 1% NaClO to bleach organic material. The sample was left to react overnight followed by centrifuging and replacement of NaClO. In total, bleaching was repeated three times.

The remaining material was washed 3 times in purified water and dried at 37°C. For XRD analyses, the material was powdered and placed on a silicon disc. Analyses were run from 0° to 60° 2-theta angle (Figure DR2) on a Philips X-ray diffractometer PW 1710 with monochromatic CuKα. The spectra showed additional peaks to those identified for dolomite. As great care was taken during the purification to avoid crystal dissolution due to extensive washing, additional peaks might originate from remnant medium components.

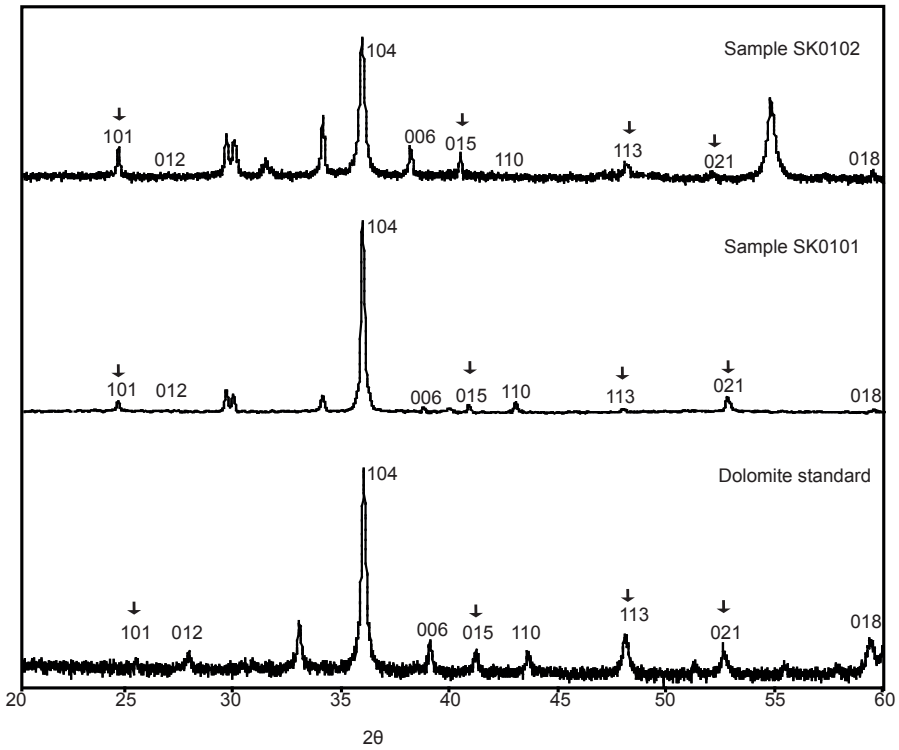

Figure DR2: X-ray diffractograms of reference dolomite material and dolomite crystals formed in *D. mediterraneus* biofilms at 21˚C (sample SK0101, sample SK0120). Note: The presence of superstructure reflections (odd labeled hkl's) indicates that the rhombohedral carbonate is an ordered dolomite (Reeder, 1983).

Methods for element concentration and Ca isotope ratio measurements

30 ml of active *D. mediterraneus* culture were inoculated into a Duran glass bottle with 1 l of sterile 196 medium with adjusted Mg/Ca ratio (see above). After 23 days of incubation, biofilm growth was stopped. The remaining medium was transferred

step wise into acid-washed 50 ml centrifuge vials and centrifuged at 4500x g for 10 minutes. The clear supernatant was transferred into acid washed 50 ml centrifuge vials. The remaining pellet, containing floating organic material was washed four times in purified water with a pH of 8-9 (adjusted with NH_4^+). The supernants of the washing steps were transferred separately into 50 ml acid washed centrifuge vials. The biofilm at the bottom was resuspended in 10 ml centrifuged medium and transferred into a 50 ml acid washed centrifuge vial. The sample was centrifuged at 4000 RPM for 10 minutes and transferred into a 15 ml Teflon beaker. 8 ml of ultra pure NaClO (1%) bleaching solution was added and left to react for 12 hours. Subsequently, the sample was centrifuged at 4000 RPM for 10 minutes and NaClO was exchanged. This procedure was repeated 3 times. After bleaching, the sample was washed 4 times in purified water with adjusted pH (see above) and the supernatants of individual washing steps were transferred separately into 50 ml centrifuge vials. Finally, the remaining pellet was transferred into a 6 ml teflon beaker.

All samples were dried at 95°C for at least 12 hrs. Organic bearing samples and blanks were additionally resuspended in 1 ml purified water and 1 ml HNO_3 8N and dried at 95°C, followed by resuspension in 1 ml HNO_3 and 20 µl $HCLO_4$ and left to react for 3 hours at 95°C. All applied HCl and HNO_3 based acids refer to 2-step Teflon cascade still (pico trace) purification of initially per analysis quality. After drying at 180°C 0.75 ml 8N HNO_3 and 0.25 ml H_2O_2 were added and left to react for at least 12 hrs, and subsequently dried at 80°C.

In order to prepare source solutions for identical aliquots for different analytical methods and reproducibility tests the samples were re-dissolved in 4ml of 2.25 HNO_3.

Table DR1. Ca isotopy of medium, organic component and crystals

Sample	Average $\delta^{44/40}$Ca (‰)	2 SE	n
Standard NIST-SRM-915a	0.00	0.11	8
Whole procedure blank	1.16	0.38	2
Chemistry blank	1.24	0.03	2
Initial medium	0.95	0.05	3
Remaining medium	1.10	0.12	6
Organic (EPS+Bacteria)	0.48	0.07	6
3rd wash Organic	0.46	0.08	5
4th wash Organic	0.48	0.26	3
Dolomite crystals	0.05	0.24	3

Simultaneous determination of element concentration (Mg, Ca, Sr) and ratios by ICP-OES (VARIAN 720-ES) was carried out on 0.5 ml of the source solution. Aliquots of up to 3000 ng Ca equivalent were taken for Ca-isotope preparation and mixed with a ^{43}Ca/^{48}Ca double spike. Spiked samples were dried at 95°C, resuspended in 2.2 N HNO_3, and Ca was separated using 600 µl columns (biorad) with MCI-Gel 75-150 µm. Whole procedure blanks were spiked at the beginning and revealed maximum amounts of 197 ng for multi-step bleach runs (dolomite crystals) and 30 to 60 ng for routine column chemistry runs (single step total dissolution).

The calcium isotope ratios of dolomite crystals, aqueous Ca of initial and remaining medium, and Ca remaining in the biological component were measured with a Finnigan Triton TI (Thermal Ionization Mass Spectrometer) following the method described in Heuser et al., (2002) and Böhm et al. (2006). Prior to filament loading samples were dried down and transferred into chloride form by evaporation in 2.2 N HCl. After uptake with loading solution, aliquots of about 300 ng were loaded with TaCl5 activator in a sandwich technique on a zone-refined Re filament.

Measurements were made on single filaments at temperatures around 1470 °C and a typical ^{40}Ca signal intensity of 9-10 V. Data acquisition was performed in dynamic mode. The double-spike correction was carried out with the algorithm used by Heuser et al. (2002).The isotope values of Ca are reported as ä$^{44/40}$Ca (‰) values relative to the NIST standard SRM915a, where

ä$^{44/40}$Ca [(^{44}Ca/^{40}Ca)$_{sample}$/(^{44}Ca/^{40}Ca)$_{SRM915\ a}$- 1] x 1000. For each sample at least 3 independent filaments were measured in one session and individually normalized to the average ^{44}Ca/^{40}Ca of four SRM915a analyses, distributed throughout the same turret. The precision is expressed as two times the standard error of the average (2SEM = 2r/n0.5). Some samples were repeated in different sessions during the study. A representative external uncertainty for the method of at least 0.11‰ is reflected in the 2 SE for NIST-SRM-915a measurements throughout the study. The results are summarized in Table DR1.

Notes: (1) Some samples were reproduced better within their single session run than the standard used for normalization regarded throughout the whole study.

(2) The last two washing supernatant liquids for the organic component had an

isotopic fractionation similar to the corresponding total dissolved sample. This result shows that the intermediate fractionation of the organic material is not due to artifacts during sample preparation, but represents the original Ca isotopic fractionation of this component.

(3) The isotope signature of the whole procedure blank was heavier than all samples.

Therefore, its only potential influence was a shift towards apparent heavier signatures, which would be mostly expressed in the smallest and multistep bleached samples, the dolomite crystals. Consequently, after blank correction original crystal isotope signature pointed to even lighter values. The fractionation step between the divalent cation reservoir, attached to the organic phase, and the dolomite precipitate must be assumed to be even larger than reflected in these initial measurements.

REFERENCES CITED

Böhm, F., Gussone, N., Eisenhauer, A., Dullo, W.-C., Reynaud, S., and Paytan, A., 2006, Calcium isotope fractionation in modern scleractinian corals: Geochimica et Cosmochimica Acta, v. 70, p. 4452-4462.

Cord-Ruwisch, R., 1985, Aquick method for the determination of dissolved and precipitated sulfides in cultures of sulfate-reducing bacteria: Journal of Microbiological Methods, v. 4, p. 33-36.

Heuser, A., Eisenhauer, A., Gussone, N., Bock, B., Hansen, B.T., and Nägler, T.F., 2002, Measurement of calcium isotopes (d44Ca) using a multicollector TIMS technique: INTERNATIONAL JOURNAL OF MASS SPECTROMETRY, v. 220, p. 387-399.

Reeder, R.J., 1983, Crystal chemistry of the rhombohedral carbonates, *in* R.J., R., ed., Carbonates, Volume 11, p. 1-47.

Sass, A., Rutters, H., Cypionka, H., and Sass, H., 2002, Desulfobulbus mediterraneus sp nov., a sulfate-reducing bacterium growing on mono- and disaccharides: Archives of Microbiology, v. 177, p. 468-474.

Zeebe, R. and Wolf-Gladrow, D., 2001, CO2 in Seawater: Equilibrium, Kinetics, Isotopes. Elsevier Oceanography Series, 65, Amsterdam, pp. 346.

Chapter 3

Enhanced calcite dissolution in the presence of aerobic methanotrophic bacteria

Stefan Krause[1], Giovanni Aloisi[1,2], Volker Liebetrau[1], and Tina Treude[1]

[1]Leibniz Institute of Marine Sciences at Kiel University (IFM-GEOMAR), Department of Marine Biogeochemistry, Wischhofstrasse 1-3, 24148 Kiel, Germany
[2]Laboratoire d'Océanographie et du Climat : Expérimentations et Approches Numériques, UMR 7159, Université Pierre et Marie Curie, 4, Place Jussieu, 75252, Paris, France

ABSTRACT

Marine aerobic methanotrophic bacteria largely contribute to methane (CH_4) removal in oxygenated marine habitats. However, the impact of metabolically produced carbon dioxide (CO_2) and cell-crystal interactions on the dissolution kinetics of carbonates are poorly constrained. The present study investigates dissolution of calcite in the presence of the methanotrophic bacterium *Methylosinus trichosporium* under brackish conditions (salinity 10) near calcite saturation. To discriminate between potential processes relevant for calcite destabilization, four dissolution experiments with calcite crystals were carried out, including the incubation of methanotrophically active cells, dead cells, and cell-free controls under air/CH_4 atmosphere, as well as methanotrophically inactive cells under air/N_2 atmosphere. Compared to cell-free controls, the amount of dissolved calcite markedly increased in all experiments containing *M. trichosporium*. Highest calcite dissolution rates, ranging between 170 (SD 5) and 90 (SD 5) Ca^{2+} µmol l^{-1} d^{-1}, were observed during the first day in experiments containing methanotrophically active and inactive cells, respectively. After this initial phase, dissolution generally decreased with highest rates remaining in experiments containing methanotrophically active and dead cells [31 (SD 9) and 29(SD 7) µmol Ca^{2+} l^{-1} d^{-1}, respectively], while calcite dissolution in experiments with methanotrophically inactive cells diminished [14 (SD 5) mmol Ca^{2+} l^{-1} d^{-1}]. In contrast, calcite dissolution in cell-free controls was not observed. Scanning electron microscopy images of calcite crystals revealed strong surface corrosion after exposure to methanotrophically active *M. trichosporium.*

The results of this study demonstrate a strong potential impact of microbial aerobic oxidation of CH_4 on calcite stability, facilitating dissolution near saturation conditions. In addition to carbonate system alteration via CO_2 production by methanotrophically active cells, interactions between cell walls and crystal surface as well as the release of acidic organic metabolites during cell lyses might also represent relevant mechanisms for enhanced calcite dissolution. Our findings support recent theories, proposing aerobic methane oxidation as a relevant process

leading to corrosion of marine authigenic carbonate deposits at methane seeps.

INTRODUCTION

Today's oceans represent an important methane (CH_4) source, producing approximately 85.3 Tg CH_4 a^{-1} (Reeburgh, 2007). In contrast, annual emission of marine CH_4 into the atmosphere contributes only 1.9% (Reeburgh, 2007), due to biological consumption in sediments (Knittel and Boetius, 2009) and in the water column (Reeburgh, 2007).

Generally, microbial consumption of CH_4 follows two different pathways, anaerobic and aerobic oxidation of methane. Anaerobic oxidation of methane is found in anoxic sediments and water bodies, where CH_4 is oxidized with sulfate by a syntrophic consortium of methanotrophic archaea and sulfate-reducing bacteria (Barnes and Goldberg, 1976; Boetius et al., 2000). Conversely, aerobic oxidation of methane is mediated by a subset of methylotrophic bacteria. Within oxygenated marine environments, this process is widespread (Hanson and Hanson, 1996), encompassing the sediment-water interface and the water column (Hovland et al., 1987). An important implication of aerobic oxidation of methane is the production of carbon dioxide (CO_2), according to the following stoichiometry:

$$CH_4 + 2O_2 \rightarrow CO_2 + 2H_2O \quad (1)$$

In the ocean, CO_2 reacts with water, producing carbonic acid (H_2CO_3), which dissociates into bicarbonate (HCO_3^-) and carbonate (CO_3^{2-}), liberating H^+ ions. Decrease of pH has adverse effects on calcium carbonate ($CaCO_3$) minerals, favoring their dissolution if undersaturation conditions with respect to calcium carbonate are attained.

Although numerous studies have been devoted to constrain carbonate dissolution under aqueous conditions (e. g. Pokrovsky et al., 2009; Berner and Morse, 1974; Archer, 1991), the microbial influence on carbonate dissolution in marine

environments has received little attention (Brewer and Goldman, 1976; Wenzhöfer et al., 2001). Although potentially relevant in the marine realm, so far influence of aerobic methanotrophic bacteria on carbonate dissolution has not been studied in depth.

This study presents results from closed-system experiments quantifying calcite dissolution in the presence of *Methylosinus trichosporium* OB3b, an aerobic methanotrophic bacterium, under brackish conditions (salinity 10). The influence of methanotrophically active and inactive, as well as dead cells and cell-free controls on calcite stability was investigated independently. Our major aims were to identify: (1) the general effect of aerobic oxidation of methane on calcite stability, and (2) the dominant mechanism for calcite dissolution. We were able to demonstrate enhanced calcite dissolution in the presence of *M. trichosporium*, applying a combination of microbiological and geochemical methods. In addition, scanning electron microscopy (SEM) imaging of calcite particles, colonized by *M. trichosporium*, revealed considerable crystal surface corrosion.

MATERIAL AND METHODS

Bacteria strain and culture conditions

Experiments were conducted with *Methylosinus trichosporium* OB3b, a type II methanotroph, donated by I. Bussmann (Biological Institute Helgoland (BAH) of the Alfred Wegener Institute, Germany). For experiments a nitrate mineral salts (NMS) medium (Whittenbury et al., 1970) without phosphate buffer was used to ensure that medium pH was regulated only by the carbonate buffer sytsem.The initial pH of the sterile medium was 6.8. The headspace was gassed with filtered air and high-grade CH_4 in a ratio of 1, to an excess pressure of 1 bar. Gases were replenished every other day.

Characterization of calcite sample

For dissolution experiments, we used a calcite sample purchased from Rheinisches Mineralien-Kontor, Germany (Catalog no: X00663). All experiments were conducted

with material from one optically homogenous crystal fragment. The calcite was broken with a hammer and subsequently grinded in an agate mortar. Particle size spectra were obtained by Laser particle count analysis (Analysette 22, NanoTec). Specific surface area was calculated using size spectra assuming sphere shaped particles. Crystal size ranged from 0.4 to 970 µm with a geometric surface area of 0.0041 (SD±0.005) $m^2 g^{-1}$. Mass spectrometry analysis (7500 CX, Agilent) revealed that the calcite was 98.7 % pure, with small amounts of Fe^{2+} (0.57 %), Mg^{2+} (0.37 %), S^{2-} (0.31 %), Sr^{2+}(0.053 %) and Cl^- (0.041 %). Additional elements were present in trace concentrations below 0.03 %.

Dissolution experiments with calcite powder

For all experiments, the NMS medium was mixed equally with brackwater medium (Eppelin, 2002) to yield major ion ratios similar to natural seawater. The combined media had the following composition (gl^{-1}): KBr, $4.50x10^{-2}$; KCl, 0.33; $CaCl_2 \cdot 2H_2O$, 0.28; $MgCl_2 \cdot 6H_2O$, 1.55; NaCl, 9.3; $CuCl_2 \cdot 2H_2O$, $5.01x10^{-4}$; KNO_3, 0.5; $MgSO_4 \cdot 6H2O$, 0.542; FeDTA, $6.86x10^{-6}$; HCl, $1.82x10^{-3}$; $FeCl_2 \cdot 4H_2O$, 9.94 $x10^{-4}$; $ZnCl_2$, $6.81x10^{-5}$; $MnCl_2 \cdot 2H_2O$, 8.09 $x10^{-5}$; H_3BO_3, $6.18x10^{-6}$; $CoCl_2 \cdot 6H_2O$, 1.19 $x10^{-4}$; $CuCl_2 \cdot 2H_2O$, $1.35x10^{-6}$; $NiCl_2 \cdot 6H_2O$, $2.38x10^{-5}$; $Na_2MoO_4 \cdot 2H_2O$, $3.63x10^{-5}$; $NaHCO_3$, 0.12., The salinity of the experimental medium was 10.

Four independent incubation experiments were carried out to investigate calcite dissolution in the presence of *M. trichosporium*. Experiments included three replicates with either methanotrophically active (with CH_4), inactive (without CH_4), or sterilized cells (with CH_4) as well as cell-free controls (with CH_4). Incubations were carried out in 12 sterile 500 ml Duran glass bottles with gas tight butyl stoppers and screw caps. Prior to experiments, 3 grams of calcite powder were transferred into each vessel and autoclaved with 5 ml NMS-brackwater medium for 20 minutes. After cooling to room temperature, 245 ml of sterile NMS-brackwater medium were added to each bottle. The headspace was aerated with sterile atmospheric air for 10 minutes. High-grade purity CH_4 was added to nine bottles to 1 bar excess pressure, giving a headspace air/CH_4 ratio of 1. To the remaining three bottles high purity grade N_2 (in alternative to CH_4) was added to 1 bar excess pressure, giving a

headspace air/N_2 ratio of 1. All vessels were shaked at 50 RPM on a rotary shaker in the dark for 8 days and inverted every other day. All preparations and experiments were carried out at 22 °C (room temperature).

For each replicate containing live cells, *M. trichosporium* from growth culture was carefully filtered to prevent aged medium from entering the reaction vessles (Whatman PC 25 mm 0.2 µm) and re-suspended in 5 ml sterile NMS-brackwater medium under sterile atmospheric conditions for 30 minutes shortly before the inoculation. Accordingly, 5 ml of sterile medium were exposed to atmosphere for each replicate of cell-free controls. To prepare experiments with dead cells, 5 ml medium with *M. trichosporium* per replicate (after filtration and re-suspension, see above) were sterilized by exposure to UV-light for 30 min. Light microscopy of sterilized cells stained with LIVE/DEAD BacLight™ after UV-treatment confirmed 100% cell mortality. The 5 ml medium containing either live, dead or no cells was finally injected into the respective experimental vessels using sterile syringes: live and dead cells were added separately to vessels with air/CH_4 in headspace (hereafter referred to as experiment "Live/CH_4 "and experiment "Dead/CH_4") (Table 1). Additionally, live cells were added to vessels with air/N_2 headspace (hereafter referred to as experiment "Live/N_2"). Cell-free control vessels with air/CH_4 in headspace were added with 5 ml sterile medium (hereafter referred to as "cell-free control").

Table 1. Overview of experimental setups. Each experiment was carried out in triplicates.

Experiment	**Setup**
Live/CH_4	Live cells + calcite powder + Air/CH_4 headspace
Dead/CH_4	Dead cells + calcite powder + Air/CH_4 headspace
Live /N_2	Live cells + calcite powder + Air/N_2 headspace
Cell-free control	No cells + calcite powder + Air/CH_4headspace

All vessels were kept on a rotary shaker at 50 RPM in the dark. Shaking was adjusted to circulate the liquid, without suspending the calcite powder. The vessels were

inverted carefully once per day to grant microbial access to all crystals. Repeated sampling of experimental liquid and headspace was carried out for monitoring temporal developments of cell numbers, pH, total alkalinity and calcium concentration. For each sampling, 3 ml aliquots were subtracted from the mixed liquid containing crystals with an air-tight sterile syringe. A pH electrode was attached to the syringe for instant liquid pH recording. After pH reading (see 2.3.1), the aliquot was centrifuged at 14.000 x g for 5 min at 22°C. The clear supernatant was subdivided for total alkalinity and Ca^{2+} concentration measurements (see 2.3.2 and 2.3.3, respectively). 200 µl of headspace gas was sampled for measurements of CH_4 concentrations using a glass syringe (see 2.3.4). The experiments were carried out for 35 days, during which the experiment vessels remained sealed.

pH measurements

pH of the mixed liquid was determined *in-situ*, under in the respective vessel's atmosphere and pressure, using a pH sensor (WTW pH 3210) tightly mounted to a syringe. Calibration of the pH-meter was carried out using reference buffer solutions according to PTB and NIST (Schott Instruments, L 4794, L 4796, L 4799).

Total Alkalinity titration

For total alkalinity (TA) determination, 0.5 ml of centrifuged liquid (see above) was titrated visually with 0.01 M HCl using a titration vessel after G. Pavlova and a MetromTitrino plus titration unit. A Methyl Red/Methylen Blue solution with the following composition was used as indicator: sodium salt of Methyl Red (37 mg) was mixed with 1.19 ml of 0.1 M NaOH and dissolved in 80 ml Ethanol (96%) (solution 1). Methylene Blue (10 mg) was dissolved in 10 ml Ethanol (96%) (solution 2). Both solutions were mixed (80 ml of solution 1 and 4.8 ml of solution 2) to obtain a greenish-brown product.

Calcium concentration measurement

Calcium (Ca^{2+}) concentrations were determined using Inductively Coupled Plasma Optical Emission Spectrometry (ICP-OES Varian 720-ES). For ICP-OES, 0.5 ml of

centrifuged aliquots was transferred into 500 µl Eppendorf vials and acidified with 5 µl of HNO_3 (Suprapure, 65%).

Methane measurements

Methane concentration of the headspace was determined by gas chromatography. Therefore, 100 µl headspace gas sample was injected into a 5890A Hewlett Packard, equipped with a 6FT Poropak Q stainless steel column and a flame ionization detector. Combustion gases were synthetic air (300 ml min^{-1}) and Hydrogen (H_2 generator PG H2 100; Schmidlin; 30 ml min^{-1}). Helium (30 ml min^{-1}) was used as carrier gas. The column temperature was 50 °C.

Cell counts

For cell counts, 50µl of liquid with suspended cells was stained with 4',6-Diamidin-2-phenylindol (DAPI) (1 µg ml^{-1}) for 20 minutes at room temperature, and in the dark. Subsequently, the solution was filtered (Whatman PC 25 mm 0.2 µm) with 10 ml of sterile phosphate buffered saline (PBS). Cells counts on filters were carried out with a Leitz Aristoplan epifluorescence microscope in random rectangular grids of 0.0121 mm^2. Enumeration was continued until > 800 cells per filter were viewed.

Dissolution experiments with large calcite crystals

In a separate experiment, we investigated the colonization and bacterial-induced erosion of calcite crystals in setups with and without *M. trichosporium* in the presence of methane. Before incubation, crystals were autoclaved in 20 ml of NMS-brackwater medium for 20 minutes. Five large calcite fragments (approx. 5x5x3 mm each) were placed at the bottom of 250 ml sterile serum vials for each of the two replicates. 100 ml of sterile NMS-brackwater medium were added. Setups containing *M. trichosporium* were inoculated with 1 ml of filtered *M. trichosporium* enrichment culture ($2x10^{-7}$ cells ml^{-1}), which was re-suspended in 1 ml sterile NMS-brackwater medium. After sealing the serum vials with rubber stoppers the headspace was aerated with filtered air for 10 minutes, followed by addition of high-grade purity methane to an excess pressure of 1 bar resulting in an air:CH_4 micture

of 1:1. Cell-free controls were prepared identically. Instead of enrichment culture, 1 ml of sterile medium was added. Vials were kept in the dark at room temperature (22 °C) without shaking for 56 days. Headspace gases were replenished weekly. After each gas renewal, the medium was gently mixed, avoiding crystal movement.

Scanning Electron Microscopy (SEM) analysis

After 56 days, the crystals were recovered and prepared for SEM analysis according to the following procedures. For surface imaging, crystals were rinsed with 70% ethanol twice to remove bacteria. Crystals from cell-free controls were treated in the same manner. After air-drying, samples were mounted on aluminum stubs. Crystals used for imaging of bacterial colonization were placed in Karnovsky's fixative (2.5 % glutaraldehyde, 2 % paraformaldehyde in 0.1 M sodium cacodylate buffer, pH 7.5) for 30 minutes. After fixation, crystals were washed twice in 0.1 M cacodylate buffer for 15 minutes. Post-fixation was done with 1 % osmium tetroxide in cacodylate buffer (pH 7.5) for 20 minutes. Subsequently, samples were washed twice in ultra-purified water and dehydrated in a 4-step ethanol series (50, 70, 90, and 100 % solution). For each concentration, an immersion time of 10 min was applied. Dehydration in 100 % ethanol was repeated three times.. Samples were then dried at temperature above the critical point of CO_2 (31°C at 73.8 bar). Reference crystals, not exposed to medium, were prepared accordingly and kept dry under sterile conditions. Finally, all crystals were mounted on aluminum stubs and stored in a dessicator. Prior to SEM analysis, all samples were gold sputter coated for 60 s at 50 mA. SEM was carried out using a Zeiss DSM 940. Digital images were captured using Orion 6.0 Digital Image Acquisition System.

Calculations

Total Alkalinity (TA) and calcite dissolution

The definition for Total Alkalinity in seawater by (Dickson, 1981) includes several contributing ions:

$$TA = [HCO_3^-] + 2[CO_3^{2-}] + [B(OH)_4^-] + [OH^-] + [HPO_4^{2-}] + 2[PO_4^{3-}] + [H_3SiO_4^-] + [NH_3] + [HS^-] - [H^+] - [HF] - [H_3PO_4] \quad (2)$$

As the liquid medium used in our experiments lacked most of the contributors, the formula was simplified to:

$$TA = [HCO_3^-] + 2[CO_3^{2-}] + [OH^-] - [H^+], \quad (3)$$

including the sum of carbonate alkalinity and water alkalinity as a suitable approximation for TA.

The dissolution and precipitation of calcite can be written as follows, accounting for carbonic acid system components:

$$CaCO_3 + H_2O + CO_2 \leftrightarrow Ca^{2+} + 2HCO_3^- \quad (4)$$

Considering equation 3 and 4, dissolution of 1 mole calcite produces 2 moles of TA. Therefore, the calcite dissolution rate can be derived from temporal change of TA according to:

$$R_{calcite\ dissolution} = \frac{1}{2}\left(\frac{dTA}{dt}\right) \quad (5)$$

Carbonate system and saturation state calculation

The concentration of CO_3^{2-} ions were calculated from the pH and total alkalinity (TA) of the solutions according to the following set of equations (Zeebe and Wolf-Gladow, 2001). Stoichiometric constants (*) where calculated for salinity = 10 and temp. = 22°C:

$$[CO_2] = \left(TA - \frac{K_B^* B_T}{K_B^* + h} - \frac{K_W^*}{h} + h\right) / \left(\frac{K_1^*}{h} + 2\frac{K_1^* K_2^*}{h^2}\right) \quad (6)$$

$$DIC = [CO_2]\left(1 + \frac{K_1^*}{h} + \frac{K_1^* K_2^*}{h^2}\right) \quad (7)$$

$$[CO_3^{2-}] = DIC / \left(1 + \frac{h}{K_2^*} + \frac{h^2}{K_1^* K_2^*}\right) \quad (8)$$

where $[CO_2]$ is the concentration of dissolved CO_2 including carbonic acid, DIC is dissolved inorganic carbon, TA is total alkalinity, K_B^* is equilibrium constant of boric acid, B_T is total dissolved boron. K_w^* is the ion product of water, K_1^* and K_2^* are the first and second acidity constants of carbonic acid, h is the concentration of H^+ ions.

The saturation state of a solution with respect to calcite indicates whether this mineral tends to precipitate (Ω>1) or dissolve (Ω<1). It is expressed as:

$$\Omega = \frac{\left[Ca^{2+}\right]\left[CO_3^{2-}\right]}{K_{sp}^{*}} \quad (9)$$

Where Ksp^{*} is the stoichiometric solubility product constant of calcite in seawater, calculated for salinity = 10 at 22°C (Mucci, 1983).

RESULTS

Closed system experiments

Bacterial growth

Initial cell density was similar in all three bacteria experiments (approximately $1x10^7$ cells ml^{-1}) (Fig. 1, A). In Exp. Live/CH_4, methanotrophically active cells doubled within the first 10 days, followed by stable cell density, indicating stationary cell growth conditions. Cell density in Exp. Live/N_2 remained stable at approximately 1 $x10^7$ cells ml^{-1} during the entire experiment. In contrast, sterilized cells of Exp. Dead/CH_4 showed a decline in cell density by one third during the first 3 days, after which density stabilized.

Temporal changes of CH_4, pH, total alkalinity, Ca^{2+} and calcite saturation state

In Exp. Live/CH_4, average headspace methane concentration decreased by 17% [3.4 $mmol^{-1}$ (SD 0.2)] during the first 20 days, indicating methane consumption by the bacteria. After 20 days, concentrations remained stable until experiment termination (35 days) (Fig. 1, B). In Exp. Dead/CH_4 and cell-free control headspace CH_4 concentrations fluctuated between 7-9% possibly due to gas chromatography accuracy limit, but generally remained close to initial concentrations.
Initial pH showed variations ranging from 8.05 (cell-free control) to 7.98 (Live/CH_4), A decrease of pH (0.03-0.08 units) was observed in experiments containing live or dead *M. trichosporium* during the first day (Fig. 1, C), while pH remained stable in

cell-free control. Between day 1 and 20 strongest pH decline of ~0.18 units was observed in Exp. Live/CH_4. In Exp. Dead/ CH_4 pH also changed considerably (~0.15), although to a lesser extent. . A smaller decline, of ~0.60 pH units, was observed in Exp. Live/N_2. Cell-free controls also showed a pH decline of 0.03 units. After day 20, pH variations in all setups were < 0.02 units.

In all experiments containing live or dead *M. trichosporium,* total alkalinity increased markedly from their starting value close to 1.6 mEq l^{-1} (Fig. 1, D). Similar to pH, a the fastest increase of TA occurred in these three experiments during the first day. Subsequently, strongest TA increase continued in Exp. Live/CH_4 and Dead/CH_4 reaching maximum values of 2.6 (SD 0.06) and 2.5 (SD 0.04) mEq l^{-1}, after 13 and 9 days, respectively. After reaching maximum, TA stabilized for the rest of the experiment. Also in Exp. Live/N_2 fastest increase of TA occurred during the first day. The maximum concentration of 2.1 mEq l^{-1} (SD ± 0.02) was reached after 9 days, thereafter stabilizing between 2 and 2.1 1 mEq l^{-1}. Total alkalinity of cell-free control increased only gradually and very slowly by 0.1 mEq l^{-1} (SD ± 0.02) over the course of the complete experiment to a maximum concentration of 1.68 (SD 0.02) mEq l^{-1}.

Initial concentration of dissolved Ca^{2+} was similar in all four experiments, with values around 2.2 mmol l^{-1} (Fig. 1, E). While Ca^{2+}concentrations remained stable in cell-free controls over the entire experiment, pronounced Ca^{2+} increase was observed during the first 10 days in all experiments containing live or dead *M. trichosporium*. Subsequently, concentrations stabilized until experiment termination. Highest increase of dissolved Ca^{2+} was observed in Exp. Live/CH_4 and Dead/CH_4, reaching maxima of 2.77 (SD 0.005) and 2.68 (SD 0.004) mmol l^{-1}, respectively. In accordance with TA, increase of Ca^{2+} was lower in Exp. Live/N_2, with final concentrations of 2.52 (SD 0.004) mmol l^{-1} towards the end of incubation period.

The development of the calcite saturation state (Ω) showed initial supersaturation in all experiments containing live or dead *M. trichosporium* (Ω $1.48 - 1.58$) (Fig. 1, F). In accordance with pH, TA and Ca^{2+} concentrations, Ω increased during the first 10 days of these experiments.

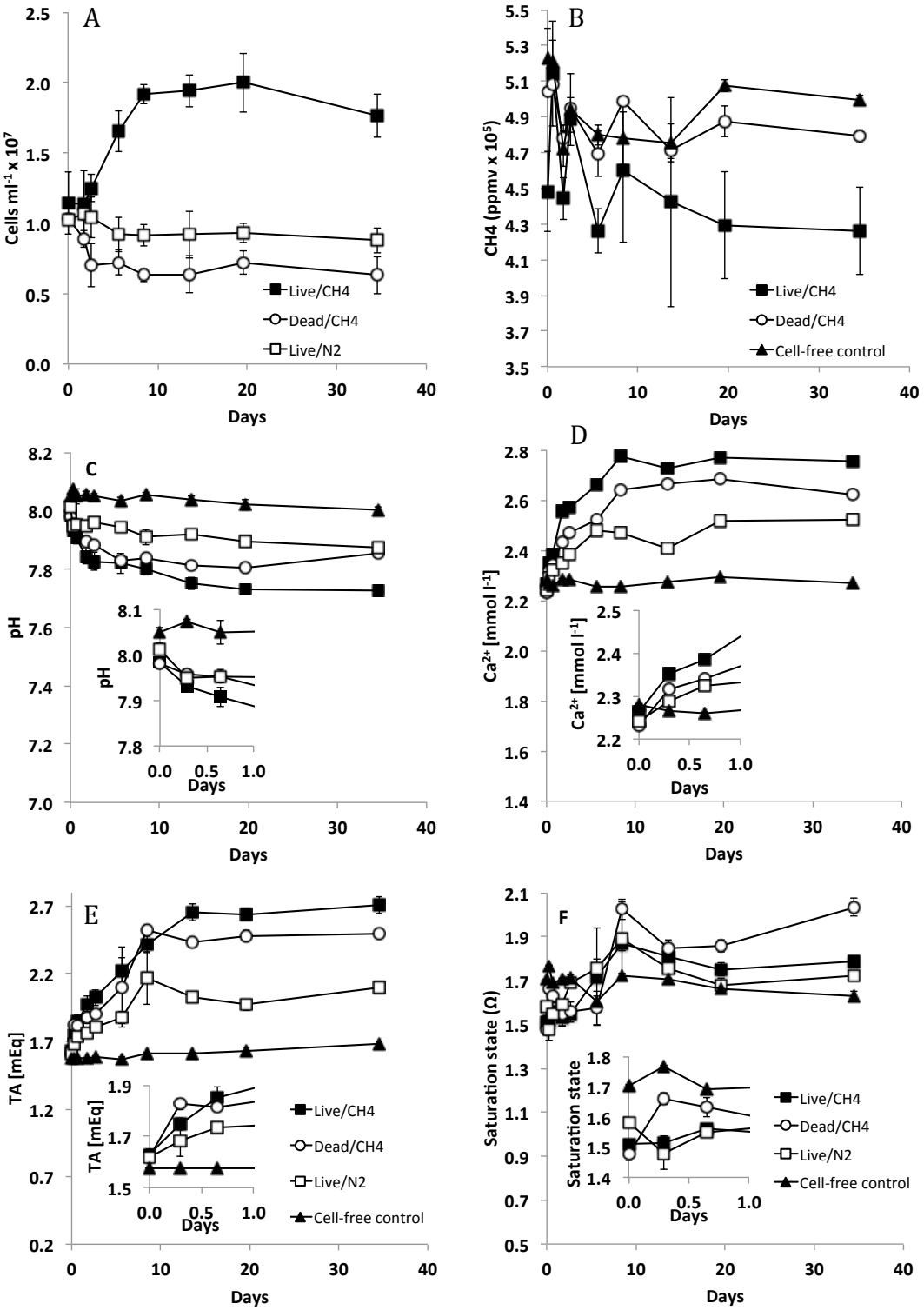

Figure 1. Temporal development of cell concentration (A), CH_4 consumption (B), pH (C), total alkalinity (D), Ca^{2+} concentration (E), and saturation state (F). Error bars represent standard deviations of three replicates.

Highest increases in saturation state were observed for Exp. Dead/CH_4 [Ω = 2.03 (SD 0.03)] and Exp. Live/N_2 [Ω = 1.89 (SD 1.70)]. Calcite saturation state in Exp. Live/CH_4 increased to a maximum value of 1.87 (SD 0.05) after 10 days. The corresponding Ω of the cell-free controls was slightly higher than observed for experiments containing live or dead *M. trichosporium* (Initial Ω = 1.71), due to the highest initial pH (8.05), and varied within 0.1 units during the course of the entire experiment.

Calcite dissolution rates

The calcite dissolution rates (R) during the initial phase of the experiments (0-0.65 days) were calculated from the increase of total alkalinity (Table 3). Dissolution rates after 0.65 days were calculated for the individual time period of TA increase in the experiments (Exp. Live/CH_4, 14 days; Exp. Dead/CH_4 and Exp. Live/N_2, 8.5 days). Thereafter, values remained generally stable.

During the initial phase (0-0.65 days) calcite dissolution rates of the experiments showed variations from 17-50%. Calcite dissolution rate was highest in Exp. Live/CH_4 [R=0.17 (SD ± 0.009)], while Exp. Live/N_2 showed the lowest rate [R=0.09 (SD ± 0.005)]. In in the subsequent phase (until 14 days) calcite dissolution rates were generally 5-6 times lower experiments containing live or dead *M. trichosporium*. Different to experiments containing *M. trichosporium*, calcite dissolution was not observed in cell-free controls over the entire course of the experiment. In Exp. Live/CH_4 the ratio between methane consumption and calcite dissolution was 6.85 (SD 0.06).

Table 3. Calcite dissolution rates (R) of the different experiments, calculated for the initial (0-0.65 days) and second (0.65- 14 days) phase of the experiment. * R and *k* for cell-free controls were calculated for the entire course of the experiment (35 days). Note: The calculated values of SD undercut the method error of 5%. Therefore SD is given as 5% variation.

	0 - 0.65 days R (mmol l^{-1} d^{-1})	0.65 - 14 days R (mmol l^{-1} d^{-1})
Live/CH_4	0.17 (SD ± 0.009)	0.031 (SD ± 0.009)
Dead/CH_4	0.14 (SD ± 0.007)	0.028 (SD ± 0.007)
Live/N_2	0.09 (SD ± 0.005)	0.014 (SD ± 0.005)

According to $CaCO_3$ stoichiometry, calcite dissolution results in a TA/Ca ratio increase of 2 (Table 2). Exp. Live/CH_4 and Dead/CH_4 followed the theoretical stoichiometry, while the ratio observed in Exp. Live/N_2 was slightly lower (1.62). However, numerous studies report strong binding of Ca^{2+} to microbial cell walls and metabolites (e. g. Dupraz et al., 2004; Heinzmann and Hunziker, 1991). To avoid false calculations, all rates were therefore calculated from temporal TA increase.

Table 2. Ratio between total alkalinity (TA) and Ca^{2+} in dissolution experiments including *M. trichosporium* calculated for the entire course of the experiment (35 days). No ratio was calculated for cell-free controls, because changes in Ca^{2+} concentrations were lower than method accuracy (5%).

Experiment	Ratio TA/Ca^{2+}
Live/CH_4	1.99
Dead/CH_4	2.06
Live/N_2	1.62

SEM Analyses of large carbonate crystals

Scanning electron microscopy (SEM) analysis was applied to surfaces of large carbonate crystals after 56 days of incubation with methanotrophically active cells of *M. trichosporium*. Crystals immersed in cell-free medium served as controls. Additionally, crystals, which were not subjected to medium at all, were imaged as a

reference for pristine initial surface conditions. Microscopic analysis of reference crystals revealed plain surfaces with clear steps between lattice layers (Fig. 2 a,b). Crystal breaks were always distinct including sharp cleavages and conchate steps. Edge pits or degraded areas could not be identified. However, natural cavities of varying shape and size were present, presumably formed during crystal formation.

Calcite crystals incubated in sterile medium (controls) revealed no sign of surface alteration after 8 weeks compared to references (Fig. 2. c, d). Plain surface areas showed an even topography, interrupted by clear steps in the crystal lattice, which appeared to be smooth and well defined. Similar to the reference material, irregularly shaped natural cavities were visible. The surface of crystals incubated with active *M. trichosporium* was covered by a biofilm consisting of multiple cell layers (Fig. 3 a, b). After cell removal, crystal surfaces displayed characteristic features, indicative for dissolution (Fig. 3. c-f). These features included irregular erosion forming knolls with hooknose tops at plain surfaces. Additionally, strongly corroded areas were frequently associated with numerous irregular trenches (Fig. 3. e). Breaks in the lattice layers did not appear as conchate structures, but showed clear signs of dissolution, visible as multiple layers with triangular edges of varying size Fig. 3. f). Additionally, surfaces with hump-like irregularities were present area-wide.

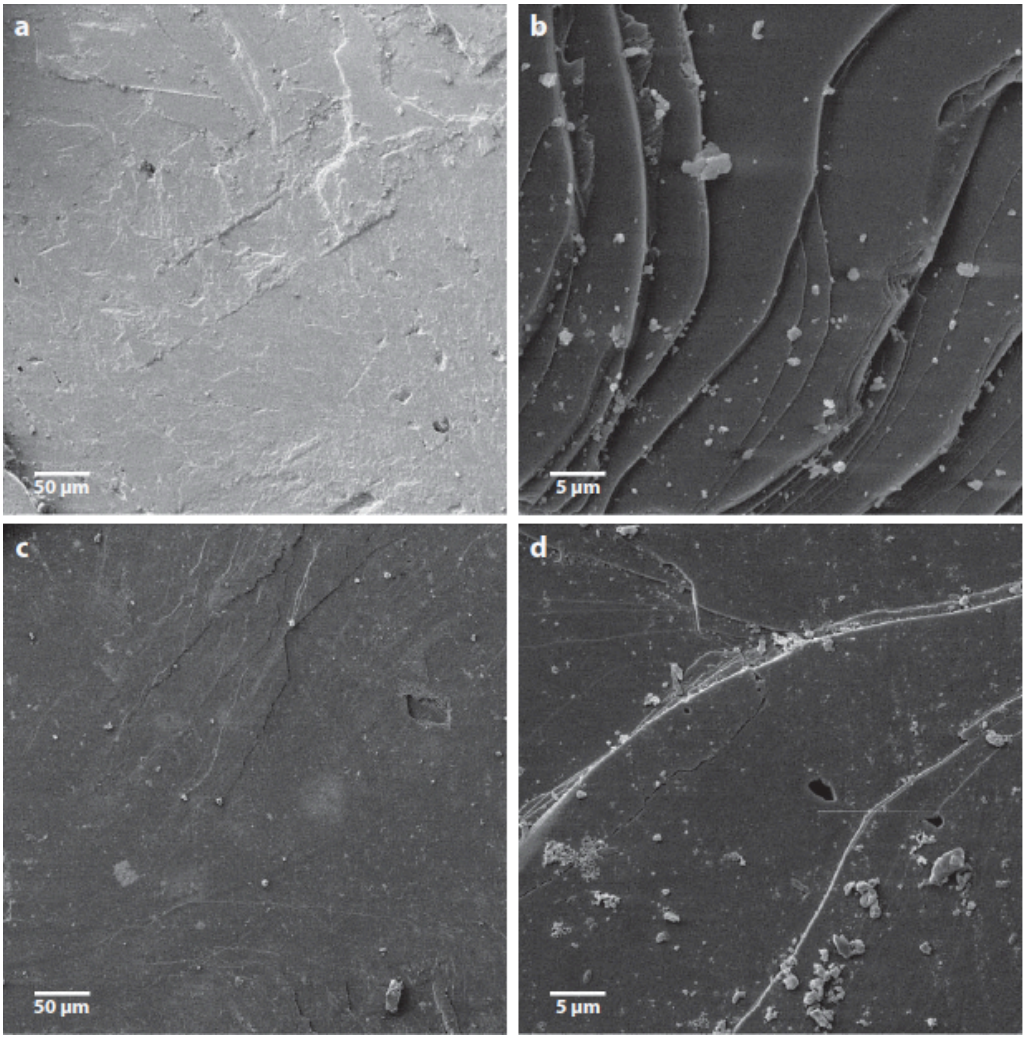

Figure 2: SEM micrographs of calcite crystal surfaces: Reference (a, b), Crystals immersed without bacteria for 56 days (c, d); No obvious signs of surface dissolution were evident in both samples (see text); a & c: Magnification 200x, acceleration voltage 4.0 and 10 kV, working distance 5 mm; b & d: Magnification 2000x, acceleration voltage 15.0 and 10 kV, working distance 10 mm and 5 mm. Scale bars are given.

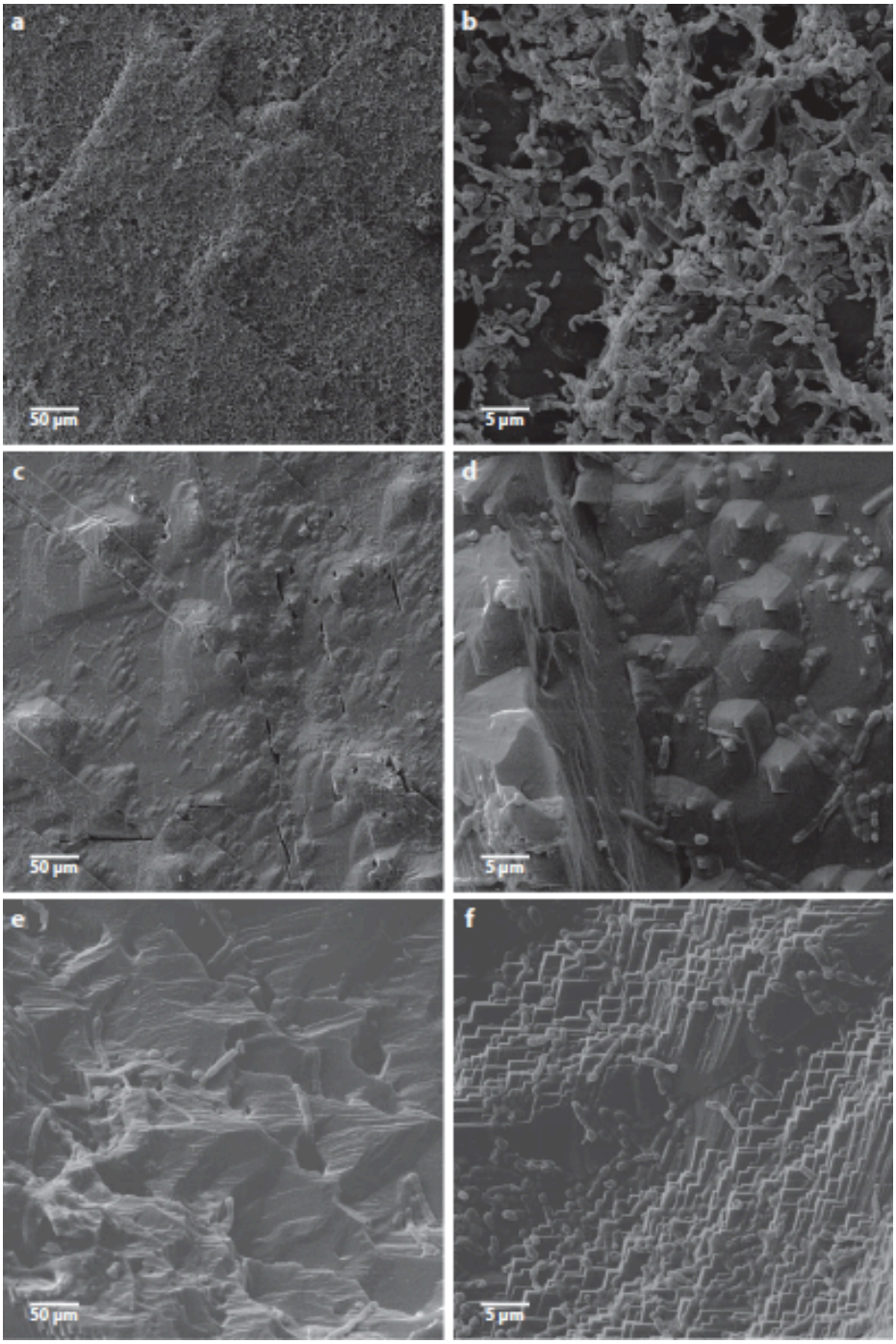

Figure 3: SEM micrographs of calcite crystals exposed to methanotrophically active *M. trichosporium* cells for 56 days. Crystal surfaces densely covered by a biofilm of *M. trichosporium* (a, b), Surface topography after biofilm removal (c-f); Dissolution features included knolls with hooknose tops (c, d), altered surface with trenches (e), and irregular layer steps (f); a, c & e: Magnification 200x, acceleration voltage 4.0 and 10 kV, working distance 5 mm; b, d & f: Magnification 2000x, acceleration voltage 15.0 and 10 kV, working distance 10 mm and 5 mm. Scale bars are given.

DISCUSSION

Our laboratory experiments were carried out under simplified conditions and thus resemble natural field-scale situations only to a limited extend, which should be kept in mind for the interpretation of the data. However, the present study provides a basic understanding of the potential effects of aerobic methanotrophic bacteria on the stability of calcite near saturation under saline conditions.

Microbial calcite dissolution

The experiments carried out clearly showed that the presence of active, inactive, and dead *M. trichosporium* cells caused increase of calcium ion concentration and total alkalinity in the liquid phase, compared to cell-free controls. The increase of calcium and total alkalinity followed a linear relationship, indicative for calcite dissolution. Highest calcite dissolution rates were observed for metabolically active cells (Exp. Live/CH_4). Dead cells (Exp. Dead/CH_4) caused generally higher dissolution rates than methanotrophically inactive ones (Exp. Live/N_2). Calcite dissolution rates during the initial period of the experiments (0-0.65 days) were similar between the three setups including bacteria (0.09 (SD 0.005) to 0.17 (SD 0.009). As dissolution was not observed in cell-free controls, we assume that bacteria-related processes were causative for this phenomenon.

About the mechanisms for dissolution in Exp. Dead/CH_4 and Live/N_2 we can only speculate. However, a possible explanation for the initial dissolution effect could be interactions between the functional groups of cell walls with the surface of calcite crystals. Friis et al. (2003) showed that calcite dissolution was enhanced after the addition of cell wall material from *Bacillus subtilis*. Microbial cell walls include a variety of organic functional groups, predominantly carboxylic, phosphonic, and hydroxyl groups (Beveridge, 1981). These functional groups bind cations, as calcium, in solution (Daughney and Fein, 1998; Morita, 1980). This binding capability for calcium might cause a local decrease of the carbonate saturation state at the surface of calcite crystals, resulting in enhanced dissolution. Direct interactions between cell

walls and crystal surfaces are considered as local phenomena restricted to the vicinity of the cell (Lüttge and Conrad, 2004), causing interference with etch pit development and excavation of carbonate material at the cell–mineral interface during attachment to the mineral surface (Davis et al., 2007). These mechanisms might have been primarily responsible for calcite dissolution in Exp. Live/N_2, including methanotrophically inactive cells.

Calcite dissolution of methanotrophically active cells (Exp. Live/CH_4) during the initial phase was probably the combined result of metabolic CO_2 production and cell-crystal surface interaction (see above). While calcite dissolution induced by CO_2 production is largely dependent on the concentrations of available O_2 and CH_4, dissolution mediated by cell wall components might be dependent on the saturation of functional groups with Ca^{2+} ions (Fredd and Folger, 1998). The latter process probably reached a saturation level at the end of the initial phase, resulting in a decrease of dissolution rates in all experiments containing live or dead *M. trichosporium* cells.

Subsequent to the initial day, dissolution rates generally declined by a factor of 5-7 in all bacteria bearing experiments. Interestingly, in our experiments dead cells (Exp. Dead/CH_4) showed a 2-fold higher dissolution rate of calcite than methanotrophically inactive ones (Exp. Live/N_2). Given the fact that the abundance of dead cells decreased by approximately 40% during the first 9 days, we assume that most of these cells were lost due to cell lysis. Cell lyses causes a considerable release of organic acids, ligands, and redox-active metabolites (Rosso et al., 2003). These organic components might have caused pH decrease in the medium and extensive binding of dissolved Ca^{2+} ions, contributing to calcite dissolution in addition to the above-mentioned interactions between cell walls and crystals. In addition, laboratory experiments have shown that the enzyme carbonic anhydrase, which is wide spread in nature, induces strong carbonate dissolution in aquatic environments (Liu, 2001). In seawater, dissolved organic substances interact with carbonate mineral surfaces, forming organo-carbonate associations (Suess, 1970), influencing equilibrium reaction rates with carbonate system components of the surrounding seawater. Due to the methane consumption, observed in Exp. Live/CH_4,

it can be assumed that microbial CO_2 production from aerobic oxidation of methane, leading to liquid acidification, was a relevant process for calcite dissolution in this setup.

In our experiments the saturation state for calcite always exceeded the threshold of 1, indicating supersaturation at all times. Consequently, calcite should have precipitated, instead of being dissolved. Although great care was taken to prevent equilibration between liquid and atmosphere, minor loss of CO_2 during pH measurements cannot be excluded. As a consequence, measured pH and calculated calcite saturation state might have been slightly too high, with regards to the bulk liquid in the reaction vessels. In addition, the contradiction between supersaturated conditions in the bulk liquid and simultaneous calcite dissolution also arises from the common approach to regard the experimental setups as homogenous liquids, which is not the case. Bacteria can create local concentration gradient, differing from bulk fluid, thus dissolving calcite at the immediate environment while surrounded by fluid supersaturated with respect to calcite (Bennett et al., 2000). In addition, also dissolved microbial organic substances, which bind calcium ions in solution, might cause a decrease in saturation state.

Considering the potential mechanisms, which might have caused a shift in pH, it seems rather likely that the calculated saturation state exceeded the actual saturation state of the experimental solutions. Therefore, not the actual values, but the temporal variations should be considered. According to the increasing saturation state in experiments with bacteria during the first 10 days of the incubations, calcite dissolution took mainly place during this time period. This finding is in good correlation with temporal increases of total alkalinity and dissolved calcium ions. As a consequence, the temporal development of the saturation state was still useful to constrain the time period of calcite dissolution in the performed experiments.

Environmental implications of aerobic oxidation of methane

At many marine locations, seepage of methane charged fluids is accompanied by the buildup of massive authigenic carbonate deposits (e. g. Greinert et al., 2001;

Bohrmann et al., 1998). This carbonate formation is mediated by anaerobic oxidation of CH_4, due to an increase in carbonate alkalinity (Ritger et al., 1987; Boetius et al., 2000; Suess, 2002). A recent investigation by Himmler et al. (2011) on secondary porosity of seep-carbonates identified microbial aerobic oxidation of CH_4 as one of the potential reasons for observed corrosion. Our studies support this hypothesis, documenting pronounced microbially mediated calcite dissolution by direct microscopy investigations in combination with dissolution experiments. For carbonates from the Amsterdam and Athina mud volcanoes (eastern Mediterranean Sea), Himmler et al. (2011) calculated an approximate loss of at least 10 vol.% caused by dissolution. In comparison, in our study approximately 0.4 % of calcite was dissolved after 35 days in incubations with active aerobic methanotrophs . As secondary porosity of seep-carbonates has been reported for a variety of locations (e.g. Teichert et al., 2005; Matsumoto, 1990; Han et al., 2004), it can be speculated that aerobic oxidation of methane might have considerable influence on carbonate stability and carbon flux, especially during periods of increasing temperature, which might induce gas hydrate destabilization and increased methane fluxes from the seafloor (Jiang et al., 2006). Also in the context of recent global warming, potentially causing gas hydrate instability, aerobic oxidation of methane might represent a relevant process affecting marine pH and carbonate stability (Biastoch et al., 2011).

Conclusion

The present study demonstrated enhanced dissolution of calcite in the presence of the aerobic methanotrophic bacterium *M. trichosporium*. Despite metabolically induced acidification during methane oxidation, dissolution was also observed when cells were methanotrophically inactive or dead. Therefore, interactions between cell and crystal surfaces might have considerable influence on dissolution kinetics. Additionally, potential liberation of organic acids after cell lysis appeared to have a pronounced influence on carbonate stability, inducing enhanced dissolution. Our studies strengthen the recently formulated hypothesis by Himmler et al. (2011), assigning aerobic methane oxidation as a possible reason for observed corrosion of natural authigenic carbonates at methane seeps.

ACKNOWLEDGEMENT

The authors would like to acknowledge A. Bleyer, B. Domeyer, A. Kolevica, M. Dibbern, R. Surberg, and J. Hommer for technical assistance during sample analyses. We thank A. Freund for his support in the particle analyses. We gratefully acknowledge the Central Microscopy Laboratory of the Christian-Albrechts-University (Kiel, Germany) for providing instrumentations as well as the help of M. Mulisch during SEM imaging. This is a publication of the Cluster of Excellence "The Future Ocean" funded by the German Research Foundation (DFG).

REFERENCES CITED

Archer, D., 1991, Modeling the Calcite Lysocline: Journal of Geophysical Research-Oceans, v. 96, no. C9, p. 17037-17050.

Barnes, R.O., and Goldberg, E.D., 1976, Methane Production and Consumption in Anoxic Marine-Sediments: Geology, v. 4, no. 5, p. 297-300.

Bennet, P., Rogers, J., Choi, W., 2001, Silicates, silicate weathering, and microbial ecology, Geochemical Journal, v. 18, no. 1, p. 3-19.

Berner, R.A., and Morse, J.W., 1974, Dissolution kinetics of calcium carbonate in sea water IV. Theory of calcite dissolution: American Journal of Science, v. 274, p. 108-134.

Beveridge, T.J., 1981, Ultrastructure, chemistry and function of the bacterial wall: International Review of Cytology, v. 147, p. 229-317.

Biastoch, A., Treude, T., Rüpke, L.H., Riebesell, U., Roth, C., Burwicz, E.B., Park, W., Latif, M., Böning, C.W., Madec, G., and Wallmann, K., 2011, Rising Arctic Ocean temperatures cause gas hydrate destabilization and ocean acidification: Geophysical Research Letters, v. 38, no. 8, p. 1-5, doi: 10.1029/2011GL047222.

Boetius, A., Ravenschlag, K., Schubert, C.J., Rickert, D., Widdel, F., Gieseke, A., Amann, R., Jorgensen, B.B., Witte, U., and Pfannkuche, O., 2000, A marine microbial consortium apparently mediating anaerobic oxidation of methane: Nature, v. 407, no. 6804, p. 623-626.

Bohrmann, G., Greinert, J., Suess, E., and Torres, M., 1998, Authigenic carbonates from the Cascadia subduction zone and their relation to gas hydrate stability: Geology, v. 26, no. 7, p. 647-650, doi: 10.1130/0091-7613(1998)026<0647:ACFTCS>2.3.CO;2.

Brewer, P.G., and Goldman, J.C., 1976, Alkalinity Changes Generated by Phytoplankton Growth: Limnology and Oceanography, v. 21, no. 1, p. 108-117.

Daughney, C.J., and Fein, J.B., 1998, The effect of ionic strength on the adsorption of H+, Cd2+, Pb2+ and Cu2+ by Bacillus subtilis and Bacillus licheniformis: a surface complexation model: Journal of Colloid Interface Science, v. 198, p. 53-77.

Davis, K.J., Nealson, K.H., and Lüttge, A., 2007, Calcite and dolomite dissolution rates in the context of microbe-mineral surface interactions: Geobiology, v. 5, no. 2, p. 191-205.

Dickson, A.G., 1981, An Exact Definition of Total Alkalinity and a Procedure for the Estimation of Alkalinity and Total Inorganic Carbon from Titration Data: Deep-Sea Research Part a-Oceanographic Research Papers, v. 28, no. 6, p. 609-623.

Dupraz, C., Visscher, P.T., Baumgartner, L.K., and Reid, R.P., 2004, Microbe-mineral interactions: early carbonate precipitation in a hypersaline lake (Eleuthera Island, Bahamas): Sedimentology, v. 51, no. 4, p. 745-765.

Eppelin, A., 2002, Charakterisierung aerob methanoxidierender Mikroorganismen an marinen Standorten:.

Fredd, C.N., and Folger, H.S., 1998, The Influence of Chelating Agents on the Kinetics of Calcite Dissolution: Journal of Colloid and Interface Science, v. 204, no. 1, p. 187-197.

Friis, A.K., Davis, T.A., Figueira, M.M., Paquette, J., and Mucci, A., 2003, Influence of Bacillus subtilis cell walls and EDTA on calcite dissolution rates and crystal surface features: Environmental Science & Technology, v. 37, no. 11, p. 2376-2382.

Greinert, J., Bohrmann, G., and Suess, E., 2001, Gas hydrate-associated carbonates and methane-venting at Hydrate Ridge (Cascadia): Their classification, distribution and origin.: Paull CK and Dillon WP (eds): Natural Gas Hydrates: Occurence, Distribution, and Detection. AGU Monograph 124,, p. 99-113.

Han, X., Suess, E., Sahling, H., and Wallmann, K., 2004, Fluid venting activity on the Costa Rica margin: new results from authigenic carbonates: International Journal of Earth Sciences,, p. 596-611, doi: 10.1007/s00531-004-0402-y.

Hanson, R.S., and Hanson, T.E., 1996, Methanotrophic bacteria: Microbiological Reviews, v. 60, no. 2, p. 439-+.

Heinzmann, C.W. and Hunziker, W., 1991, Intracellular calcium-binding proteins: more sites than insights: Trends in Biochemical Sciences, v. 16, p. 98-103.

Himmler, T., Brinkmann, F., Bohrmann, G., and Peckmann, J., 2011, Corrosion patterns of seep-carbonates from the eastern Mediterranean Sea: Terra Nova, v. 23, no. 3, p. 206-212, doi: 10.1111/j.1365-3121.2011.01000.x.

Hovland, M., Talbot, M.R., Qvale, H., Olaussen, S., and Aasberg, L., 1987, METHANE-RELATED CARBONATE CEMENTS IN POCKMARKS OF THE NORTH SEA: Journal of Sedimentary Petrology, v. 57, no. 5, p. 881-892.

Jiang, G.Q., Shi, X.Y., and Zhang, S.H., 2006, Methane seeps, methane hydrate destabilization, and the late Neoproterozoic postglacial cap carbonates: Chinese Science Bulletin, v. 51, no. 10, p. 1152-1173.

Knittel, K., and Boetius, A., 2009, Anaerobic Oxidation of Methane: Progress with an Unknown Process: Annual Review of Microbiology, v. 63, p. 311-334.

Liu, Z., 2001, Role of Carbonic Anhydrase as an Activator in carbonate Rock Dissolution and Its Implications for Atmosphere CO2 Sink: Acta Geologica Sinica, v. 75, no. 3, p. 275-278.

Lüttge, A., and Conrad, P.G., 2004, Direct observation of microbial inhibition of calcite dissolution: Applied and Environmental Microbiology, v. 70, no. 3, p. 1627-1632.

Matsumoto, R., 1990, Vuggy carbonate crust formed by hydrocarbon seepage on the continental shelf of Baffin Island, northeast Canada: Geochemistry Journal, v. 24, p. 143-158.

Morita, R., 1980, Calcite precipitation by marine bacteria: Geomicrobiology Journal, v. 2, no. 1, p. 63-82, doi: 10.1080/01490458009377751.

Mucci, A., 1983, The Solubility of Calcite and Aragonite in Seawater at Various Salinities, Temperatures, and One Atmosphere Total Pressure: American Journal of Science, v. 283, no. 7, p. 780-799.

Pokrovsky, O.S., Golubev, S.V., Schott, J., and Castillo, A., 2009, Calcite, dolomite and magnesite dissolution kinetics in aqueous solutions at acid to circumneutral pH, 25 to 150 degrees C and 1 to 55 atm pCO(2): New constraints on CO2 sequestration in sedimentary basins: Chemical Geology, v. 265, no. 1-2, p. 20-32.

Reeburgh, W.S., 2007, Oceanic methane biogeochemistry: Chemical Reviews, v. 107, no. (2, p. 486-513.

Ritger, S., Carson, B., and Suess, E., 1987, Methane-derived authigenic carbonates formed by subduction-induced pore-water expulsion along the Oregon/Washington margin: Geological Society of America Bulletin, v. 98, p. 147-156.

Rosso, K.M., Zachara, J.M., Fredrickson, J.K., Gorby, Y.A., and Smith, S.C., 2003, Nonlocal bacterial electron transfer to hematite surfaces: Geochimica Et Cosmochimica Acta, v. 67, no. 5, p. 1081-1087.

Suess, E., 2002, Gashydrat—Eine Verbindung aus Methan und Wasser: Nova Acta Leopoldina, v. 85, no. 323, p. 123-146.

Suess, E., 1970, Interaction of organic compounds with calcium carbonate-r . Association phenomena and geochemical implications *: Geochimica et Cosmochimica Acta, v. 34, p. 157-168.

Teichert, B.M.A., Bohrmann, G., and Suess, E., 2005, Chemoherms on Hydrate Ridge - unique microbially mediated carbonate build-ups growing into the water column: Palaeogeography, Palaeoclimatology, Palaeoecology, v. 227, p. 67-85.

Wenzhöfer, F., Adler, M., Kohls, O., Hensen, C., Strotmann, B., Boehme, S., and Schulz, H.D., 2001, Calcite dissolution driven by benthic mineralization in the deep-sea: In situ measurements of Ca2+, pH, pCO(2) and O-2: Geochimica Et Cosmochimica Acta, v. 65, no. 16, p. 2677-2690.

Whittenbury, R., Phillips, K.C., and Wilkinson, J.F., 1970, Enrichment, isolation, and some properties of methane-utilizing bacteria: J. Gen. Microbiol., v. 59, p. 2771-2776.

Zeebe, R.E., and Wolf-Gladow, D., 2001, CO2 IN SEAWATER: EQUILIBRIUM; KINETICS; ISOTOPES: Elsevier, Amsterdam, Boston, London, New York, Oxford, Paris, San Diego, San Francisco, Singapore, Sydney.

Chapter 4

A simple method for the quantification of microbially-induced calcification rates in marine sediment slurries using ^{14}C and ^{45}Ca radioisotopes

Stefan Krause[1] and Tina Treude[1]

[1]Helmholtz Centre for Ocean Research GEOMAR, Wischhofstr. 1-3, 24148 Kiel

ABSTRACT

Authigenic calcium carbonate precipitation represents an important carbon sink in marine sediments. To date, benthic carbonate precipitation rates are commonly deduced from numerical models, while methods for direct rate measurements are scarce. In order to establish a method for direct measurements of calcium carbonate precipitation, microbially active and sterilized slurries (dilution 1:6) of three marine cold-seep sediments, featuring different levels of methane-dependent sulfate reduction [210 (SD 30), 40 (SD 5), and 0 nmol SO_4^{2-} cm^{-3} slurry d^{-1}, respectively], were incubated separately with ^{14}C-bicarbonate and $^{45}Ca^{2+}$ radiotracers. Both active and sterilized sediment slurries showed an increase of the ^{14}C and ^{45}Ca radioisotopes in the solid phase during the experiments (30 days), which allowed for a differentiation between microbially-induced and abiotic precipitation. The two sediment slurries with considerable methane-dependent sulfate reduction showed an overall linear increase of ^{14}C and ^{45}Ca radioisotopes in the solid phase over the course of the experiment, which was positively correlated ($R^2 > 0.95$ and >0.96, respectively) with increase in bulk fluid total alkalinity and sulfide concentration. In the case of ^{45}Ca, this linear increase was lagged by 10 days, during which substantial fluctuations of ^{45}Ca in the solid phase occurred, potentially caused by initial interaction between ^{45}Ca and living or non-living organic substances. Bulk precipitation rates of the three sediment slurries, calculated via ^{14}C [0.49 (SD 0.16), 0.06 (SD 0.10), and 0.04 (SD 0.106 nmol C cm^{-3} slurry day^{-1}, respectively], were generally lower compared to rates obtained via ^{45}Ca [2.06 (SD 0.50), 1.55 (SD 3.69), and 0.21 (SD 0.50) nmol Ca cm^{-3} slurry day^{-1}, respectively]. In the third active sediment slurry, featuring non-detectable methane-dependent sulfate reduction, bulk precipitation rates of total C and Ca were 0.04 (SD 0.10) and 0.21 (SD 0.50) nmol cm^{-3} slurry day^{-1}, respectively, and were most likely correlated with abiotic processes. In summary, microbially-mediated calcification rates obtained with radiotracers were in good agreement with recent modeling approaches determining carbonate precipitation from geochemical parameters at fluid venting sites. Our study demonstrates that incubations with ^{14}C-bicarbonate and $^{45}Ca^{2+}$ radiotracers are principally suitable to quantify carbonate

precipitation rates in slurries of natural sediments, allowing for the discrimination between abiotic and microbially-induced precipitation. However, discrepancies between precipitation rates calculated via ^{14}C and ^{45}Ca, possibly arising from additional calcium binding to sediment components or dilution of the bicarbonate radioisotopes, suggest the need for further methods refinements.

INTRODUCTION

Cold seeps are defined as regions of the seafloor where ascending, methane-charged fluids reach the surface sediment (Suess, 2010). These locations are commonly characterized by the presence of authigenic carbonates. Seep sediments are host to syntrophic microbial consortia that are mediating anaerobic oxidation of methane (AOM) (Boetius et al., 2000; Zehnder and Brock, 1979), and that play an outstanding role in the formation of authigenic carbonates in sediments (Greinert, Bohrmann, and Suess, 2001a; Bohrmann et al., 1998; Peckmann et al., 2001). During AOM, sulfate (SO_4^{2-}) is used as the terminal electron acceptor (Barnes and Goldberg, 1976) to oxidize methane (CH_4), according to the following net reaction:

$$CH_4 + SO_4^{2-} \rightarrow HCO_3^- + HS^- + H_2O \quad (1)$$

The resulting increase of carbonate alkalinity elevates the saturation state for carbonates, and in case of supersaturation, induces formation of authigenic mineral phases according to:

$$Ca^{2+} + CO_3^{2-} \rightarrow CaCO_3 \quad (2)$$

The precipitation rate (R) of carbonate is calculated, using the saturation state, the mineral phase depending kinetic constant k and the equilibrium constant (k_{sp}), as well as bulk fluid concentrations of calcium [Ca^{2+}] and carbonate [CO_3^{2-}] according to the following equation (e.g. Luff and Wallmann, 2003):

$$R = k\left(\frac{[Ca^{2+}]\,[CO_3^{2-}]}{k_{SP}} - 1\right)^n \quad (3)$$

where *n* represents the reaction order.

Rates of authigenic carbonate formation in natural marine sediments are commonly derived indirectly, i.e., by considering carbonate, sediment, and porewater characteristics combined with fluxes of relevant chemical components (e.g. Naehr et al., 2007; Luff et al., 2004). In contrast, direct measurements of microbial carbonate precipitation, suitable to quantify precipitation rates, are scarce and usually carried out in sediment-free conditions with isolated bacterial strains (e.g. Hammes and Verstraete, 2002; Yates and Robbins, 1999), not representing marine sedimentary conditions.

In the present study, incubations with ^{14}C-bicarbonate and $^{45}Ca^{2+}$ radiotracer were performed, to directly quantify microbially-induced calcification (carbonate precipitation) rates in marine sediments. The use of these radioisotopes has been widely accepted to determine the calcification potential of corals and algae (Riebesell et al., 2000; Marshall and Wright, 1998; Tambutté et al., 1995). To date, approaches to assess extracellular calcification rates in sediments using ^{14}C and ^{45}Ca radioisotopes have, to our knowledge, not been established. However, radiotracers have been employed for beta imager mapping of microbial mats to obtaining spatial information and semi-quantitative rates of calcification (Michaelis et al., 2002; Treude et al., 2007; Ludwig et al., 2005). We used three slurries of natural marine cold-seep sediments, featuring different levels of methane-dependent sulfate reduction (≅AOM) activity and employed time series to determine carbonate precipitation rates with the respective radiotracers. Careful analysis of method limitations and potential error sources was carried out to identify refinements, necessary for routine application.

MATERIAL AND METHODS

Sediment samples used in this study were collected with TV-guided multicorers during the two research cruises M66 offshore Costa Rica, and SO191 offshore New Zealand (Table 1) with the research vessels RV "Meteor" and RV "Sonne", respectively. Samples were obtained from seafloor regions, characterized by different seep and AOM activity (Linke et al., 2005; Sommer et al., 2010). Costa Rica (CoRi) sediment was obtained from a seep habitat with live chemosynthetic sibuglinid (pogonophoran) polychaetes. New Zealand sediments were sampled from a habitat type termed “raindrop” (NZRa) consisting of a dense bed of live heterotrophic ampharetid polychaetes (Sommer et al., 2010), as well as from a habitat that was characterized by empty polychaete sheats (NZPo).

Table 1: List of cold-seep sediments used in this study.

Sediment	Cruise	Year	Study area offshore	Station	Water depth (m)	Lat	Lon	Sampled from cmbsf	Habitat
CoRi	M66/2	2009	Cost Rica	88	1660	09:07.39 N°	84:50.88 W°	0-10	active Pogonophora
NZRa	SO191	2007	New Zealand	232	1172	40:02.1421 S°	177:43.143 E°	0-5	"Raindrop" sediment
NZPo	SO191	2007	New Zealand	309	1054	41:46.47 S°	175:25.699 E°	0-5	Polychaete sheats

Sampling was carried out immediately after retrieval at *in situ* temperature (4°C). On board, sediment samples were transferred into Duran ® glass bottles without headspace, sealed with butyl rubber stoppers and stored at 4°C in the dark until further use.

Preparation of experimental sediment slurries

For experimental sediment slurry preparation, a modified marine sulfate-reducer medium (Medium 196, German Collection of Microorganisms and Cell Cultures) was used. The concentrations of Mg^{2+} and Ca^{2+} were adjusted to resemble modern seawater concentrations. Carbonate alkalinity was adjusted to ~2 mEq by adding 0.17 g Na bicarbonate l^{-1}. The medium had the following composition (g l^{-1}): $NaSO_4$,

3; KH_2PO_4, 0.2; NH_4Cl, 0.3; NaCl, 21; $MgCl_2$ x 6 H_2O, 10.83; KCl, 0.5; $CaCl_2$ x 2 H_2O, 1.53; resazurin solution 0.2 ml l^{-1}; Na_2S x 9 H_2O, 0.4; Se/Wo solution, trace element solution SL-10, 1 ml l^{-1}; 6-vitamin solution (4-aminobenzoat, D-(+)-biotin, nicotinic acid, calcium-D-(+)-panthothenate, pyridoxaminedihydrochloride); Solutions of thiamine, cyanocobalamine, riboflavin (1 ml l^{-1}, each). Medium pH was adjusted to 7.4.

In the laboratory, the sediments were transferred into 500 ml Duran glass bottles in a glovebox under N_2/CO_2 (80%/20%) atmosphere. Subsequently, an equal volume of sterile medium was added anaerobically, resulting in a 1:1 diluted stock slurry, from which the actual experimental setups (see below) were later produced. Bottles were sealed with butyl stoppers. The sediment slurry headspace of was gassed with CH_4 for 10 min to an excess pressure of 1 bar.

Time series experiments with ^{14}C-bicarbonate and $^{45}Ca^{2+}$ radiotracers

Preparation of samples

From each of the three stock slurries (CoRi, NZRa, and NZPo sediment), 15 subsamples with a volume of 4 ml each were transferred into autoclaved, anoxic 50 ml serum glass vials under N_2/CO_2 (80%/20%) atmosphere. For the production of sterile controls, additional 9 subsamples (4 ml) were transferred into open petri dishes (ø 10 cm) under N_2/CO_2 (80%/20%) atmosphere and sterilized by the exposure to UV-light (2x6 Watt, distance 10 cm) for 30 min. Petri dishes were gently shaken occasionally. Subsequently, control samples were transferred into anoxic 50 ml serum glass vials. Microscopy imaging of sterilized slurries with BacLight® Live/Dead stain (Invitrogen) confirmed > 99 % cell mortality after UV-treatment. To each serum vial, 8 ml of modified sterile seawater medium was added anaerobically, resulting in a final sediment dilution of 1:6. All vials were sealed with butyl rubber stoppers. The headspace was gassed for 10 min with high purity CH_4 to a final excess pressure of 1 bar. The samples were sub-sampled for initial total alkalinity, total sulfide, and Ca^{2+} determinations (see below) and were then stored for 6 days at 10

°C in the dark to allow for an adaptation of the microbial community to experimental conditions and for an equilibration of chemical parameters such as pH, total alkalinity, and mineral saturation state before addition of radiotracers. Samples were gently re-suspended every other day.

Addition of radioisotopes

After preparation of the serum glass vials, 10 microbially active and 6 sterilized samples from each of the CoRi, NZRa, and NZPo sediment slurries were used for incubation with radiotracers. Half of the respective samples (5 active samples and 3 sterilized controls) were incubated with ^{14}C-bicarbonate tracer by injection of 150 kBq dissolved in 14 µl water, specific activity 50 mCi/mmol. The other half of the respective samples was incubated accordingly with $^{45}Ca^{2+}$ tracer (500 kBq dissolved in 14 µl water, specific acticity 10 mCi/mmol). The remaining five active and 3 sterilized samples of each slurry served as non-radioactive replicates to monitor the development of sulfide, alkalinity and Ca^{2+}. All samples were incubated at 10°C in the dark. Five replicates of each radiotracer, i.e., 5 x 14 µl ^{14}C-bicarbonate and 5 x 2 µl $^{45}Ca^{2+}$, respectively, were added to 1 ml of ultra purified water and 3 ml Ultima Gold® in a 6 ml scintillation vial and vigorously shaken. Samples were left to react for 4 hours, before liquid scintillation counting of total radioactivity, to avoid additional chemical quenching.

Sub-sampling during time-series incubation

Sampling of radioactive and non-radioactive replicates was carried out immediately after experiment start and after 1, 3, 5, 10, 15, 23 and 30 days. For monitoring of sulfide, total alkalinity and Ca^{2+} concentration, a total amount of 400 µl of clear supernatant was sampled from each non-radioactive control sample. To determine the precipitation of radioisotopes in the solid phase, 300 µl from ^{14}C and ^{45}Ca radioisotopes containing slurry, respectively, was sub-sampled anaerobically with a sterile syringe from the radioactive replicates. Samples were transferred into 2.5 ml Eppendorf caps and centrifuged at 14.000 x g for 10 min. The clear supernatant was discarded. The remaining sediment pellet was washed in 2 ml sterile medium and centrifuged at 14.000 x g for 10 min. This washing procedure was repeated 5 times.

After the last washing step, 100 µl of the clear supernatant was withdrawn and transferred into a 6 ml scintillation vial with 1 ml ultra purified water, 3 ml Ultima Gold®, shortly shaken and measured after 4 hours for radioactivity by liquid scintillation counting. Measurements confirmed that radioactivity reached background levels between 8 and 20 CPM. The remaining liquid was discarded. The sediment pellet was re-suspended in 800 µl of ultra purified water and transferred to a 6 ml scintillation vial filled with 1 ml ultra purified water and 3 ml Ultima Gold®. After 4 hours, the radioactivity of precipitated radioisotopes was measured with liquid scintillation counting. Values were expressed in counts per minute (CPM).

Determination of light-quenching factors for liquid scintillation counting of sediment samples

To account for light-quenching effects during liquid scintillation counting of radioactive samples containing sediment, the individual light-quenching factor of the three sediment slurries used in this study was determined. From each of the three stock slurries, 0.5 ml was sampled and diluted with sterile medium to a final dilution of 1: 6, matching slurry dilution in the experiments. From this diluted slurry, 10 replicates of 300 µl were transferred into 2.5 ml Eppendorf caps and centrifuged at 14.000 x g for 10 min. The clear supernatant was removed and replaced by 800 µl of ultra purified water. After re-suspension, slurries were transferred into 6 ml scintillation vials, filled with 1 ml ultra purified water. ^{14}C-bicarbonate tracer (70 kBq dissolved in 6 µl water; specific activity 50 mCi/mmol) and $^{45}Ca^{2+}$ tracer (245 kBq dissolved in 6 µl water, specific activity 10 mCi/mmol) was added to five replicates each. In addition, the same amounts of tracers were added to five sediment-free controls, each containing 2 ml of ultra purified water. After addition of 3 ml Ultima Gold® liquid scintillation cocktail, all samples were shaken and measured with liquid scintillation counting after 4 hours. The individual light-quenching factor of the three sediments was calculated by:

$$\text{Quench factor} = \text{average CPM}_{water}/\text{average CPM}_{slurry} \quad (4)$$

Sulfide measurements

Total sulfide concentration of the liquid phase was determined photometrically after Cord-Ruwisch (1985). For determinations, 100 µl of clear supernatant was sampled and immediately transferred into a cuvette with 4 ml of 5 mM $CuSO_4$. Absorbance was measured at 480 nm wavelength. Calibration was carried out with a sulfide standard series from 0 to 20 mmol l^{-1}.

Determination of Ca^{2+} concentration

Ca^{2+} concentrations of clear supernatant were measured photometrically using the the O-Cresol Phtalein Complexone (CPC) method after (Moorehead and Briggs, 1974). For determinations, 10 µl of clear supernatant were transferred liquid into a 4.5 ml cuvette. Subsequently, 1 ml of CPC reagent, 1 ml of dietylamin buffer and 1 ml of ultra purified water was added and mixed. A chemical blank was produced by adding 10 µl of ultra purified water to the reagents mentioned above. Samples and blank were left to react for five minutes. Subsequently, the photometer was set to zero with the blank at 575 nm. After absorption measurements of the samples, 50 µl of ethylene glycol, bis-(2-aminoethyl ether) tetraacetic acid (EGTA) solution was added to each cuvette, including chemistry blank, and mixed by stirring. Subsequently, the photometer was zeroed again with the chemistry blank, and absorption of samples after EGTA addition was measured. For each sample the difference between the absorbance before the addition of EGTA and the absorbance after addition of EGTA was calculated. Calibration was carried out with a Ca^{2+} standard series from 0 to 20 mmol l^{-1}.

Total alkalinity measurement

Total alkalinity was measured by titration of 50 µl clear supernatant with 0.01 molar HCl and methyl red/methylen blue indicator under N_2 ventilation in a reaction vessel after Pavlova. IAPSO standard seawater was used for calibration.

Calculations

Total alkalinity (TA)

Total alkalinity (TA) of the sample fluids was characterized by three components: (1) carbonate alkalinity (CA), initially set to 2 mEq, (2) sulfide alkalinity (SA), and (3) residual alkalinity (RA), caused by alkaline medium components (e.g. alkaline trace element solutions). RA was assumed to be constant (RA_{const}). Given initial (t_0) average concentrations of TA and total sulfide concentration, and assuming an initial CA of 2 mEq, the residual alkalinity for each of the three sediment slurries at t_0 was calculated according to:

$$RA_{const} = TA_{to} - (2\ mEq + SA_{t0}) \quad (5)$$

The carbonate alkalinity of time series samples taken at later time points (t_x) was then calculated according to:

$$CA_{tx} = TA_{tx} - (RA_{const} + SA_{tx}) \quad (6)$$

Carbonate ion (CO_3^{2-}) concentrations were calculated according to Zeebe and Wolf-Gladow (2001) using CA.

Saturation state (Ω)

Calcite (with varying admixtures of magnesium) is the dominant mineral in surface sediments with AOM activity (e.g. Greinert et al., 2001; Bohrmann et al., 1998). Therefore, calcite saturation state (Ω) of sample bulk liquids was calculated according to:

$$\Omega = \frac{[Ca^{2+}] \cdot [CO_3^{2-}]}{K_{sp}^{*}}, \quad (7)$$

where $[Ca^{2+}]$ and $[CO_3^{2-}]$ are the Ca^{2+} and CO_3^{2-} concentrations of the liquids, respectively. *K*sp* is the temperature and salinity dependent stoichiometric solubility product constant for calcite, calculated after Mucci (1983).

Total calcite precipitation rates

CPM (counts per minute) values of precipitated ^{14}C and ^{45}Ca obtained by liquid scintillation counting were corrected for radionuclide half-life time (in case of ^{45}Ca) and the light-quenching factor. Values were finally extrapolated to obtain the activity (CPM) of the total sediment slurry volume (Step 1).

^{14}C and ^{45}Ca [CPM] precipitation rates were determined by calculating the slope of linear regression lines from 3 or more linear data points in time-series graphs of either ^{14}C or ^{45}Ca activity, respectively (Step 2).

For the determination of total calcite precipitation rates, CPM values were translated into total concentrations of precipitated C and Ca, respectively, according to the following equations (Step 3):

$$C_{precip} = \frac{^{14}_{0}C_{precip}}{^{14}_{0}C{-}HCO_{3\,to}^{-}} \; x \; [HCO_{3\,to}^{-}] \tag{8}$$

$$Ca_{precip} = \frac{^{45}_{0}Ca_{precip}}{^{45}_{0}Ca_{to}} x \; [Ca_{to}] \tag{9}$$

where C_{precip} and Ca_{precip} is the total concentration of C and Ca precipitated per cm^{-3} sediment slurry [nmol cm^{-3}], respectively; $^{14}C_{precip}$ and $^{45}Ca_{precip}$ is the activity of total precipitated ^{14}C and ^{45}Ca [CPM], respectively; $^{14}C\text{-}HCO_{3\,t0}^{-}$ and $^{45}Ca_{t0}$ is the activity of ^{14}C-bicarbonate and $^{45}Ca^{2+}$ added at time zero [CPM], respectively; $[HCO_{3\,t0}^{-}]$ and $[Ca_{t0}]$ are the concentrations of dissolved bicarbonate and Ca^{2+} at time zero [nmol cm^{-3}], respectively.

Finally, total calcite precipitation rates were determined by calculating the slope of linear regression lines from 3 or more linear data points in time-series graphs of either total C or Ca concentrations, respectively (Step 4). Since Step 3 represents an intermediate calculation, only the results of Step 4 are presented.

Kinetic constant for calcite precipitation (k)

Assuming first-order reaction for calcite precipitation (Luff et al., 2004), *k* was calculated according to the following rate law:

$$R = k(\Omega - 1)^n \quad (10)$$

using the final average value of Ω, obtained for each of the three slurries.

Comparison of linear regressions

For statistical control, rates of radioactivity increase in the solid phase obtained for RoRi, NZRa and NZPo slurries were analyzed for similarity using the one-way Analysis of Covariance (ANCOVA) for independent samples. For ANCOVA calculation the interactive spreadsheet of the Vassar College was used (http://faculty.vassar.edu/lowry/VassarStats.html).

RESULTS

Total alkalinity (TA), sulfide and Ca^{2+}

During the time-series incubations, CoRi sediment slurries showed the steepest increases from initial TA (15.76 mEq) and total sulfide concentration (1.57 mmol l^{-1}), reaching final averaged values of 32 mEq (SD 1.38 mEq) and 12 (SD 1.29) mmol l^{-1}, respectively (Fig. 1, blue curves). In comparison, NZRa sediment slurries featured shallower increases of initial TA (14.34 mEq) and total sulfide (0.19 mmol l^{-1}), with final averaged concentrations of 19.39 (SD 0.33) mEq and 2.24 (SD 0.49) mmol $l^{-1}$of TA and sulfide, respectively. The smallest increase (<3%) in TA and sulfide was found

in the NZPo sediment slurries. None of the three active sediment slurries revealed a change in bulk calcium ion (Ca^{2+}) concentrations.

Sterilized controls of CoRi, NZRa, and NZPo sediment slurries showed no change in TA concentrations over the course of the entire experiment (Fig. 1, red curves). Sulfide concentrations increased by ~0.2 mmol l^{-1} during the first 9 to 22 days of the experiment in all controls, and reached stable values thereafter. In all three controls, a marked decline of ~2 mmol l^{-1} Ca^{2+} concentrations occurred during the first 6 days of the experiment.

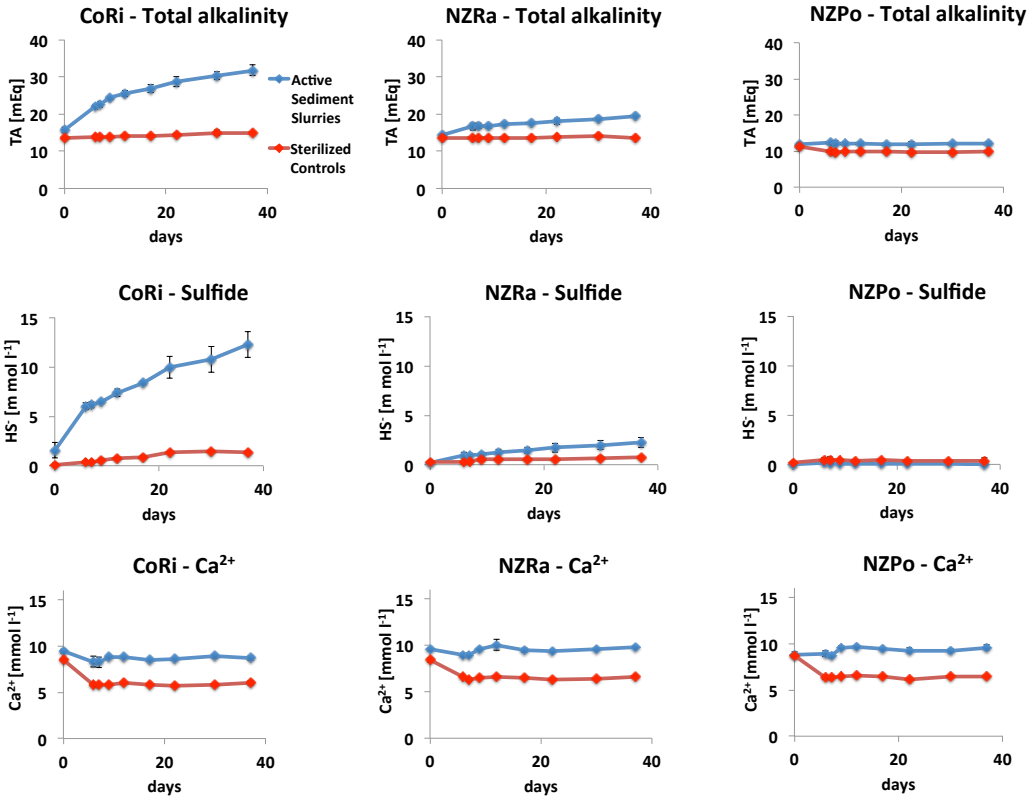

Figure 1. Temporal development of bulk liquid total alkalinity, sulfide, and Ca^{2+} concentrations of radioactivity-free slurries of CoRi, NZRa, and NZPo sediment. Error bars represent standard deviations. Note: radioisotopes were added at day 6 (second data point) to accordant replicates.

Saturation state (Ω)

The initial calcite saturation state for slurries from all three sediments ranged between 1.9 and 2.5 (Fig. 2). Sterilized controls did not show changes in Ω during the course of the experiment. Slurries from CoRi and NZRa sediment showed an increase in saturation state by a factor of 3 and 2, respectively, during the first nine

days oft the experiment. Subsequently, Ω increase followed a linear trend. Final saturation states for CoRi and NZRa slurries reached averaged values of 7.5 (SD 1.4) and 6.6 (SD 0.3), respectively. Calcite saturation state of NZPo slurries maintained average values between 1.8 (SD 0.7) and 2.3 (SD 0.5) during the entire incubation.

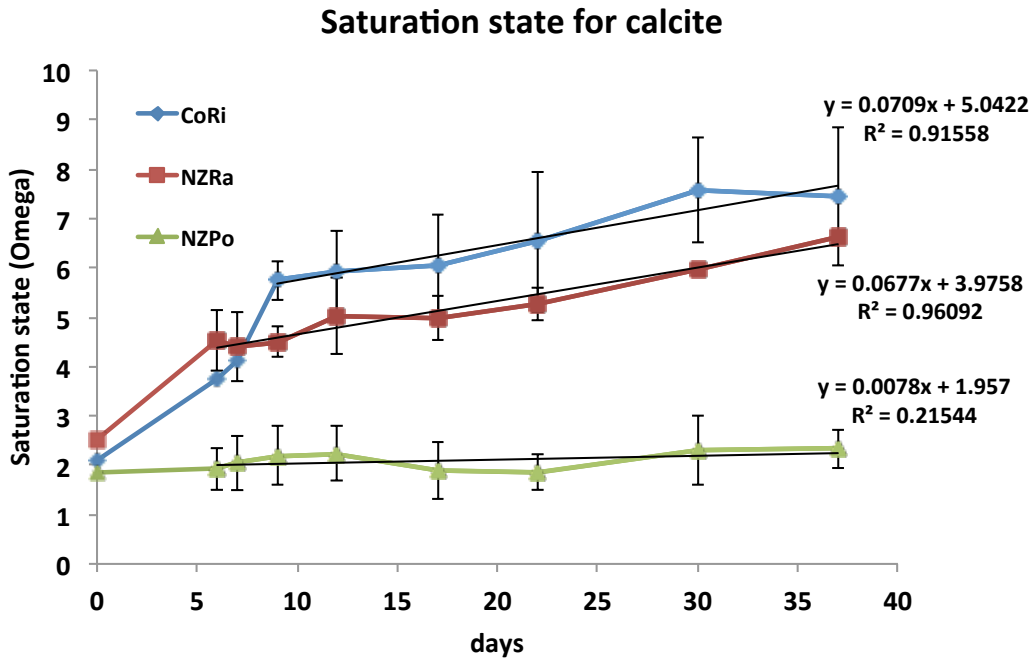

Figure 2. Temporal development of the calcite saturation state (Ω) for CoRi, NZRa, and NZPo sediment slurries. Linear regression lines and equations are given. Error bars represent standard deviations. Correlation equations: top - CoRi sediment, middle – NZRa sediment, bottom – NZPo sediment.

Precipitation of ^{14}C and ^{45}Ca radioisotopes

During time-series incubations, both active sediment slurries and sterilized controls showed the precipitation of ^{14}C and ^{45}Ca radioisotopes into the solid phase over the course of the experiment (Fig. 3 and 4). All sediment slurries incubated with ^{14}C-bicarbonate showed a linear increase in ^{14}C in the solid phase (Fig. 3). Statistical analysis of the linear regressions of the net precipitation of ^{14}C radioisotopes revealed that regression slopes differed significantly between the three active sediment types (One-Way ANCOVA for independent samples, $F= 26.17$, $p < 0.001$).

The precipitation rate of ^{14}C was generally higher in active sediment slurries compared to sterilized controls. The discrepancy between the ^{14}C precipitation rate of active and sterilized slurries was highest in CoRi sediment slurries (145.4 and 88.6 CMP cm^{-3} d^{-1}, respectively). The corresponding ^{14}C net precipitation rate, derived from the difference between active and sterilized sediment slurry, was 56.8 CPM cm^{-3} d^{-1}. In active slurries of NZRa sediment slurries, ^{14}C precipitated with a rate of 127.1 CPM cm^{-3} d^{-1}, while a precipitation of 121.8 CPM cm^{-3} d^{-1} was observed in sterilized controls. The resulting net precipitation of ^{14}C radioisotopes was 5.3 CPM cm^{-3} d^{-1}. Slurries of NZPo sediment featured the smallest difference in ^{14}C precipitation between active and sterilized controls (54.8 and 51.0 CPM cm^{-3} d^{-1}, respectively), resulting in a net precipitation of 3.8 CPM cm^{-3} d^{-1}.

In contrast to the linear increase of ^{14}C radioisotopes in the solid phase, ^{45}Ca precipitation revealed a marked peak in active and sterilized sediments at the second day of the experiment, followed by a drop almost to the initial level at day 3 and a stagnation until day 10 (Fig. 4). Thereafter, ^{45}Ca radioisotopes increased in the solid phase until experiment termination. Linear ^{45}Ca radioisotopes concentration increase from day 15 to 30 was used for precipitation rate calculations. Due to the reduced amount of data point used for linear regressions, statistical analysis of regression slope difference between the three sediments types could not be applied. Similar to ^{14}C incubations, active sediment slurries showed higher precipitation rates of ^{45}Ca radioisotopes than sterilized controls. CoRi sediment slurries, again, exhibited the largest difference in ^{45}Ca precipitation between active (371.1 CPM cm^{-3} d^{-1}) and sterilized (218.3 CPM d^{-1}) slurries, yielding a net precipitation of 152.8 CPM cm^{-3} d^{-1}. In active NZRa sediment slurries, ^{45}Ca precipitation was similar to CoRi sediment (377.4 CPM cm^{-3} d^{-1}), while sterilized controls yielded relatively high levels (271.4 CPM cm^{-3} d^{-1}). The corresponding ^{45}Ca net precipitation was 106.0 CPM cm^{-3} d^{-1}. Similar to ^{14}C experiments, NZPo sediment slurries showed the smallest difference in precipitation between active (183.3 CPM cm^{-3} d^{-1}) and sterilized (89.5 CPM cm^{-3} d^{-1}) slurries. To mitigate occurring negative values, net precipitation of ^{45}Ca radioisotopes (14.9 CPM cm^{-3} d^{-1}) was calculated over the entire course of the experiment.

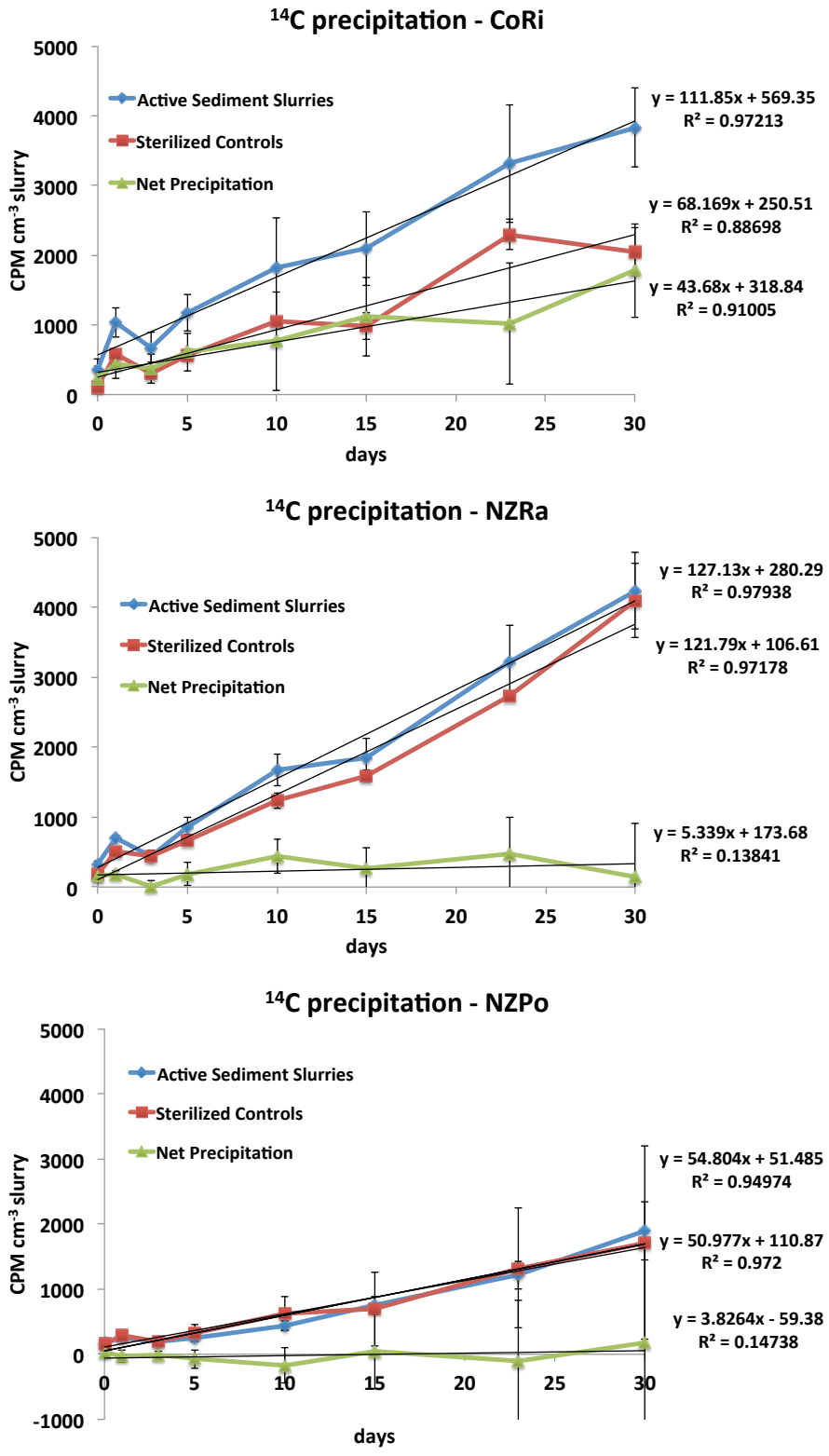

Figure 3. ^{14}C precipitation in active sediments slurries and sterilized controls with resulting net precipitation. Linear regression lines and equations are given. Error bars represent standard deviations between replicates. CPM = Counts per minute. Correlation equations: top - active sediment slurries, middle – sterilized sediment slurries, bottom – net precipitation. Note: net precipitation of NZPo calculated over the entire course of the experiment.

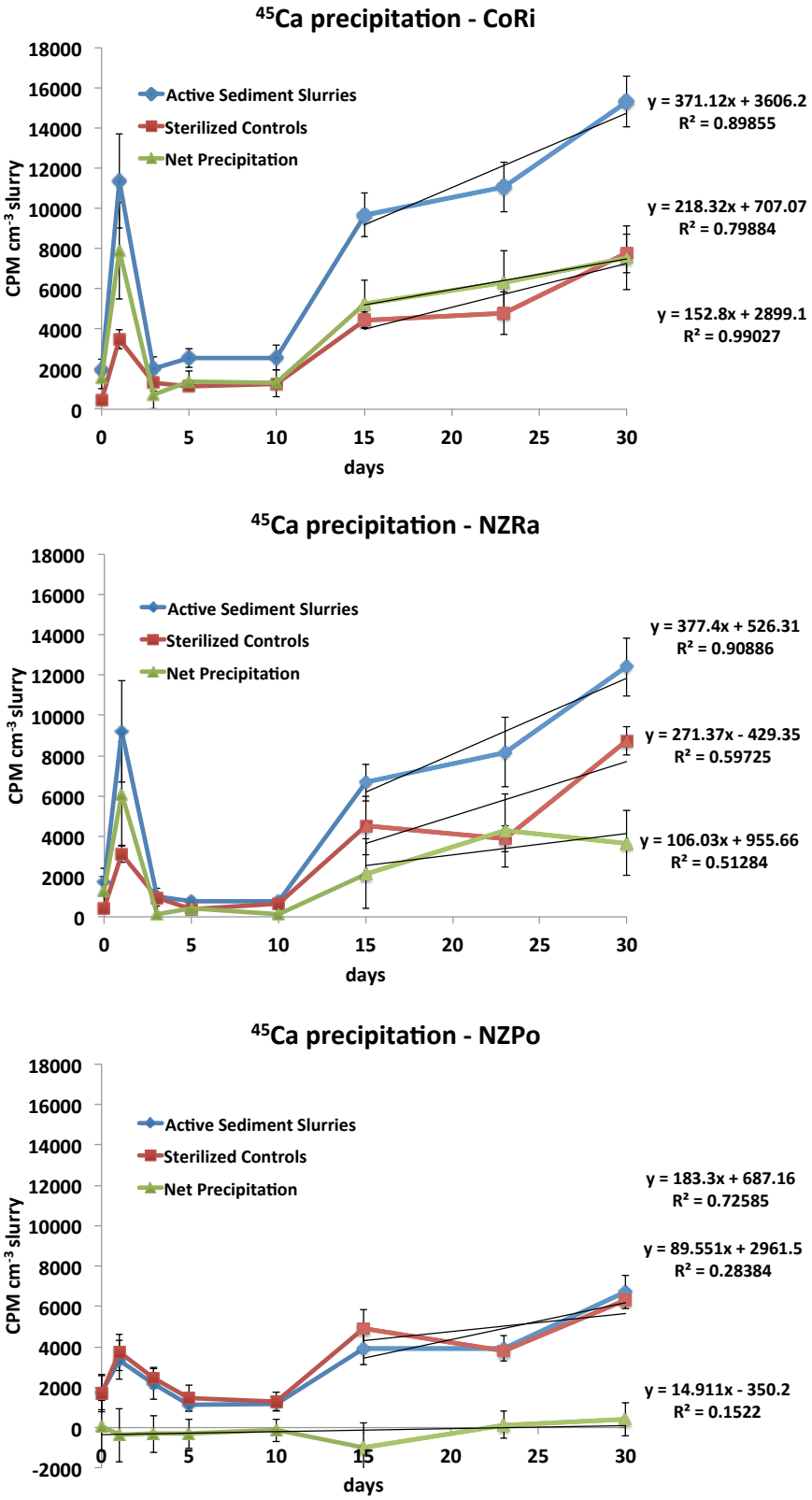

Figure 4. ^{45}Ca precipitation rates of active sediments slurries and sterilized controls with resulting net precipitation. Linear regression lines and equations are given. Error bars represent standard deviations between replicates. CPM = Counts per minute. Correlation equations: top - active sediment slurries, middle – sterilized sediment slurries, bottom – net precipitation.

Total calcite precipitation rates and kinetic constants

Rates of total calcite precipitation were calculated from net ^{14}C and ^{45}Ca precipitation in sediment slurries according to equations 9-10 (Table 2). Rates derived from ^{14}C-bicarbonate incubations were generally smaller compared to ^{45}Ca incubations, varying by a factor between 4 and 26. Smallest differences were observed for CoRi sediment slurries, while NZRa showed largest variations.

In CoRi sediment slurries, highest calcification rates were determined with either ^{14}C or ^{45}Ca [0.49 (SD 0.16) nmol C cm^{-3} slurry $d^{-1}$and 2.06 (SD 0.50) nmol Ca cm^{-3} slurry d^{-1}, respectively]. In comparison, NZRa sediment slurries featured much more different calcite precipitation rates, depending on the radioisotope used for calculation [0.06 (± 0.16) and 1.55 (SD 3.39) nmol cm^{-3} slurry d^{-1}, respectively]. NZPo slurries were characterized by calcification rates ranging one order of magnitude lower compared CoRi sediment, showing values of 0.04 (SD 0.10) and 0.21 (SD 0.50) nmol cm^{-3} slurry d^{-1}, respectively.

Table 2. Total precipitation rates (R), calculated from ^{14}C and ^{45}Ca precipitation, and corresponding kinetic constants (*k*). All values in nmol cm^{-3} slurry day^{-1}. Confidence intervals given in brackets.

Sediment	R_{14C}	k_{14C}	R_{45Ca}	k_{45Ca}
CoRi	**0.49 (± 0.16)**	**0.08**	**2.06 (± 0.50)**	**0.32**
NZRa	**0.06 (± 0.16)**	**0.01**	**1.55 (± 3.69)**	**0.27**
NZPo	**0.04 (± 0.10)**	**0.03**	**0.21 (± 0.50)**	**0.16**

The kinetic constant *k*, was calculated according to equation 10 for intervals with linear increase of ^{14}C (day 0-30), ^{45}Ca (day 15-30), and the corresponding final saturation state of each sediment, (Figure 2). For incubations with ^{14}C radioisotopes, *k* varied between 0.08 and 0.01 nmol cm^{-3} slurry day^{-1}. Kinetic constants of sediment slurries incubated with ^{45}Ca ranged between 0.16 and 0.32 nmol cm^{-3} slurry day^{-1}.

Correlations between microbial activity and calcification rates

Active sediment slurries from CoRi and NZRa sediments showed strong linear correlations ($R^2 > 0.95$) between calculated carbonate precipitation and

corresponding increase of sulfide and total alkalinity in the bulk liquid (Table 3) for both radioisotope experiments.

Table 3. List of linear regression coefficients (R^2) for correlations between carbonate increase, i.e., calcification determined either via ^{14}C or ^{45}Ca, vs. increase of sulfide, total alkalinity, and saturation state for the three different types of sediment slurries. ^{14}C n=8, ^{45}Ca n=3. The minus symbol depicts a negative correlation.

Sediment Slurry	Calcification vs. Sulfide		Calcification vs. Total alkalinity		Calcification vs. Saturation state	
	^{14}C	^{45}Ca	^{14}C	^{45}Ca	^{14}C	^{45}Ca
CoRi	0.98	0.96	0.96	0.99	0.80	0.69
NZRa	0.99	0.99	0.99	0.99	0.96	0.99
NZPo	0.65	0.83	0.04 (-)	0.94	0.22 (-)	0.83 (-)

Correlations between calcification and saturation state increase were generally less strong, with R^2 ranging between 0.69 and 0.96. NZPo sediment slurries incubated with ^{45}Ca also showed strong positive correlations between calcification vs. sulfide increase (R^2= 0.83), and calcification vs. total alkalinity increase (R^2= 0.94). In contrast, calcification calculated from ^{14}C incubations did not show a clear positive linear relationships with sulfide (R^2= 0.65), total alkalinity (R^2= 0.04), or saturation state (R^2= 0.22). For both radioisotopes, calcification and saturation state appeared to be strongly negatively correlated (R^2= 0.83) in NZPo sediment slurries.

DISCUSSION

Suitability of the introduced method

The present method is a direct determination of calcification (e.g. calcium carbonate precipitation) rates in slurries of marine sediments. The calcification rates were determined via the increase of ^{14}C and ^{45}Ca radioisotopes in the solid phase, indicative for radioactive calcium carbonate ($^{45}Ca^{14}CO_3$) precipitation, after the addition of ^{14}C-bicarbonate and $^{45}Ca^{2+}$ radiotracers to the liquid phase.

According to the stoichiometry of calcium carbonate ($CaCO_3$) the increase of ^{14}C and ^{45}Ca radioisotopess should yield a molar ratio of 1, which was not observed in the incubation experiments. In general, ^{45}Ca showed higher increases by a factor of 4 to 26 between the sediments used, compared to ^{14}C incubations. ^{14}C was added in the form of bicarbonate ($H^{14}CO_3^-$), representing a component of carbonate alkalinity. Rate calculations were based on the initial concentration of bicarbonate ions at the start of the experiment. As carbonate alkalinity increased over time due to AOM activity in the slurries, the ratio of HCO_3^- to $H^{14}CO_3^-$ was increased, in turn resulting in a relative decrease of $H^{14}CO_3^-$ contributing to carbonate precipitation. As a consequence, ^{14}C-bicarbonate incubations bare the danger of underestimating calcification rates. On the other hand, $^{45}Ca^{2+}$ ions might have been complexed by organic sediment components in addition to precipitation with carbonate (Ercole et al., 2007). Therefore, calcification rates from ^{45}Ca incubations might be overestimated.

The dilution of natural sediments to slurries is a necessary pre-requisite for the introduced method to provide sufficient bulk liquid for measurements of pH, sulfide, and total alkalinity. By diluting, the characteristics of natural sediment, including porosity, water content, gradients of chemical elements and distribution of micro-niches is strongly altered. Therefore, calcification rates determined by slurry incubations might considerably differ from undiluted marine sediment. However, since anaerobic oxidation of methane (AOM) rates determined in cold-seeps sediments remain principally unaffected by dilutions to the level applied in the present study (Treude et al. 2003), we think that our method can provide a rough approximation of microbial calcification rates at cold seeps.

The combination of active and sterilized slurries allowed the differentiation between abiotic and microbially-related precipitation. The deduced calcification rates were highly correlated to the temporal increase of sulfide and total alkalinity, which are products of AOM. Two of three sediment slurries used, including the most and least active regarding AOM, showed variations in calcification rates by a factor of 4 to 6 between ^{14}C and ^{45}Ca incubations. Considering the precipitation rates obtained by ^{14}C and ^{45}Ca incubations as the lower and upper boundary, respectively, the method

used provides a suitable tool to constrain the range of calcification in marine sediment slurries.

Method sensitivity and potential error sources

The measurements of total dissolved calcium did not show any change in concentration for the bulk medium of all three sediment slurries, and were consequently not sensitive enough to constrain calcification rates. In contrast, the incubation of sediment slurries with ^{14}C or ^{45}Ca radioisotopes was generally suitable to deduce potential calcification rates in the range of pmol to nmol cm^{-3} slurry day^{-1}. According to supersaturated conditions for calcite in all experimental setups, calcification was observed in active as well as in sterilized control sediment slurries. Net calcification rate was constrained from the difference in radioisotope precipitation between active sediment slurries and sterilized controls. It was interesting to find that Ca^{2+} declined by 35 to 40% in sterilized controls after six days (Figure 1), although initial Ca^{2+} concentrations were similar in all experimental setups. We can exclude that carbonate precipitation occurred during exposure of control sediment slurries to UV-light, since temperature, pCO_2, and total alkalinity remained stable during the sterilization process. Strong Ca^{2+} binding to released intracellular components after cell deterioration provides a potential explanation for the observed loss of bulk fluid Ca^{2+} in sterilized slurries. Substantial Ca^{2+} binding to organic intracellular proteins, forming stable chelate complexes, has well been documented (e.g. Heinzmann and Hunziker, 1991; Hauschka et al., 1975; Oswald and MacLennan, 1974).

The independent incubation of ^{14}C-bicarbonate and $^{45}Ca^{2+}$ radiotracers with sediment slurries showed a strong dependence of calcification rates on microbial AOM activity. Incubations with ^{14}C-bicarbonate yielded calcification ratios between 0.49 (SD 0.16) for the sediment slurry showing highest AOM activity, and 0.04 (SD 0.10) nmol C cm^{-3} slurry day^{-1} for slurries with the undetectable AOM activity. Carbonate precipitation during this study, was assumed to be a first-order reaction (Luff et al., 2004). The kinetic constant (*k*), calculated for the two slurries (CoRi, 0.08

nmol C cm^{-3} slurry day^{-1}; NZPo 0.03 nmol C cm^{-3} slurry day^{-1}) varied by a factor of 2.7, showing rather similar reaction speed. A similar *k* value, in turn, indicates that the same chemical reaction (e.g. carbonate precipitation) took place in both slurries, justifying comparison of individual precipitation rates. Although within the same order of magnitude, the value for the kinetic constant obtained from the sediment NZRa was lower (0.01 nmol C cm^{-3} slurry day^{-1}), compared to the other two sediments. This discrepancy might be caused by sediment features, as the amount of carbonates present as seed crystals or the concentration of organic substances, differing in NZRa sediment slurries compared to the other two.

In contrast to the strong variations regarding precipitation rate, the error margin appeared to be independent of the AOM activity and calcification rate, ranging between 0.10 and 0.16 nmol C cm^{-3} slurry day^{-1}. Considering 0.16 nmol C cm^{-3} slurry day^{-1} as the accuracy limit of ^{14}C incubations (Table 2), net calcification should exceed 0.32 nmol C cm^{-3} slurry day^{-1}, to avoid error margins > 50%. Incubations with ^{45}Ca were also positively correlated with AOM activity, generally showing calcification rates 4 to 26 times higher than for ^{14}C incubations. Similar to ^{14}C incubations, values for the kinetic constant varied by a factor of 2, indicating that the same chemical reaction (carbonate precipitation) took place. Sediment NZRa calcification rate (1.55 nmol Ca cm^{-3} slurry day^{-1}) showed a considerable error margin of 3.69 nmol Ca cm^{-3} slurry day^{-1} and is therefore considered unreliable. Considering the error margins within replicates of the three sediments, it can be speculated that individual replicates were enriched with organic matter and bound additional calcium ions (Kinniburgha et al., 1999), including ^{45}Ca, which eventually contributed to the calculation of precipitation rates. With the exemption of ^{45}Ca incubations with NZRa sediments slurries, the confidence interval for radioisotope precipitation ranged between 0.47 and 0.69 nmol ml $slurry^{-1}$ day^{-1}, irrespective of the AOM rate and calcification rate. Therefore 0.69 nmol Ca cm^{-3} slurry day^{-1} is considered as the accuracy limit of ^{45}Ca incubations. Consequently, net calcification should exceed 1.4 nmol Ca cm^{-3} slurry day^{-1}, to constrain error margins < 50%. Considering the accuracy limits of the methods one has to keep in mind that values refer to six-fold diluted

sediment slurries. Consequently, the method accuracy might change in accordance to the dilution factor of the sediment. Ma

tter of diminishing returns:

Microbial activity and net calcification rates

Obtained net calcification rates from ^{14}C and ^{45}Ca incubations ranged from 0.04 (± 0.10) to 2.06 (± 0.50) nmol cm^{-3} slurry. A direct comparison to precipitation rates obtained for natural sediments proves to be difficult as the precipitation rate (R) is usually integrated over depth. However, calcification rates obtained from sediments characterized by high AOM activity as Hydrate Ridge (Luff et al., 2004) and the convergent margin offshore Costa Rica, generally vary by one orders of magnitude between 10 and 450 nmol $CaCO_3$ cm^{-2} d^{-1} (Karaca et al., 2010;) for sediment cores of 15-45 cm in length. Conversion of these areal rates into volume rates yields values, which are in good agreement with the results of the present study.

Although absolute values for calcification rates differed between ^{14}C and ^{45}Ca incubations, both methods showed that net calcification rates were strongly dependent on methane-dependent sulfate reduction, i.e., AOM, activity, as also assumed in recent transport reaction models (Luff and Wallmann, 2003; Karaca et al., 2010). Active sediment slurries of CoRi sediment showed fastest increase of bulk liquid sulfide and total alkalinity (TA) concentration, which are indicators of microbial AOM (Nauhaus et al., 2002), in correspondence with highest net calcification rates. In contrast, NZPo sediment slurries, in which AOM was below detection, limit yielded net calcification rates one order of magnitude lower compared to CoRi sediment slurries.

During AOM, carbon is assimilated into the consortia biomass from CH_4 and CO_2 with a low efficiency ≤ 1.3 mol% (Wegener et al., 2008). Consequently, microbial carbon assimilation can be neglected for the carbon pool in our experiments. Microbial cell walls are usually strongly negatively (Hoyle and Beveridge, 1984; Beveridge, 1981) charged, prohibiting adsorption of HCO_3^- and CO_3^{2-} ions. Therefore, we can assume that precipitation of ^{14}C over time largely represents calcification.

While incubations with ^{14}C radioisotopes showed linear increase for all sediment slurries over time, the increase of ^{45}Ca did not follow any linear trend during the first 10 days of the experiment. For in CoRi and NZRa sediments, high fluctuations were observed during the initial phase after inoculation, followed by marginal increase of ^{45}Ca until day ten. This temporal variability was less pronounced in the least microbially active NZPo sediment. Therefore, it can be speculated that microbial activity was causative for initial variations in ^{45}Ca precipitation. Radioisotope studies, using the unicellular marine green alga *Nannochloris atomus* as a model organism for microbial influence on extracellular calcification (Yates and Robbins, 1999), revealed considerable differences for Ca^{2+} and inorganic carbon regarding intracellular residence time. While inorganic carbon leaked out of the cells within 10 s after introduction, Ca^{2+} was retained intracellular over several hours, due to enzymatic activity (Partida-Sánchez et al., 2001; Gangola and Rosen, 1987). Additionally, Ca^{2+} ions easily bind to negatively charged functional groups of microbial cell surfaces (Morita, 1980) or excreted extracellular polymeric substances (EPS) (Dupraz et al., 2009), being temporarily unavailable for chemical reactions. According to our experimental results, reactions of ^{45}Ca radioisotopes with biological sediment components equilibrated after 10-15 days, thereafter showing linear increase, similar to ^{14}C incubations.

Outlook

The introduced protocol for the quantification of microbially-induced calcification in sediments indicates that further experiments might be required before this method can routinely applied. Additional studies should be conducted to constrain the strength of interactions between ^{45}Ca radioisotopes and sediment components. Furthermore, additional sediments differing strongly in AOM activity should be tested against each other to constrain the method accuracy limit. And finally, calcification rates should be compared between sediments with different amounts of carbonate minerals to evaluate the effect of seed crystals on precipitation rates.

Summary and conclusions

Incubation experiments of sediment slurries with ^{14}C-bicarbonate and $^{45}Ca^{2+}$ radiotracers proved to be suitable for determing calcification rates, both abiological and microbially-induced. Although ^{14}C incubations yielded generally lower values compared to ^{45}Ca incubations, the combination of both methods might indicated the lower and upper limit of the calcification rates. For each of the two methods, precipitation rates were strongly dependent on microbial AOM activity, while the reaction velocity remained largely unaffected. Obtained calcification rates were in accordance with field studies. Experimental results suggested a method accuracy limit of ~0.16 nmol C cm^{-3} $slurry^{-1}$ day^{1} for ^{14}C incubations and ~0.7 nmol Ca cm^{-3} $slurry^{-1}$ day^{1} for incubations with ^{45}Ca. Further incubation experiments with ^{45}Ca are required to constrain radioisotope interaction with sediment components.

ACKNOWLEDGEMENTS

This study was conducted within the "The Future Ocean" Cluster of Excellence funded by the German Research Foundation (DFG). We thank J. Farkas for her help during pre-studies and method refinement. J. Hommer and K. Kretschmer are thanked for their help measuring samples with liquid scintilation counting. L. Haffert is thanked for fruitful discussions on aspects of precipitation kinetics. A. Boetius is thanked for offering the sediment material used in this study, which were collected within the GEOTECHNOLOGIEN project MUMM “Methane in the Geo/Bio-System - Turnover, Metabolism and Microbes”; grants 03G0554A and 03G0608A, BMBF.

REFERENCES CITED

Barnes, R.O., and Goldberg, E.D., 1976, Methane Production and Consumption in Anoxic Marine-Sediments: Geology, v. 4, no. 5, p. 297-300.

Beveridge, T.J., 1981, Ultrastructure, chemistry and function of the bacterial wall: International Review of Cytology, v. 147, p. 229-317.

Boetius, A., Ravenschlag, K., Schubert, C.J., Rickert, D., Widdel, F., Gieseke, A., Amann, R., Jorgensen, B.B., Witte, U., and Pfannkuche, O., 2000, A marine microbial consortium apparently mediating anaerobic oxidation of methane: Nature, v. 407, no. 6804, p. 623-626.

Bohrmann, G., Greinert, J., Suess, E., and Torres, M., 1998, Authigenic carbonates from the Cascadia subduction zone and their relation to gas hydrate stability: Geology, v. 26, no. 7, p. 647-650.

Cord-Ruwisch, R., 1985, A quick method for the determination of dissolved and precipitated sulfides in cultures of sulfate-reducing bacteria: Journal of Microbiological Methods, v. 4, p. 33-36.

Dupraz, C., Reid, R.P., Braissant, O., Decho, A.W., Norman, R.S., and Visscher, P.T., 2009, Processes of carbonate precipitation in modern microbial mats: Earth-Science Reviews, v. 96, no. 3, p. 141-162, doi: 10.1016/j.earscirev.2008.10.005.

Ercole, C., Botta, A.L., Centi, V., Lepidi, A., and Cacchio, P., 2007, Bacterially Induced Mineralization of Calcium Carbonate: The Role of Exopolysaccharides and Capsular Polysaccharides: Microscopy and Microanalysis, v. 13, no. 1, p. 42-50.

Gangola, P., and Rosen, B.P., 1987, Maintenance of intracellular calcium in Escherichia coli.: The Journal of biological chemistry, v. 262, no. 26, p. 12570-4.

Greinert, J., Bohrmann, G., and Suess, E., 2001, Gas Hydrate-associated carbonates and methane-venting at Hydrate Ridge : Classification , distribution , and origin of authigenic lithologies, *in* Paull, C.K. and Dillon, W.P. eds., GEOPHYSICAL MONOGRAPH SERIES, AGU, Washington, D. C., p. 99-113.

Hammes, F., and Verstraete, W., 2002, Key roles of pH and calcium metabolism in microbial carbonate precipitation: Reviews in Environmental Science and Technology [Rev. Environ. Sci. Technol.]., v. 1, no. 1, p. 3-7.

Hauschka, P.V., Lian, J.B., and Gallop, P.M., 1975, y-carboxyglutamate , in mineralized tissue: October, v. 72, no. 10, p. 3925-3929.

Heinzmann, C.W., and Hunziker, W., 1991, Intracellular calcium-binding proteins: more sites than insights: Trends in Biochemical Sciences, v. 16, p. 98-103.

Hoyle, B.D., and Beveridge, T.J., 1984, Metal binding by the peptidoglycan sacculus of Escherichia coli K-12: Canadian Journal of Microbiology, v. 30, no. 2, p. 204-211.

Karaca, D., Hensen, C., and Wallmann, K., 2010, Controls on authigenic carbonate precipitation at cold seeps along the convergent margin off Costa Rica: Geochemistry Geophysics Geosystems, v. 11, no. 8, p. 1-19, doi: 10.1029/2010GC003062.

Kinniburgha, D.G., Riemsdijkb, W.H. van, Koopalc, L.K., Borkovecd, M., Benedettie, M.F., and Avenac, M.J., 1999, Ion binding to natural organic matter: competition, heterogeneity, stoichiometry and thermodynamic consistency: Colloids and Surfaces A: Physicochemical and Engineering Aspects, v. 151, no. 1-2, p. 147-166.

Linke, P., Wallmann, K., Suess, E., Hensen, C., and Rehder,G., 2005, In situ benthic fluxes from an intermittently active mud volcano at the Costa Rica convergent margin: Earth and Planetary Science Letters, v. 235, no. 1-2, p. 79-95.

Ludwig, R., Al-horani, F.A., Beer, D.D., and Jonkers, H.M., 2005, Photosynthesis-controlled calcification in a hypersaline microbial mat: Limnol. Oceanogr., v. 50, no. 6, p. 1836-1843.

Luff, R., and Wallmann, K., 2003, Fluid flow, methane fluxes, carbonate precipitation and biogeochemical turnover in gas hydrate-bearing sediments at Hydrate Ridge, Cascadia Margin: numerical modeling and mass balances: Geochimica Et Cosmochimica Acta, v. - 67, no. - 18, p. - 3421.

Luff, R., Wallmann, K., and Aloisi, G., 2004, Numerical modeling of carbonate crust formation at cold vent sites: significance for fluid and methane budgets and

chemosynthetic biological communities: Earth and Planetary Science Letters, v. 221, no. 1-4, p. 337-353.

Marshall, A.T., and Wright, A., 1998, Coral calcification: autoradiography of a scleractinian coral Galaxea fascicularis after incubation in 45 Ca and 14 C: Coral Reefs, v. 17, no. 1, p. 37-47, doi: 10.1007/s003380050092.

Michaelis, W., Seifert, R., Nauhaus, K., Treude, T., Thiel, V., Blumenberg, M., Knittel, K., Gieseke, A., Peterknecht, K., Pape, T., Boetius, A., Amann, R., Jørgensen, B.B., Widdel, F., et al., 2002, Microbial reefs in the Black Sea fueled by anaerobic oxidation of methane.: Science (New York, N.Y.), v. 297, no. 5583, p. 1013-5, doi: 10.1126/science.1072502.

Moorehead, H.G., and Briggs, W.R., 1974, 2-Amino-2-methyl-1-propanol as the Akalizing Agent in an Improved Continous-Flow Cresolphtalein Complexone Procedure for Calcium in Serum: Clin. Chem., v. 20, p. 1458-1460.

Morita, R., 1980, Calcite precipitation by marine bacteria: Geomicrobiology Journal, v. 2, no. 1, p. 63-82, doi: 10.1080/01490458009377751.

Mucci, A., 1983, The Solubility of Calcite and Aragonite in Seawater at Various Salinities, Temperatures, and One Atmosphere Total Pressure: American Journal of Science, v. 283, no. 7, p. 780-799.

Naehr, T.H., Eichhubl, P., Orphan, V.J., Hovland, M., Paull, C.K., Ussler, W., Lorenson, T.D., and Greene, H.G., 2007, Authigenic carbonate formation at hydrocarbon seeps in continental margin sediments: A comparative study: Deep-Sea Research Part Ii-Topical Studies in Oceanography, v. 54, no. 11-13, p. 1268-1291.

Nauhaus, K., Boetius, A., Kruger, M., and Widdel, F., 2002, In vitro demonstration of anaerobic oxidation of methane coupled to sulphate reduction in sediment from a marine gas hydrate area: Environmental Microbiology, v. 4, no. 5, p. 296-305.

Oswald, T.J., and MacLennan, D.H., 1974, Isolation Protein of a High Affinity from Sarcoplasmic Calcium-binding Reticulum *: Journal of Biological Chemistry, v. 249, no. 3, p. 974-979.

Partida-Sánchez, S., Cockayne, D. a, Monard, S., Jacobson, E.L., Oppenheimer, N., Garvy, B., Kusser, K., Goodrich, S., Howard, M., Harmsen, a, Randall, T.D., and

Lund, F.E., 2001, Cyclic ADP-ribose production by CD38 regulates intracellular calcium release, extracellular calcium influx and chemotaxis in neutrophils and is required for bacterial clearance in vivo.: Nature medicine, v. 7, no. 11, p. 1209-16, doi: 10.1038/nm1101-1209.

Peckmann, J., Reimer, A., Luth, U., Luth. C., Hansen, B.T., Heincke, C.,Hoefs, J., and Reitner, J., 2001, Methane-derived carbonates and authigenic pyrite from the northwestern Black Sea: Marine Geology, v. 177, no. 1-2, p. 129-150.

Riebesell, U., Revill, A.T., Holdsworth, D.G., and Volkman, J.K., 2000, The effects of varying CO 2 concentration on lipid composition and carbon isotope fractionation in Emiliania huxleyi: Geochimica et Cosmochimica Acta, v. 64, no. 24, p. 4179-4192.

Sommer, S., Linke, P., Pfannkuche, O., Niemann, H., and Treude, T., 2010, Benthic respiration in a seep habitat dominated by dense beds of ampharetid polychaetes at the Hikurangi Margin (New Zealand): Marine Geology, v. 272, no. 1-4, p. 223-232, doi: 10.1016/j.margeo.2009.06.003.

Suess, E., 2010, Handbook of hydrocarbon and lipid microbiology (K. N. Timmis, Ed.): Springer-Verlag, Berlin, Heidelberg.

Tambutté, E., Allemand, D., Bourge, I., Gattuso, J.-P., and Jaubert, J., 1995, An improved 45Ca protocol for investigating physiological mechanisms in coral calcification: Marine Biology, v. 122, no. 3, p. 453-459.

Treude, T. Knittel, K., Wallmann, K., Jørgensen B.,B., 2003, Anaerobic oxidation of methane above gas hydrates at Hydrate Ridge, NE Pacific Ocean: Mar Ecol Prog Ser, v. 264, p. 1-14.

Treude, T., Orphan, V., Knittel, K., Gieseke, A., House, C.H., and Boetius, A., 2007, Consumption of methane and CO2 by methanotrophic microbial mats from gas seeps of the anoxic Black Sea.: Applied and environmental microbiology, v. 73, no. 7, p. 2271-83, doi: 10.1128/AEM.02685-06.

Wegener, G., Niemann, H., Elvert, M., Hinrichs, K.-U., and Boetius, A., 2008, Assimilation of methane and inorganic carbon by microbial communities mediating the anaerobic oxidation of methane.: Environmental microbiology, v. 10, no. 9, p. 2287-98, doi: 10.1111/j.1462-2920.2008.01653.x.

Yates, K., and Robbins, L., 1999, Radioisotope tracer studies of inorganic carbon and Ca in microbially derived CaCO3: Geochimica et Cosmochimica Acta, v. 63, no. 1, p. 129-136, doi: 10.1016/S0016-7037(98)00297-X.

Zeebe, R.E., and Wolf-Gladow, D., 2001, CO2 IN SEAWATER: EQUILIBRIUM; KINETICS; ISOTOPES: Elsevier, Amsterdam, Boston, London, New York, Oxford, Paris, San Diego, San Francisco, Singapore, Sydney.

Zehnder, A.J.B., and Brock, T.D., 1979, Methane formation and methane oxidation by methanogenic bacteria: J Bacteriol, v. 137, p. 420-432.

Chapter 5

Fluid discharge characteristics of two neighboring mounds along the Pacific Costa Rican continental margin classified by direct measurements of microbial methane turnover and carbonate isotopic analyses

Stefan Krause [1], Philip Steeb [1], Christian Hensen[1], Tina Treude [1]

[1] Helmholtz Centre for Ocean Research (GEOMAR), Wischhofstr. 1-3, 24148 Kiel

ABSTRACT

Subduction of the oceanic Cocos plate offshore Costa Rica causes strong advection of methane-charged fluids leading to high microbial anaerobic oxidation of methane (AOM) and sulfate reduction (SR) in surface sediments. Previous benthic chamber experiments and numerical modeling indicated the upward flow of methane charged fluid is differing by approximately one order of magnitude between two neighboring mounds, Mound 11 and 12, potentially affecting local AOM and SR rates. Presented here are the first direct measurements, using, of microbial AOM and SR rates in sediments from the two mounds, applying radiotracer techniques during cruise RV-SO206. Additionally, analysis of carbonate $\delta^{18}O$ and $\delta^{13}C$ were performed to constrain the origins of the carbonate precipitating fluid. Peak rates of microbial activities showed differences with a factor of 4.8 to 6.3 between Mound 11 [AOM 140.71 (SD 40.84); SR 117.25 (SD 82.06) mmol m^{-2} d^{-1}, respectively] and Mound 12 [AOM 22.37 (SD 0.85); SR 23.99 (SD 5.79) mmol m^{-2} d^{-1}, respectively]. Analysis of stable oxygen and carbon isotope variations of authigenic carbonates from the two locations showed higher values for Mound 11 ($\delta^{18}O$ 4.7 to 5.9‰, $\delta^{13}C$ -21.0 to -29.6‰), compared to Mound 12 ($\delta^{18}O$ 4.1 to 4.5‰, $\delta^{13}C$ -45.7 to -48.9‰). These results are in accord with previous work, defining the investigated cores of this study as representative and supporting a dominated deep fluid source for Mound 11 versus a rather shallow source of biogenic methane for Mound 12. The present study demonstrates that the combination of microbial rate measurements in combination with the analyses of carbonate archives, provide a suitable approach to constrain temporal and spatial variations of methane charged fluid flow at the Costa Rican continental margin.

INTRODUCTION

Areas of oceanic plate subduction represent sites of convection driven down welling of the oceanic plate below the continental plate, an essential process for

geochemical cycling between the crust and mantle. Along with oceanic crust material, water and volatiles are subducted into the mantle. During the decent, these components are exposed to increasing pressure and temperature, causing alteration of the chemical (Manning, 2004) and isotopic signatures (Ellam and Hawkesworth, 1988). As a result of hydraulic pressure, pore water buoyancy, diagenetic and higher metamorphic mineral reaction as well as dewatering processes, upward directed fluid fluxes can be observed in the area of the fore arc (Scambelluri et al., 2007).

During the ascent, fluids are often charged with elements, ions and gasses encountered. Depending on velocity and flux, fluid exits at the sediment surface, commonly known as cold seeps, can be associated with different geological formations such as crater-like structures (pockmarks) or mud extrusions (mounds, volcanoes) (Judd et al., 2002). Cold seeps are often characterized by authigenic carbonate concretions produced by microbial activity (Suess, 2010).

The prerequisite for microbial related authigenic carbonates at cold seeps is the advection of methane (CH_4). In marine sediments, CH_4 is formed either as the result of microbial (biogenic CH_4) or thermal (thermogenic CH_4) degradation of organic matter (Schoell, 1988; Thauer, 1998). In anoxic sediments, CH_4 removal is mediated by microbial sulfate (SO_4^{2-})-dependent anaerobic oxidation of methane (AOM) (Boetius et al., 2000). The general reaction of AOM is (Barnes and Goldberg, 1976):

$$CH_4 + SO_4^{2-} \rightarrow HCO_3^- + HS^- + H_2O \quad (1)$$

AOM and sulfate reduction (SR) increases porewater alkalinity, producing bicarbonate (HCO_3^-), which can partly dissociate into carbonate (CO_3^{2-}). In the case of supersaturation, carbonate minerals may form, predominantly with Ca^{2+} ions (Peckmann et al., 2001). Previous field studies have confirmed that authigenic carbonate formation is closely associated to high CH_4 flux and AOM activity (e.g. Bohrmann et. al., 1998; Greinert et. al., 2001). The resulting carbonates usually exhibit micritic crystal morphology and are frequently aggregated to larger

concretions (Naehr et al., 2007). Massive crusts of authigenic carbonates in surface sediments are frequently encountered at fluid venting locations as a direct result of microbial AOM (Luff et al., 2004). The chemical and isotopic compositions of authigenic carbonates provide information concerning the fluids present during precipitation (Naehr et al., 2007; Peckmann et al., 2001). Therefore, authigenic carbonates represent a suitable archive of the palaeo- hydrological and geological settings present during precipitation.

The present study reports AOM and SR rates, obtained during the SO206 research cruise, from two adjacent mud extrusions (Mound 11 and 12) located at the subduction zone forearc off the Pacific Costa Rican coast. Microbial turnover rates and stable isotope signatures of carbonate samples retrieved from the same sites are in accordance with hypothesized fluid discharge processes.

MATERIAL AND METHODS

Geological Settings and study sites

The Middle American Trench is a large-scale subduction zone with a length of 2750 km located off the southwestern coast of Central America. Offshore Costa Rica, the trench is formed by the eastward subduction of the oceanic Cocos plate beneath the Carribbean plate. A characteristic feature of this trench is the subduction of seamounts and ridges (Hensen et al., 2004). As these structures are thrusted into and below the continental plate, subduction of material may cause fractures in the upper plate and overlying shelf sediments through which fluids rise towards the surface (Ranero et al., 2000).

Fluid uprise within the forearc of the continental plate is accompanied with mud extrusions that form aggregations, which are termed mounds. These structures are ubiquitous at the continental margin off Costa Rica (Hensen and Wallmann, 2005). The present study focused on the two neighboring mounds, Mound 11 and 12 (Fig. 1 & 2), which are situated north-east of the Osa Peninsula (Greinert et al., 2001;

Bohrmann et al., 1998) in water depths at ~1000 m (Klaucke et al. 2008). Mound 11 is located at 08°55'20"N and 84°18'14"W, including two summits that are ~ 300 m apart, each ~ 250 m in diameter (Klaucke et al. 2008). Previous investigations, including sediment sampling and video survey, showed that the Mound 11 surface consists of fine-grained sediment with mats of sulfur bacteria (Schmidt et al., 2005; Mörz et al., 2005; Mau et al., 2006).

Mound 12 is located about 1 km north of Mound 11 and is characterized by a differing geological morphology, including a solitary summit with a diameter of ~ 800 m (Klaucke et al. 2008). Sediment sampling and video surveys of the sediment surface revealed fine-grained sediment and typical cold-seep features, such as mats of sulfur bacteria, fields of chemosymbiotic mytilid mussles and carbonate precipitates (Mau et al., 2006; Linke et al., 2005).

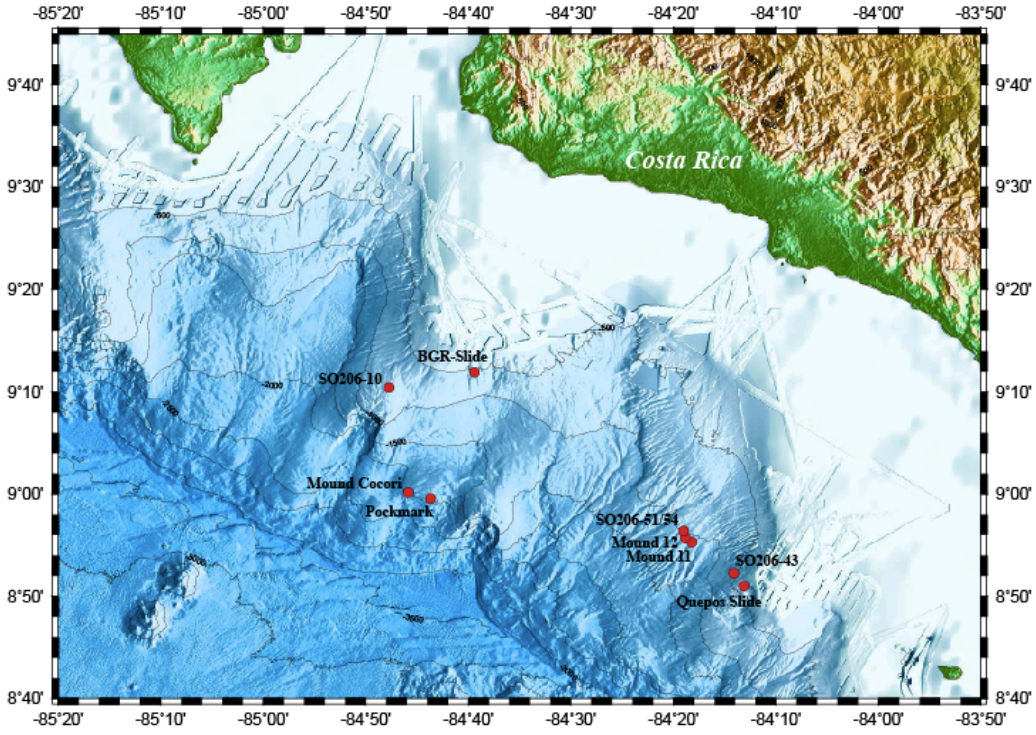

Figure 1. Bathymetric map of the pacific continental slope of Costa Rica, sampling sites during SO206 are indicated (Source: GEOMAR, Cruise Report SO206).

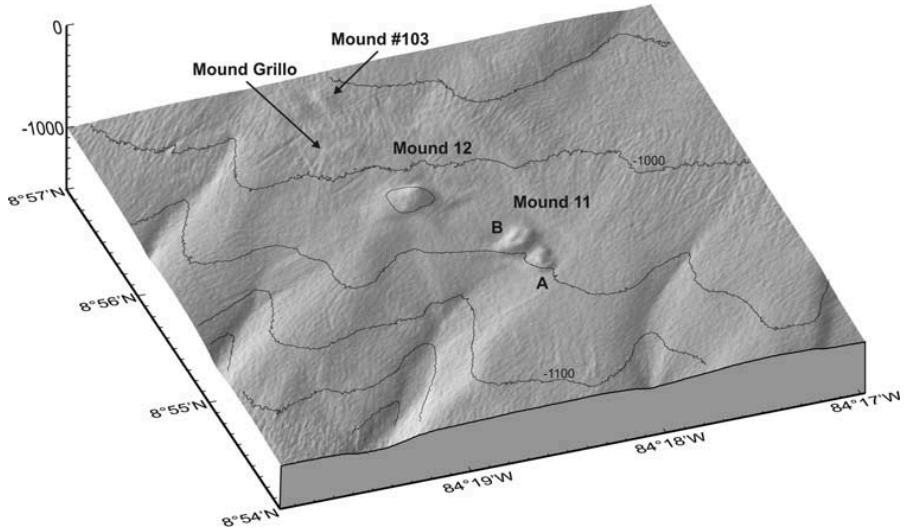

Figure 2. Relief map of the study area offshore Costa Rica showing Mound 11 and 12. Source: Klaucke et al. (2008).

Sampling and analytical methods

Sediment samples from Mound 11 and 12 were obtained during the research expedition SO206 (30.05.-19.06.2010) onboard the German RV Sonne. Sediment recovery stations on both mounds were situated in water depths between 1000 - 1010 m water depth (Table 1.), at Mound 11 partially accompanied by the occurrence of gas hydrates. Samples were collected with a gravity corer (GC) and a video-guided multicorer (MUC). MUC sampling was performed at locations with microbial mats of filamentous sulfur-oxidizing bacteria (Fig. 3, b) visible on the sediment surface, indicating areas of high CH_4 flux (Treude et al., 2003).

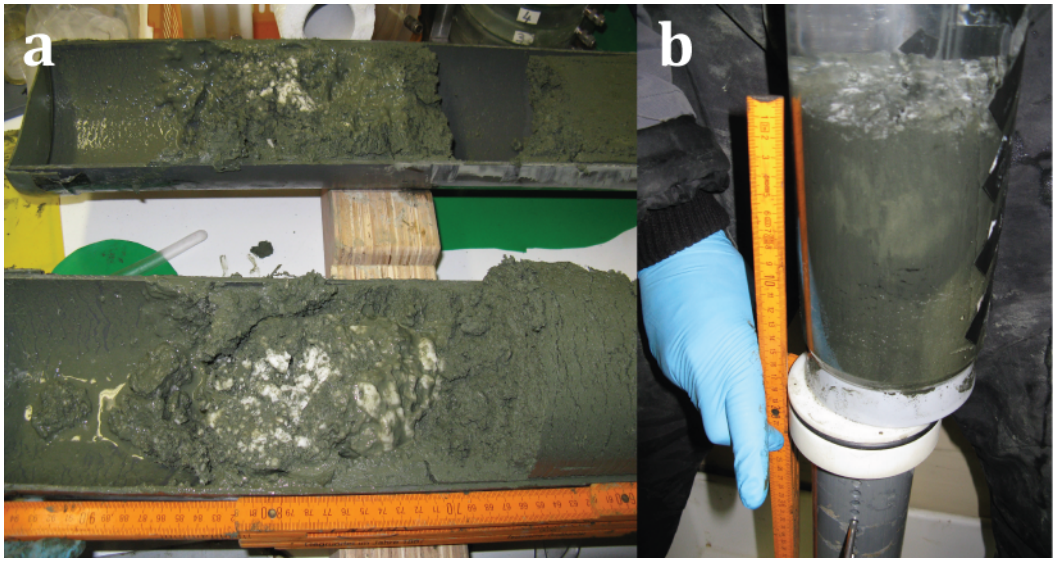

Figure 3**.** Pictures from retrieved sediments: (a) solid piece of gas hydrate captured in GC 50 (Mound 11); (b) core liner of MUC 46 filled with Mound 11 surface sediment covered by a mat of white sulfur bacteria.

Table 1. List of stations, sampled at Mound 11 and 12.

St. No	Location	Instrument	Lat. N°	Lon. W°	Water depth (m)	Sediment	Features
SO206-39	Mound 11	TV-MUC	8° 55.34′	84° 18.23′	1005	black-grey, soft	Bacterial mat
SO206-50	Mound 11	GC	8° 55.33′	84° 18.23′	1003	Green-gray, soft	Gas hydrate
SO206-44	Mound 12	TV-MUC	8° 55.69′	84° 18.79′	1007	black-grey, soft	Bacterial mat
SO206-46	Mound 12	TV-MUC	8° 55.72′	84° 18.83′	1009	black-grey, soft	Bacterial mat

Core processing for porewater extraction

GC 50 was sectioned into 1 m intervals and cut in half. One half was stored at 4°C, serving as archive. The other half was used for sediment and porewater sampling. Nine samples were obtained in 30- 45 cm intervals over a total length of 300 cm for porewater extraction. From each MUC cast (Mound 11, MUC 39; Mound 12, MUC 44

& 46), one core was assigned for sediment porewater analysis. Sediment obtained by the three MUCs was sampled at 7 depths between core top and bottom.

Porewater analysis

Porewater was gained from sediments using a pressure filtration system (argon 3-4 bars, 0.2 µm regenerated cellulose filters). Retrieved porewater was analyzed on board for total alkalinity, silicate (SiO_4), sulfide (HS^-), and ammonium (NH_4^+). The remaining porewater was stored frozen at -20°C for analysis of dissolved ions with inductively coupled plasma optical emission spectrometry (ICP-OES) at facilities at GEOMAR, Kiel.

***Ex situ* microbial turnover rates of methane and sulfate**

Immediately after retrieval of the MUC, six replicate polycarbonate push- cores (3 for AOM rates, 3 for SR rates, inner diameter 26 mm, length 25 cm) were sampled from pristine surface sediment of one multicorer core (inner diameter 100 mm). Sediment from gravity corers was sampled with six 5 ml glass tubes, closed with syringe puncheons, dipped in Antifoam®, to enable a better gliding. Open ends of push-cores and glass tubes were closed with rubber stoppers for anoxic incubation. In addition, 10 controls (5 ml each) were sampled from sediment from the same core using 5 ml syringes with cut off tips.

Anaerobic oxidation of methane (AOM)

On board radioactive CH_4 ($^{14}CH_4$ dissolved in water, 15 µl injection volume, activity 1-2 kBq, specific activity 2.28 GBq $mmol^{-1}$) was injected into replicate push cores at 1-cm intervals according to the whole-core injection method of Jørgensen (1978). After tracer injection, push cores were incubated at in situ temperature (8°C) for 24 hrs in the dark. Subsequently, microbial activity was terminated by sectioning 1-cm intervals of sediment into 50 ml glass vials with 25 ml of sodium hydroxide (2.5%

w/w). Vials were closed immediately after sediment transfer and shaken vigorously before storage. Controls were first transferred into sodium hydroxide before addition of radiotracer. At GEOMAR (Kiel), AOM rates were determined after (Treude et al., 2005) (gas chromatography and $^{14}CH_4$ combustion) and (Joye et al., 2004) ($^{14}CO_2$ trapping).

Sulfate reduction (SR) rates

Sampling, injection, and incubation conditions were identical to that of the AOM samples. The injected radiotracer was $^{35}SO_4$ (dissolved in water, 6 µl injection volume, activity 200 kBq, specific activity 37 TBq $mmol^{-1}$). After 24 hrs, microbial activity was terminated by sectioning 1-cm intervals of sediment into 50-ml plastic centrifuge vials filled with 20 ml zinc acetate (20% w/w). Controls were first transferred into zinc acetate before addition of radiotracer. SR rates were determined using the cold-chromium distillation method by Kallmeyer et al. (2004).

Carbonate sampling

Carbonate blocks present in GC and MUC samples that were between 2 and 12 cm in length, were picked with gloves, wrapped in aluminum foil, and subsequently stored at -20 °C. Two bivalve shell fragments found within sediment from SO206-MUC 39 were sampled accordingly (Table 2).

Determination of methane (CH_4) concentrations

CH_4 was stripped from sediments according to the method of McAullife (1971). Sediment plugs were recovered using a 10 ml clean disposable polypropylene syringe that had the end cut off. The sediment plug was immediately injected in a 30 ml glass vial filled with 10 ml of 10% aqueous solution of potassium chloride (KCl). The vial was sealed and vigorously shaken to disaggregate the mud and to stop all bacterial activity via KCl poisoning (Bowes and Hornibrook, 2006). The sample was stored upside down, to minimize potential gas exchange with the atmosphere, and

allowed to equilibrate with the vial headspace for 48 hrs. The gas was extracted with a syringe while injecting an equivalent amount of 10% KCl solution. A blank sample (air equilibrated with 10% KCl solution) was taken for background corrections. The KCl solution was not acidified so as to avoid production of CO_2 by dissolution of carbonate minerals. The headspace gas was later transferred into either a 10 or 20 ml sterile serum vial, filled (bubble-free) with a pH 1, 10% KCl solution, by displacement of an equivalent amount of solution. The vials were stored upside down. The CH_4 concentration was determined onboard by Gas Chromatography-Flame Ionization Detection (GC-FID) using a Shimadzu GC14A instrument fitted with a Restek Rt® Alumina Bond/KCl capillary column (50m, 0.53mm ID) operated at 60°C. N2 was used as a carrier gas.

X-ray diffraction of carbonates

Carbonate samples and bivalve shell fragments were dried at 37°C for 12 hrs and gently cleaned of sediment remains. The top surface from each carbonate piece was scoured away in an area of ~5 x 5 mm. Subsequently, a small cavity was drilled to yield mineral powder. Powder from carbonate samples were analyzed for mineralogy using x-ray diffraction (Philips X-ray diffractometer PW 1710 with monochromatic CuKα) between 2 and 70 2θ. The resulting spectra were analyzed with the software XPowder (XPowder, Spain).

Table 2. List of carbonate samples from Mound 11 and 12 used for mineralogy and stable isotope analysis. Grey background indicates samples of bivalve shell fragments. cmbsf = centimeters before seafloor.

Area	Sample ID	Depth (cmbsf)
Mound 11	SO 206-38-GC	172-185
Mound 11	SO 206-39-MUC	8
Mound 11	SO 206-39-MUC	10-12
Mound 11	SO 206-39_MUC	11
Mound 11	SO 206-39-MUC	20-25
Mound 11	SO 206-39-MUC	26-30
Mound 11	SO 206-39-MUC, **Shell**	25
Mound 11	SO 206-39-MUC, **Shell**	26-30
Mound 12	SO 206-44-MUC	5-8
Mound 12	SO 206-46-MUC	6-7

Stable isotope analysis of carbonates

From each homogenized carbonate powder sample (see above), an aliquot of 10 mg was separated for carbon $\delta^{13}C$ and oxygen $\delta^{18}O$ stable isotope analysis. A fraction from this (approximately 1 mg) was dissolved by water-free phosphoric acid at 73°C in a "Carbo-Kiel" (Thermo Fischer Scientific Inc.) online carbonate preparation line and measured for carbon and oxygen stable isotope ratios with a MAT 253 mass spectrometer (Thermo-Fischer Inc.). The $\delta^{13}C$ and $\delta^{18}O$ values are reported as ‰ deviations from laboratory standard referred to the PDB scale.

RESULTS

Porewater chemistry and microbial turnover rates

Biogeochemical profiles obtained at Mound 11 (Figure 4) by MUC 39 and GC 50, respectively, revealed considerable differences regarding the vertical extension of the sulfate-methane transition zone (SMT) and the location of peak microbial

turnover rates of CH_4 and SO_4^{2-}. Sediment from MUC 39 was characterized by a rapid decline of SO_4^{2-} from a surface concentration of 27.4 mmol l^{-1} to < 0.5 mmol l^{-1} within the first 6 cm below seafloor (cmbsf). CH_4 concentration increased from 2 mmol l^{-1} at 21 cmbsf to 17.9 mmol l^{-1} at 7.5 cmbsf. Towards the surface, values further declined to 0.6 mmol l^{-1} sediment. The SMT was located at ~5 cmbsf.

In contrast, SO_4^{2-} in GC 50 decreased from a surface concentration of 27.5 mmol l^{-1} to < 0.5 mmol l^{-1} at 150.5 cmbsf. CH_4 concentration declined from 5.1 mmol l^{-1} sediment at the bottom of the core (290 cmbsf) to 1.9 mmol l^{-1} sediment at 210 cmbsf. At 190 cmbsf methane increased to 20.9 mmol l^{-1} sediment, followed by a rapid decline to a surface concentration of 0.06 mmol l^{-1} sediment. Compared to MUC 39, the SMT of GC 50 sediment was located much deeper, ~125 cmbsf. Peak rates for AOM and SR were 0.01, and 0.017 µmol cm^{-3} d^{-1}, respectively. Corresponding areal rates, integrated, over the sampled core length (290 cm) yielded 4.76 (SD 2.21) mmol m^{-2} day^{-1} for AOM and 45.48 (SD 53.67) mmol m^{-2} day^{-1} for SR, respectively However, highest HS^- (2.3 and 4.4 mmol l^{-1}) and total alkalinity (2.1 and 4.2 mEq) levels of MUC 39 and GC 50 were in the same order of magnitude.

The two cores, MUC 44 and 46, retrieved at Mound 12 (Figure 5) revealed different profiles of SO_4^{2-} and CH_4 concentration. In MUC 44, SO_4^{2-} decreased gradually from surface concentrations of 28.4 to 4.2 mmol l^{-1} between 5-7 cmbsf. Subsequently, SO_4^{2-} concentration declined to 1.4 mmol l^{-1} at the core bottom (13 cmbsf). CH_4 concentrations in MUC 44 fluctuated between 1 and 12 mmol l^{-1} sediment below 7.5 cmbsf. Between 6.5 to 2.5 cmbsf, CH_4 increased to ~14 mmol l^{-1} sediment, consecutively declining to 3.5 mmol l^{-1} sediment at the surface. Due to the presence of massive carbonate layers in the sediment, MUC 46 core liner penetration depth was limited to 12 – 15 cmbsf. SO_4^{2-} declined from surface concentrations of 28.3 mmol l^{-1} to 11.5 mmol l^{-1} at 9 cmbsf. CH_4 increased from 1.3 to 19.1 mmol l^{-1} sediment between 11 and 9 cmbsf, declining rapidly to < 0.2 mmol l^{-1} sediment. Highest rates for AOM and SR at Mound 12 were measured between 3 and 5 cmbsf with peak values of 1.7 and 2.3 µmol cm^{-3} d^{-1}, respectively. Integration from the sediment–water interface to a sediment depth of 10 cm yielded rates of 22.37 (SD 0.85) and 23.99 (SD 5.79) mmol m^{-2} day^{-1} for AOM and SR, respectively. At Mound 11

AOM and SR rates showed peak values between 2 and 5 cmbsf of 4.4 and 8.1 µmol cm^{-3} d^{-1}, respectively. Corresponding areal rates, integrated rates over a core length of 10 cm, were 140.71 (SD 40.84) mmol m^{-2} day^{-1} for AOM and 117.25 (SD 82.06) mmol m^{-2} day^{-1} for SR, respectively.

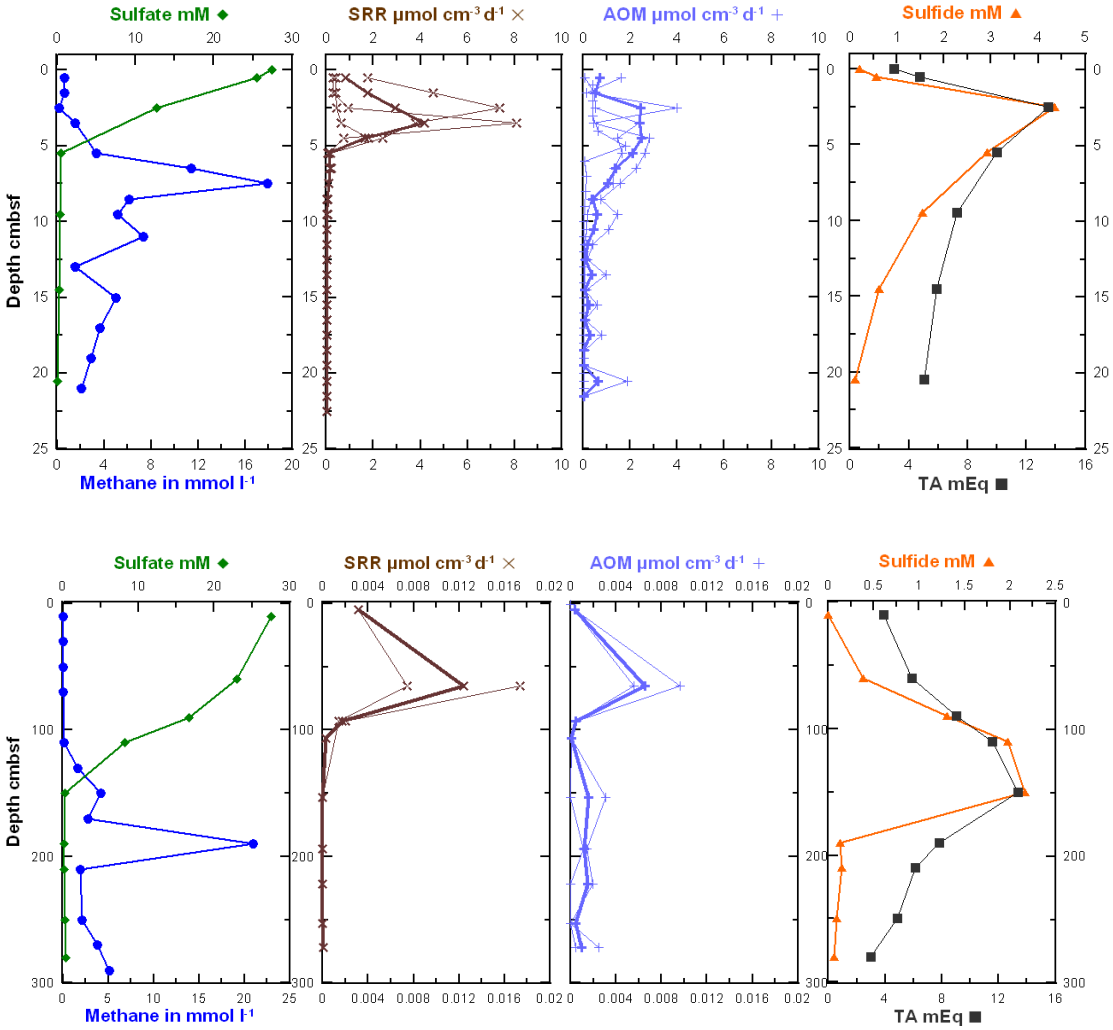

Figure 4. Mound 11 porewater profiles for sulfate, methane, SR, AOM, sulfide, and total alkalinity (TA). Top: MUC 39 (covered by bacterial mat), bottom: GC 50.

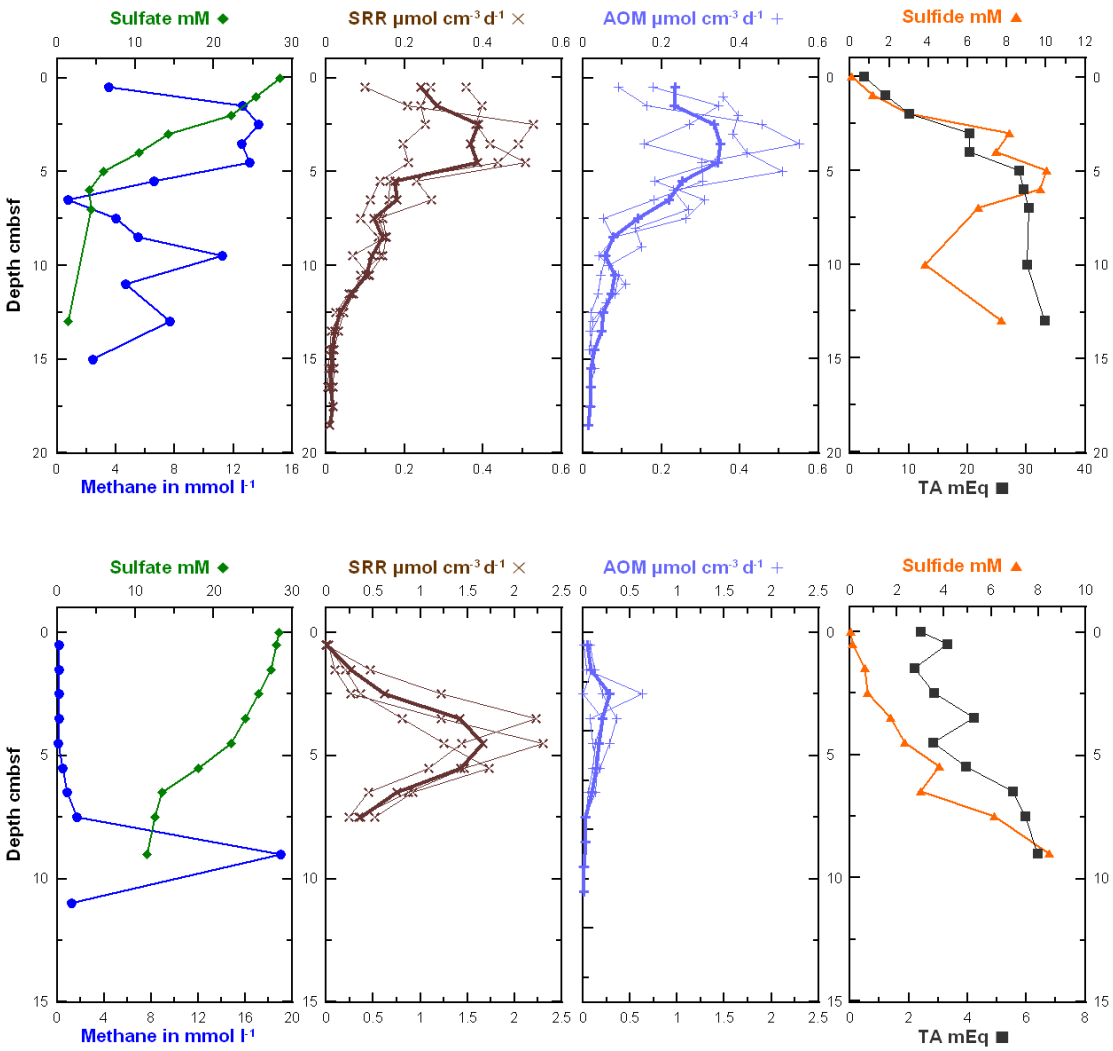

Figure 5. Mound 12 porewater profiles for sulfate, methane, SR, AOM, sulfide, and total alkalinity (TA). Top: MUC 44 (covered by bacterial mat), bottom: MUC 46 cores (covered by bacterial mat).

In accordance with peak AOM and SR, highest concentrations of total alkalinity and sulfide, end products of AOM, were also located within the SMT (Figure 4 and 5). In both cores, the methane profile revealed a sharp peak located below the SMT zone. In the GC 50 core, the CH_4 peak coincided with a large block of gas hydrate located at ~12 cmbsf (Figure 2). Therefore, we assume that gas hydrate dissociation during core retrieval has caused the local CH_4 peak in the sediment.

Carbonate mineralogy and isotopic composition

The results for carbonate mineralogy and isotopic composition of oxygen and carbon of sampled carbonate concretions are compiled in Table 3. XRD analyses confirmed

high carbonate concentrations of the concretions, ranging between 77% and 82% at Mound 11 and 12. XRD spectra further showed that the carbonate samples mainly consisted of Mg-calcite, generally accounting for > 51% of the carbonate mass. Mg-free calcite was also present, contributing between 23% and 30% to the carbonate mass. At Mound 11, also ferric dolomite and kutnohaurite appeared in samples collected from sediment depths >10 cmbsf. However, relative contribution to the carbonate mineral phases did not exceed 8 %. Bivalve shell fragments from Mound 11 differed from authigenic carbonate samples, consisting of organic material and aragonite as the dominant mineral phase.

Table 3. Mineralogy and stable isotope composition of carbonate samples obtained from Mound 11 and 12. Grey background indicates samples of bivalve shell fragments.

Area	Sample ID	Carbonate content	Carbonate minerals				$\delta^{13}C$	$\delta^{18}O$
Mound 11	SO 206-38-GC, 172-185 cm	81.70%	Mg calcite	56.30%	Calcite	25.40%	-27.135	5.649
Mound 11	SO 206-39-MUC, 8 cm	81.10%	Mg calcite	57.70%	Calcite	23.40%	-26.214	5.871
Mound 11	SO 206-39-MUC, 10-12 cm	72.80%	Mg Calcite	65.20%	Dolomite, ferr.	7.60%	-21.202	4.724
Mound 11	SO 206-39-MUC, 11 cm	81.60%	Mg calcite	52.30%	Calcite	29.30%	-27.492	5.712
Mound 11	SO 206-39-MUC, 20-25 cm	75.20%	Mg Calcite	68.80%	Kutnohaurite	6.40%	-29.562	6.148
Mound 11	SO 206-39-MUC, 26-30 cm	70.80%	Aragonite	57.00%	Mg calcite	13.80%	-29.008	5.845
Mound 11	SO 206-39-MUC, **Shell**, 25 cm	50.80%	Aragonite	38.80%	Mg calcite	12.00%	-6.98	3.547
Mound 11	SO 206-39-MUC, **Shell**, 26-30 cm	58.70%	Aragonite	58.70%	organic	41.30%	-9.61	3.961
Mound 12	SO 206-44-MUC, 5-8 cm	77.40%	Mg calcite	51.70%	Calcite	25.70%	-48.981	4.147
Mound 12	SO 206-46-MUC, 6-7 cm	77.00%	Mg calcite	52.60%	Calcite	24.40%	-45.702	4.476

Stable isotope analyses of carbonates

The carbonate samples from Mound 11 were characterized by $\delta^{13}C$ values ranging from -30‰ to -21‰ (Table 3, Fig. 6). Corresponding $\delta^{18}O$ values varied between 4.7‰ and 6.2‰. The carbon and oxygen isotopic signatures of the two carbonate samples obtained from Mound 12 were in general more negative. Values for $\delta^{13}C$ were -49‰ and -46‰, $\delta^{18}O$ ranged between 4.1 and 4.5‰. Isotopic signatures of the two bivalve shell fragments deviated from the authigenic carbonate samples with $\delta^{18}O$ being more negative (3.5 - 4.0‰) and $\delta^{13}O$ values being considerably more positive (-9.6 – 6.9‰).

DISCUSSION

In the present study, the considerable differences of AOM and SR as well as $\delta^{18}O$ and $\delta^{13}C$ isotopic signatures of carbonates from surface sediment samples of the two neighboring mounds are indicative for different fluid regimes underlying them. AOM and SR rates obtained from Mound 11 were one order of magnitude higher compared to Mound 12, and were in the same order of rates reported for high-advective cold-seep systems such as Hydrate Ridge (Treude et al., 2003) and Håkon Mosby Mud Volcano (Niemann et al., 2006) (Table 4). To our knowledge, areal AOM rates of Mound 11 exceed highest values published for marine cold-seep locations so far (e.g. Treude et al., 2003; Joye et al., 2004; Krüger et al., 2005). The observed difference in AOM and SR rates between the two mounds might be due to different advectice transport velocities of methane charged fluid. This hypothesis is supported by previous reactive-transport modeling (Mound 11) and benthic flux chamber experiments (Mound 12) (Karaca et al., 2010; Linke et al., 2005). According to these studies, fluid flux at Mound 11 might be as high as 200 cm yr^{-1}, while only approximately 10 cm yr^{-1} was calculated for Mound 12.

It should be mentioned that the here observed differences in AOM and SR rates of one order of magnitude in surface sediments covered by thick sulfur bacteria mats illustrates the wide range of methane turnover that can be connected with this type of chemosynthetic habitat. Sulfur bacteria are capable of oxidizing sulfide (Jørgensen and Nelson, 2004), and are typically present at localities of high anaerobic methane turnover (Treude et al., 2003). However, the variability of AOM rates underneath sulfur bacteria mats observed in our study, calls for caution with respect to extrapolations of methane turnover rates based solely on visual seafloor observations.

Table 4. *Ex situ*-rates of anaerobic oxidation of methane (AOM) and sulfate reduction (SR) obtained from SO206 MUC sediment cores, in comparison with previous studies.

	AOM mmol m^{-2} day^{-1}	SRR mmol m^{-2} day^{-1}	Depth of integration (cm)	AOM Modeled[†]	Depth of integration (cm)
Pockmark[#]	4.01 (± 3.86)	1.19 (± 0.21)	0-10	9.17	0-15
Quepos slide[#]	36.67 (± 11.70)	208.36 (±165.05)	0-10	58.4	0-41.5
Mound 11[#]	140.71 (± 40.84)	117.25 (± 82.06)	0-10	9.64	0-27.5
Mound 12[#]	22.37 (± 0.85)	23.99 (± 5.79)	0-10		
Hydrate Ridge	99.00 (± 102.00)	65.00 (± 58.00)	0-10	Treude et al. 2003	
Mound 12	16.11		0-10	Linke et al. 2005	
Håkon Mosby	19.45 (± 5.48)		(± 102.00)	Niemann et al. 2006	

standard variation given as ±

[#] Steeb & Krause, unpubl. data; data gained during expedition SO206

[†] Karaca et al. 2010

The more positive $\delta^{18}O$ values of carbonates from Mound 11 indicate that this location might be under considerable influence of a deep-source fluid, supporting previous investigations (Han et al., 2004; Mavromatis et al., submitted). In contrast, less positive $\delta^{18}O$ values of Mound 12 carbonates suggest extended mixing of deep-source fluid with oceanic bottom water, also postulated by Mavromatis et al. (submitted). Carbon isotopic signatures of methane largely depend on its formation process, with thermogenic methane being generally less depleted than biogenic (Coleman and Risatti, 1981).

While the observed microbial turnover rates of methane indicate differences in fluid flux and corresponding methane supply, the discrepancy of $\delta^{18}O$ and $\delta^{13}C$ isotopic signatures of carbonate suggest a different origin of fluids at Mound 11 and 12. Carbonates of the two mounds were mainly composed of Mg-calcite that was strongly depleted in ^{13}C. Mound 11 showed $\delta^{13}C$ values between -21 and -30‰, while $\delta^{13}C$ values ranged between -45 and -49‰ at Mound 12. Corresponding $\delta^{18}O$ values showed enrichment in ^{18}O at Mound 11 (4.7 – 6.2‰) and Mound 12 (4.1 – 4.5‰). These results confirmed previous analyses of samples from the study area (Han et al., 2004). Depletion of the heavier ^{13}C and accumulation of heavier ^{18}O isotope in carbonates is a consequence of a kinetic carbon isotope fractionation

during AOM (Bohrmann et al., 1998; Reitner et al., 2005; Teichert et al., 2005). Hence, the isotopic signature of the carbonate concretions, sampled at the two mounds, reflect fluid characteristics present during precipitation. According to Hensen et al. (2004), the observed positive $\delta^{18}O$ values of carbonates from the study area are the result of clay-mineral dehydration at temperatures between 85 and 130°C in ~12 km depth and subsequent upward fluid transport. Thus, the observed difference in ^{18}O enrichment of carbonates from Mound 11 and 12 might be the result of different admixing of deep source fluid with bottom water. In comparison, carbonate concretions at Mound 11 were less depleted in $\delta^{13}C$, suggesting methane of thermogenic origin predominantly present during concretion formation (Schmidt et al., 2005). In contrast, methane of biogenic origin from a shallower source might have been causative for strongly depleted $\delta^{13}C$ in Mound 12 carbonates (Hensen and Wallmann, 2005).

Han et al. (2004) identified five types of authigenic carbonate associated to fluid vent locations at the Costa Rica margin, based on morphological, petrological, and stable isotope criteria (referred to the PDB scale): chemoherm carbonates, seepage-associated concretions, gas hydrate-associated concretions, as well as calcareous and dolomitic concretions. Regarding the isotopic composition, the carbonate samples obtained for Mound 11 and 12 during the SO191 cruise can visually be divided into two groups (Fig. 6). Group 1 was comprised of Mound 11 carbonates samples, while group 2 included samples from Mound 12. Carbonates from group 1 were characterized by $\delta^{18}O$ values between + 5.6 to +6.7‰. Corresponding $\delta^{13}C$ values ranged from -21 to -29‰. According to the carbonate classification mentioned above, group 1 carbonate-isotope composition is indicative for gas hydrate-associated concretions ($\delta^{18}O$ 5.2 – 6.8‰, $\delta^{13}C$ -18.6 - -29.8‰) (Han et al. 2004). This type of carbonate is characterized by layered high Mg-calcite and aragonite precipitated into spaces, previously occupied by gas hydrates before dissociation (Bohrmann et al., 2002; Suess, 2002). The carbonates from group 2 had a more negative $\delta^{18}O$ signature, while depletion of ^{13}C was stronger compared to group 1. According to Han et al. (2004), carbonates of group 2 showed an isotopic combination typical for seepage-associated concretions ($\delta^{18}O$ 4.3 – 5.4‰, $\delta^{13}C$ -44.6

– -53.0‰). This type of carbonate occurs at or near the seafloor, forming small, individual carbonate blocks, concretions and crusts of high Mg- calcite. Bivalve shell material from Mound 11 was mainly composed of aragonite and organic components. Corresponding values of $\delta^{13}C$ showed an isotopic signature considerably more positive compared to the carbonates, indicating shell formation in seawater with atmospheric CO_2 as a carbon source (Emrich et al., 1970).

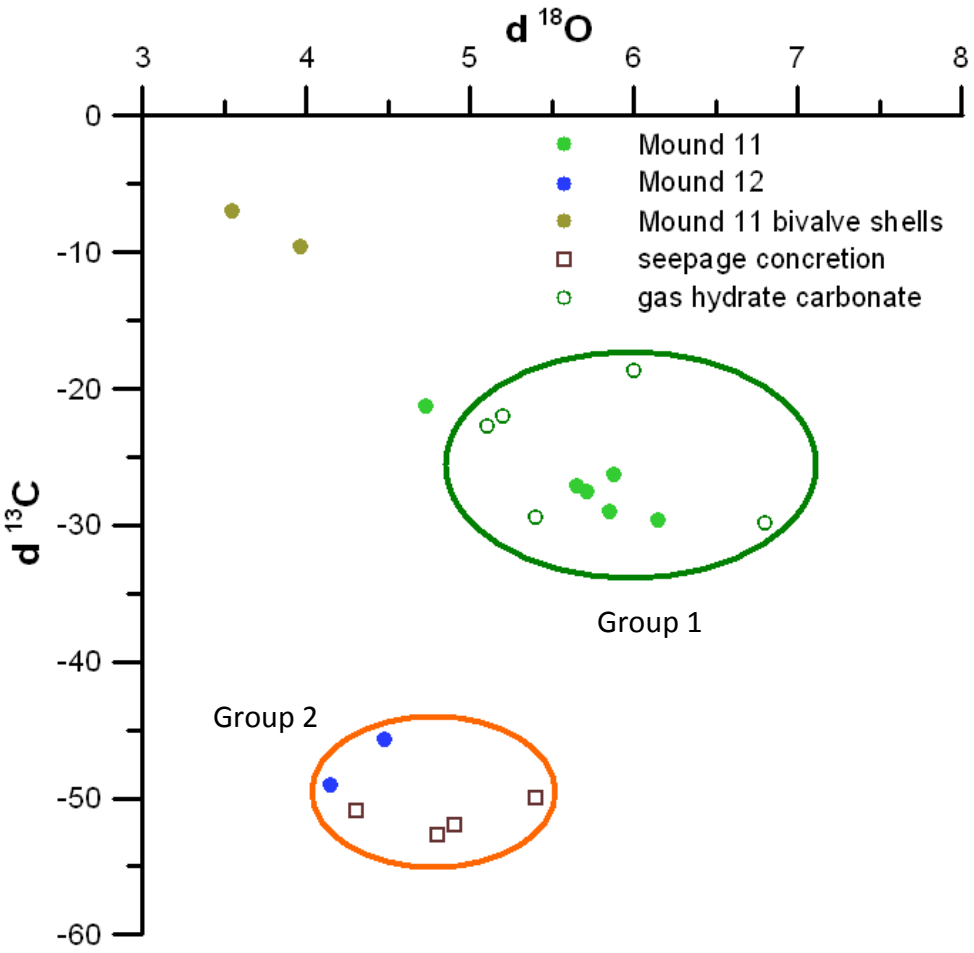

Figure 6. $\delta^{13}C$ vs. $\delta^{18}O$ plot of carbonate material sampled from various locations during SO206 (solid symbols). Open symbols and non-stochastic grouping, based on isotopic, petrographic, mineralogic and morphological similarities represent results from Han et al. (2004). All values referred to the PDB scale.

According to U/Th dating on carbonates and sediment layers from the two locations (Kutterolf et al., 2008), Mound 11 is considered as currently active, i.e. it is emanating mud onto the surrounding seafloor since ≥15 ka (Fig. 7). In contrast, pelagic surface sediments at Mound 12 indicated that vertical mud transport is currently inactive and has been since at least 5 ka.

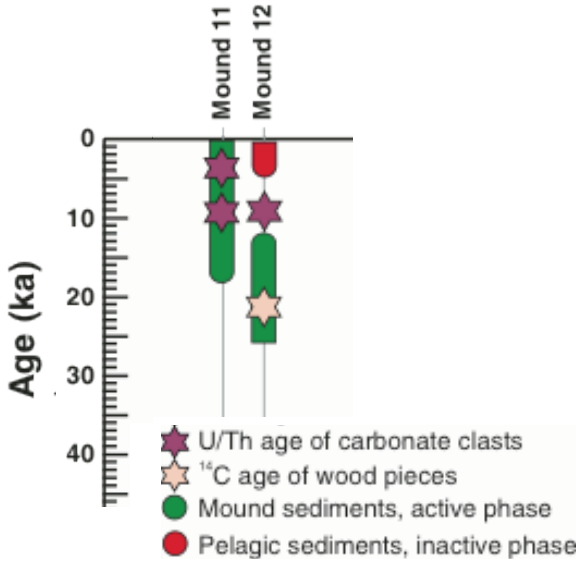

Figure 7. Ages of sediment packages generated during active venting (green bars) and of intervals of pelagic background sedimentation (red bars). Colored stars indicate ages of authigenic carbonate cements, carbonate clasts, and wood pieces, which overlap with active periods. Extracted from Kutterolf et al. (2008).

In contrast, the results of the present study and previous work (Linke et al., 2005) clearly demonstrated recent methane-related microbial activity at both mounds. Consequently, Mound 12 has to be anticipated as a site of active fluid venting, delivering sufficient methane to support related microbial activity. Contrary to Mound 11, fluid advection is currently insufficient to induce vertical transport and extrusion of mud. As both mounds are situated on the same fault zone, ascending fluids originate from the same source (Hensen et al., 2004). Due to past tectonic activities, the fluid pathway of Mound 12 might have been compromised, reducing deep source fluid advection at this location. The more negative $\delta^{18}O$ values of Mound 12 carbonates suggest that surfacing fluid at this location represents a mixture of deep source fluid with diagenetic bottom water. While carbonate $\delta^{13}C$

values indicated that fluids at Mound 11 are primarily charged with deep source thermogenic methane, ascending fluids at Mound 12 include a mixture of thermogenic and biogenic methane, the latter originating from a shallower source.

CONCLUSIONS

Methane charged fluid advection is causative for high microbial activity in surface sediments of two neighboring mounds, Mound 11 and 12. Anaerobic oxidations of methane (AOM) and sulfate reduction (SR) rates determined *ex situ* in surface sediments were one order of magnitude higher at Mound 11. The observed difference in microbial activity is positively correlated with previous transport reaction modeling results (Mound 11) and calculations from benthic chamber experiments (Mound 12), indicating fluid flow velocities one order of magnitude higher at Mound 11. Differences in carbonate stable isotope composition of the two mounds indicated that ascending fluid at Mound 11 originated from a deep source transporting primarily thermogenic methane. In contrast, Mound 12 was characterized by a mixture of deep source fluid and bottom water. At this location, the fluid was considerably charged with biogenic methane from a shallower source. Our study demonstrated that direct measurements of microbial AOM and SR activity, in combination with carbonate archives, provides a suitable approach to constrain spatial and temporal variations of methane charged fluid flow at the Costa Rica continental margin.

ACKNOWLEDGEMENTS

Funding for the present study was provided by the SFB-574: "Volatiles and Fluids in Subduction Zones“ and "The Future Ocean" Cluster of Excellence funded by the German Research Foundation (DFG). We thank the captain and the crew of R/V Sonne and all staff members who supported work onboard. V. Liebetrau and S. Kutterolf is thanked for stimulating discussions about aspects of mud mound genesis and carbonate isotopy. We also thank A. Bleyer, R. Ebbinghaus, E.Corrales-Cordero, E.Piñero Melgar, M. Nuzzo, and A. Dale for porewater sampling and chemical

analyses. J. Heinze and L. Haxhiaj are thanked for carbonate mineralogy and stable isotope measurements.

REFERENCES CITED

Barnes, R.O., and Goldberg, E.D., 1976, Methane Production and Consumption in Anoxic Marine-Sediments: Geology, v. 4, no. 5, p. 297-300.

Boetius, A., Ravenschlag, K., Schubert, C.J., Rickert, D., Widdel, F., Gieseke, A., Amann, R., Jorgensen, B.B., Witte, U., and Pfannkuche, O., 2000, A marine microbial consortium apparently mediating anaerobic oxidation of methane: Nature, v. 407, no. 6804, p. 623-626.

Bohrmann, G., Greinert, J., Suess, E., and Torres, M., 1998, Authigenic carbonates from the Cascadia subduction zone and their relation to gas hydrate stability: Geology, v. 26, no. 7, p. 647-650, doi: 10.1130/0091-7613(1998)026<0647:ACFTCS>2.3.CO;2.

Bohrmann, G., Heeschen, K., Jung, C., Weinrebe, W., Baranov, B., Cailleau, B., Heath, R., Hühnerbach, V., Hort, M., Masson, D., and Trummer, I., 2002, Widespread fluid expulsion along the seafloor of the Costa Rica convergent margin: Terra Nova, v. 14, no. 2, p. 69-79.

Bowes, H.L., and Hornibrook, E.R.C., 2006, Emission of highly 13C-depleted methane from an upland blanket mire: Geophysical Research Letters, v. 33, p. 1-4.

Colemann, D., Risatti, J., 1981, Fractionation of carbon and hydrogen isotopes by methane-oxidizing bacteria, Geochimica et Cosmochimica Acta, v. 45, p. 1033-1037.

Ellam, R.M., and Hawkesworth, C.J., 1988, Elemental and isotopic variations in subduction related basalts: evidence for a three component model: Contributions to Mineralogy and Petrology, v. 98, no. 1, p. 72-80, doi: 10.1007/BF00371911.

Emrich, K., Erhalt, D.H., and Vogel, J.C., 1970, Carbon isotope fractionation during precipitation of calcium carbonate: Earth and Planetary Science Letters, v. 8, p. 363-371.

Greinert, J., Bohrmann, G., and Suess, E., 2001, Gas Hydrate-associated carbonates and methane-venting at Hydrate Ridge : Classification , distribution , and origin of authigenic lithologies, in Paull, C.K. and Dillon, W.P. eds., GEOPHYSICAL MONOGRAPH SERIES, AGU, Washington, D. C., p. 99-113.

Han, X., Suess, E., Sahling, H., and Wallmann, K., 2004, Fluid venting activity on the Costa Rica margin: new results from authigenic carbonates, Int. J. Earth Sci., v. 93, p. 596-611.

Hensen, C., and Wallmann, K., 2005, Methane formation at Costa Rica continental margin—constraints for gas hydrate inventories and cross-décollement fluid flow: Earth and Planetary Science Letters, v. 236, no. 1-2, p. 41-60, doi: 10.1016/j.epsl.2005.06.007.

Hensen, C., Wallmann, K., Schmidt, M., Ranero, C.R., and Suess, E., 2004, Fluid expulsion related to mud extrusion off Costa Rica—A window to the subducting slab: Geology, v. 32, p. 201-204.

Joye, S.B., Boetius, A., Orcutt, B.N., Montoya, J.P., Schulz, H.N., Erickson, M.J., and Logo, S.K., 2004, The anaerobic oxidation of methane and sulfate reduction in sediments from Gulf of Mexico cold seeps: Chemical Geology, v. 205, no. 3-4, p. 219-238, doi: 10.1016/j.chemgeo.2003.12.019.

Judd, A.G., Hovland, M., Dimitrov, L.I., Gil, S.G., and Jukes, V., 2002, The geological methane budget at Continental Margins and its influence on climate change: Geofluids, v. 2, no. 2, p. 109-126.

Jørgensen, B.B., and Nelson, D.C., 2004, Sulfide oxidation in marine sediments: Geochemistry meets microbiology: Geological Society of America Special Paper, v. 379, p. 63-81.

Kallmeyer, J., Ferdelman, T.G., Weber, A., Fossing, H., and Jørgensen, B.B., 2004, A cold chromium distillation procedure for radiolabeled sulfide applied to sulfate reduction measurements: Limnology and Oceanography-Methods, v. 2, p. 171-180.

Karaca, D., Hensen, C., and Wallmann, K., 2010, Controls on authigenic carbonate precipitation at cold seeps along the convergent margin off Costa Rica: Geochemistry Geophysics Geosystems, v. 11, no. 8, p. 1-19, doi: 10.1029/2010GC003062.

Klaucke, I., Masson, D.G., Petersen, C.J., Weinrebe, W., and Ranero, C.R., 2008, Multifrequency geoacoustic imaging of fluid escape structures offshore Costa Rica: Implications for the quantification of seep processes: Geochemistry Geophysics Geosystems, v. 9, no. 4, p. 1-16, doi: 10.1029/2007GC001708.

Krüger, M., Treude, T., Wolters, H., Nauhaus, K., and Boetius, A., 2005, Microbial methane turnover in different marine habitats: Palaeogeography, Palaeoclimatology, Palaeoecology, v. 227, no. 1-3, p. 6-17, doi: 10.1016/j.palaeo.2005.04.031.

Kutterolf, S., Liebetrau, V., Mörz, T., Freundt, A., Hammerich, T., Garbe-Schönberg, D., 2008, Lifetime and cyclicity of fluid venting at forearc mound structures determined by tephrostratigraphy and radiometric dating of authigenic carbonates, Geology, v. 36, no. 9, p. 707-710.

Linke, P., Wallmann, K., Suess, E., Hensen, C., and Rehder, G., 2005, In situ benthic fluxes from an intermittently active mud volcano at the Costa Rica convergent margin: Earth and Planetary Science Letters, v. 235, no. 1-2, p. 79-95, doi: 10.1016/j.epsl.2005.03.009.

Luff, R., Wallmann, K., and Aloisi, G., 2004, Numerical modeling of carbonate crust formation at cold vent sites: significance for fluid and methane budgets and chemosynthetic biological communities: Earth and Planetary Science Letters, v. 221, no. 1-4, p. 337-353.

Manning, C., 2004, The chemistry of subduction-zone fluids: Earth and Planetary Science Letters, v. 223, no. 1-2, p. 1-16, doi: 10.1016/j.epsl.2004.04.030.

Mau, S., Sahling, H., Rehder, G., Suess, E., Linke, P., and Soeding, E., 2006, Estimates of methane output from mud extrusions at the erosive convergent margin off Costa Rica: Mar. Geol., v. 225, p. 129-144.

Mavromatis, V., Botz, R., Schmidt, M., Liebetrau, V., and Hensen, C. (submitted) Formation of carbonate concretions in surface sediments of two mud mounds , offshore Costa Rica – a stable isotope study

McAullife, C., 1971, GC Determination of solutes by Multiple Phase Equilibration: Chemical Technology, v. 1, no. 1, p. 46-51.

Mörz, T., Fekete, N., Kopf, A.J., Brueckmann, W., Kreiter, S., Huehnerbach, V., Masson, D.G., Hepp, D.A., Schmidt, M., Kutterolf, S., Sahling, H., Abegg, F., Spiess, V., Suess, E., et al., 2005, Styles and productivity of mud diapirism along the Middle American Margin, Part II, Mound Culebra and Mounds 11 and 12, in Martinelli, G. and Panahi, B. eds., Mud volcanoes, geodynamics and seismicity, Springer, Dordrecht, Netherlands, p. 49-76.

Naehr, T.H., Eichhubl, P., Orphan, V.J., Hovland, M., Paull, C.K., Ussler, W., Lorenson, T.D., and Greene, H.G., 2007, Authigenic carbonate formation at hydrocarbon seeps in continental margin sediments: A comparative study: Deep-Sea Research Part Ii-Topical Studies in Oceanography, v. 54, no. 11-13, p. 1268-1291.

Niemann, H., Lösekann, T., de Beer, D., Elvert, M., Nadalig, T., Knittel, K., Amann, R., Sauter, E.J., Schlüter, M., Klages, M., Foucher, J.P., and Boetius, A., 2006, Novel microbial communities of the Haakon Mosby mud volcano and their role as a methane sink.: Nature, v. 443, no. 7113, p. 854-8, doi: 10.1038/nature05227.

Peckmann, J., Reimer, A., Luth, U., Luth, C., Hansen, B.T., Heinicke, C., Hoefs, J., and Reitner, J., 2001, Methane-derived carbonates and authigenic pyrite from the northwestern Black Sea: Marine Geology, v. 177, no. 1-2, p. 129-150.

Ranero, C., and von Huene R, 2000, Subduction erosion along the Middle America convergent margin: Nature, v. 404, no. 6779, p. 748-52, doi: 10.1038/35008046.

Reitner, J., Peckmann, J., Blumenberg, M., Michaelis, W., Reimer, a., and Thiel, V., 2005, Concretionary methane-seep carbonates and associated microbial communities in Black Sea sediments: Palaeogeography, Palaeoclimatology, Palaeoecology, v. 227, no. 1-3, p. 18-30, doi: 10.1016/j.palaeo.2005.04.033.

Scambelluri, M., Malaspina, N., and Hermann, J., 2007, Subduction fluids and their interaction with the mantle wedge : a perspective from the study of high-pressure ultramafic rocks: PERIODICO di MINERALOGIA, v. 76, no. 2-3, p. 253-265, doi: 10.2451/2007PM0028.

Schmidt, M., Hensen, C., Mörz, T., Müller, C., Grevemeyer, I., Wallmann, K., Maub, S., and Kaule, N., 2005, Methane hydrate accumulation in "Mound 11" mud volcano, Costa Rica forearc: Marine Geology, v. 216, no. 1-2, p. 83-100.

Schoell, M., 1988, Multiple origins of methane in the Earth: Chemical Geology, v. 71, no. 1-3, p. 1-10, doi: 10.1016/0009-2541(88)90101-5.

Suess, E., 2002, Gashydrat—Eine Verbindung aus Methan und Wasser: Nova Acta Leopoldina, v. 85, no. 323, p. 123-146.

Suess, E., 2010, Handbook of hydrocarbon and lipid microbiology (K. N. Timmis, Ed.): Springer-Verlag, Berlin, Heidelberg.

Teichert, B.M.A., Bohrmann, G., and Suess, E., 2005, Chemoherms on Hydrate Ridge - unique microbially mediated carbonate build-ups growing into the water column: Palaeogeography, Palaeoclimatology, Palaeoecology, v. 227, p. 67-85.

Thauer, R.K., 1998, Biochemistry of Methanogenesis: a Tribute to Marjory Stephenson: Microbiology, v. 144, p. 2377-2406.

Treude, T., Knittel, K., Wallmann, K., Jørgensen B., B., 2003, Anaerobic oxidation of methane above gas hydrates at Hydrate Ridge, NE Pacific Ocean: Mar Ecol Prog Ser, v. 264, p. 1-14.

Treude, T., Krüger, M., and Jørgensen, B.B., 2005, Environmental control on anaerobic oxidation of methane in the gassy sediments of Eckernförde Bay (German Baltic): Limnol. Oceanogr., v. 50, no. 6, p. 1771-1786.

Chapter 6

1. Final discussion

In the present study different aspects of microbial effects on carbonate minerals were investigated, including:

- Influence of microbial biofilms on carbonate precipitation
- Influence of microbial activity on carbonate dissolution
- Carbonate precipitation dependent on anaerobic oxidation of methane

In section 1, results of the present thesis will be summarized. Section 2 is devoted to the discussion of implications derived from the results of this thesis. In section 3, the used methods are critically evaluated. Section 4 addresses future research questions, which are formulated based on the present thesis.

1.1 Chapter summary

The present thesis demonstrated that aerobic and anaerobic methanotrophic, as well as sulfate-reducing microbes strongly influence the fate of marine carbonates. The results emphasized the important role of microbes as a geological force, which impacts marine carbonate sinks and sources.

In Chapter 2, investigations of biofilms produced by the marine sulfate-reducing bacterium *Desulfobulbus mediterraneus* are described. The results showed that extracellular polymeric substances (EPS) played an outstanding role facilitating the nucleation of dolomite nano-crystals. Within the EPS, calcium ions were accumulated at a similar molar ratio to magnesium ions, which deviated from the molar magnesium/calcium ratio of the bulk liquid medium. Medium concentrations

of both ions represented seawater concentrations of. In addition, EPS were involved in calcium isotopy fractionation. The biofilm related fractionation provided a reservoir within the organic matter of a $\delta^{44/40}$Ca value smaller than the surrounding liquid. The dolomite within the EPS, forming from that reservoir, fractionated again in this direction, resulting in a dolomite depleted in ^{44}Ca relative to both, the biofilm and the surrounding fluid. Based on these results, a two-step fractionation process might be involved for calcium sequestration from the bulk liquid into the crystal lattice.

Chapter 3, reports results from incubation experiments with calcite powder and metabolically active, inactive, and dead cells of the aerobic methanotrophic bacterium *Methylosinus trichosporium*. Calcite dissolution of varying degrees was observed in all of the three experiments, while abiotic controls did not show calcite dissolution. Strongest dissolution of calcite crystals was observed for incubations with active and dead cells. Also inactive cells induced calcite dissolution, although less strong compared to experiments with active and dead cells. The results showed that in addition to microbial carbon dioxide production, also the release of intracellular substances and direct contact between cells and crystals induced considerable dissolution of calcite.

In Chapter 4, incubation experiments of natural marine sediment slurries with ^{14}C and ^{45}Ca radiotracers are described. Both methods proved to be principally suitable to constrain calcification rates, and were highly correlated ($R^2 > 0.94$) with measureable microbial anaerobic oxidation of methane (AOM) activity. However, rates obtained from ^{45}Ca incubations were generally higher compared to incubations with ^{14}C, indicating additional calcium binding by organic components of the sediment.

Chapter 5 reports results from a field study, including measurements of sediment AOM rates, carried out at two neighboring mud mounds at the active continental margin of Costa Rica (Mound 11 and 12). Carbonates from both sites were analyzed for δ^{18}O and δ^{13}C. The results showed considerably higher areal rates of AOM at Mound 11 compared to Mound 12, supporting results of benthic chamber

experiments (Linke et al., 2005) and numerical modeling (Karaca et al., 2010) of the study area. In addition, carbonates from Mound 11 showed higher $\delta^{18}O$ and $\delta^{13}C$ values than observed at Mound 12. The combination of current AOM rates and stable isotope signatures of carbonates indicated differences in fluid flow and origin between the two mounds.

Over all, the present thesis confirms that the activity of microbes commonly present in or near the ocean floor has direct implications for the fate of marine carbonates. The results emphasize that, in addition to microbial impact on the marine carbonate system, also organic substances of microbial origin have to be considered with regards to carbonate precipitation and dissolution.

1.2 Influence of microbial biofilms on carbonate precipitation

Biofilms probably comprise the normal environment for most microbial cells in numerous habitats, and represent complex associations of cells and extracellular polymeric substances (EPS) (Sutherland, 2001; Christensen, 1989). Considering the results of the present thesis on microbial biofilms, EPS might be of utmost importance for the genesis of primary dolomite. Facilitation of dolomite might be the result of selective concentration (element fractionation) of divalent ions, as Ca^{2+} and Mg^{2+}, by EPS functional groups (Dupraz et al., 2009) at a different ratio compared to the surrounding bulk liquid. Abiotic dolomite precipitation at modern Earth's surface conditions is largely inhibited due to the strong hydration shell of magnesium ions, providing a kinetic barrier. Our results suggest that EPS might overcome this barrier, allowing for dolomite precipitation. Biologically induced fractionation, as shown in the present thesis, has been postulated to explain discrepancies between calculated and observed calcium fractionation in carbonate minerals (Böhm et al., 2006; Russell et al., 1978), while prove could not be provided to date. The accumulation of light Ca isotopes by EPS may have important implications for the reconstruction of paleo-environmental conditions. Calcium ion fractionation might be caused by microbial substances (our study) and also coral

tissue (Böhm et al., 2006), therefore limiting the use as as paleo-proxy. At least, careful re-consideration of calcium isotope studies might be required.

Our biofilm studies showed the development of dolomite crystals at the nanometer scale with a granular surface in close proximity to EPS. Our results are in accordance with previous investigations (Sánchez-Román et al., 2008), identifying granular dolomite nano-crystals in natural dolomites from different locations of various geologic ages. These results support our findings suggesting that microbial activity might also have been involved in past dolomite formation. Throughout the Phanerozoic, intensified dolomite formation occurred during distinct periods (Given and Wilkinson, 1987). These periods were characterized by lowered concentrations of atmospheric (Lasaga, 1989) and, consequently, marine oxygen levels. Low oxygen concentrations surely had adverse effects on numerous marine live forms, causing mass decay and increased transfer of organic substrates to the seafloor. Here, the increased availability of organic material might have stimulated activity of sulfate reducing bacteria. Additionally, low oxygen concentrations might have reduced the pressure of benthic metazoan grazers. Both, the increased availability of organic substrate and the reduction of grazers might have been beneficial for an intensified development of biofilms by sulfate-reducers. Periods of low oxygen concentration persisted over several millions of years, potentially favoring long-term establishment of undisturbed sulfate-reducing bacteria biofilms, in which considerable quantities of dolomite might have precipitated.

Biofilms represent the normal mode of microbial life (e.g. Flemming et al., 2007; Donlan, 2002; Sutherland, 2001). Therefore, biofilm components have to be considered with regards to mineral stability. However, the composition of biofilm components may vary greatly among the microbial community due to their genetic diversity. In addition, biofilm specifics might also be depending on the specific environmental circumstances (Jefferson, 2004). In natural environments, biofilms are commonly inhabited by a multi-species microbial community (Sutherland, 2001), further adding to the complexity of simultaneously ongoing processes. Therefore,

functional mechanisms of biofilms may vary as a result of the mutual relationship between microbes and the adjacent environment.

1.3 Influence of microbial activity on carbonate dissolution

We demonstrated that microbial aerobic methanotrophic activity favors calcite dissolution. Comparing different experimental setups, it appeared that in addition to metabolically active cells, also metabolically inactive and dead cells induced calcite dissolution, however at lower rates. These results suggest that, in addition to carbon dioxide production, also organic microbial substances induced calcite dissolution. In case of metabolically inactive cells, direct contact between cells and calcite crystal surfaces might have caused dissolution. Microbial cell walls include organic functional groups as carboxylic, phosphonic, and hydroxyl groups (Beveridge, 1981), which can bind cations in solution (Daughney and Fein, 1998; Morita, 1980). This binding capability might cause a local decrease of the carbonate saturation state at the surface of calcite crystals, resulting in enhanced dissolution. Potential mechanisms of dissolution might also include interference with etch pit development and excavation of carbonate material at the cell-mineral interface during attachment to the mineral surface (Davis et al., 2007). Our results also suggested that intracellular components, possibly organic acids, ligands, chelating, and redox-active metabolites, released after cell deterioration (Rosso et al., 2003), caused dissolution of calcite. In addition, laboratory experiments have shown that the enzyme carbonic anhydrase, which are wide spread in nature, induced strong carbonate dissolution in aquatic environments (Liu, 2001).

These organic components might affect carbonate dissolution in different ways, including pH decrease of the bulk liquid by organic acids in combination with binding of dissolved Ca^{2+} ions to organic molecules. In seawater, dissolved organic substances interact with carbonate mineral surfaces, forming organo-carbonate associations (Suess, 1970), reducing or even inhibiting equilibrium reaction rates with carbonate system components of the surrounding seawater. It can be speculated that dissolved organic substances in surface waters, primarily of

microbial origin, might be partly explanatory for inhibition of carbonate precipitation despite supersaturation (Chave, 1965).

Aerobic methanotrophy might have been of considerable importance during periods of rapid global temperature increase causing large scale gas hydrate destabilization, as reported for the Paleocene-Eocene Thermal Maximum (PETM) (~55.5 Ma) (Bice and Marotzke, 2002). During this time period, also massive dissolution of seafloor carbonate occurred as a consequence of rapid ocean acidification (Zachos et al., 2005). The increased carbon dioxide levels during the PETM, might have resulted from microbial aerobic oxidation of methane. Also recent investigations indicate that aerobic methanotrophy might be partly causative for observed corrosion patterns of authigenic marine carbonate buildups (Himmler et al., 2011). Considering also the results of our study, the dissolution of carbonates in marine environments might be the combined result of both, microbial effects on the carbonate system and contact between microbial organic substances.

1.4 Carbonate precipitation dependent on anaerobic oxidation of methane

In marine sediments, AOM is largely responsible for authigenic carbonate formation (e.g. Bohrmann et al., 1998; Michaelis et al., 2002; Knittel and Boetius, 2009; Luff et al., 2005). The calculation of carbonate precipitation rates is commonly derived from geochemical models (e.g. Luff et al., 2004; Karaca et al., 2010) or reconstructed from the rock record (e.g. Liebetrau et al., 2010; Summer et al., 1996; Greinert et al., 2002). In contrast, measurements of current carbonate precipitation rates in marine sediment are scarce.

A previous investigation used ^{45}Ca for beta imaging to yield semi-quantitative precipitation rates and to identify regions of intensified carbonate precipitation within microbial mats (Ludwig et al., 2005). However, this method is not applicable for measurements in bulk sediment. To date, ^{45}Ca and ^{14}C isotopes have been successfully employed to quantify only biologically controlled carbonate precipitation, which includes studies on corals (Barnes and Crossland, 1977),

molluscs (Dillaman and Ford, 1982; Ireland and Scheuer, 1979), coccolithophores (van der Wal et al., 1994) and foraminifera (Kuile and Erez, 1987; McEnery and Lee, 1970). Whereas the method introduced in this thesis allows for quantification of biologically influenced calcification outside the cell and therefore can have a range of applications. The combined measurement of biologically controlled and biologically influenced carbonate precipitation might be useful to account for all major biological processes influencing marine carbonate stability. Once the introduced method has been refined and applied, comparative studies of seafloor regions, which vary in AOM activity, might provide a global overview of AOM-related carbonate precipitation rates. These rates might also be used to re-evaluate reconstructions of carbonate precipitation throughout the geological record. In addition, experimental investigations of precipitation rates under varying environmental conditions could contribute to current understanding of the effects of climate change on marine sedimentary carbonate formation.

AOM and carbonate precipitation are not continuous processes, as these activities strongly depend on the advection of methane from deeper parts of the sediment. Various studies reported active and inactive periods fluid flow during the existence of modern or ancient seep sites (e.g. Peckmann et al., 1999; Kutterolf et al., 2008), presumably caused by temporal fluid flow variations. To date, the understanding of temporal and spatial fluid flow variations is still fragmentary and the origin and dynamics of seafloor and sub-seafloor fluid flow expressions are not well understood.

Within the scope of the present thesis, investigations of AOM activity and carbonate isotopic signature were carried out along the pacific continental margin offshore Costa Rica. Combining current measurements of AOM and sulfate reduction rates (SR) with carbonate stable isotopes, it was shown that mound structures, which did not show vertical sediment transport for ~ 5 ka (Kutterolf et al., 2008), were characterized by considerable advection of methane-charged fluids. These fluids supported considerable AOM activity and authigenic carbonate formation. The combination of AOM rates and carbonate isotopy might help to determine the

"livetime" of a seep location and constrain alternating periods of high and low fluid flow.

Numerous studies have been devoted to understand the relationship between fluid advection and methane-related microbial activity (e.g. Hensen & Wallmann, 2005; Niemann et al., 2006; Wallmann et al., 2006). However, it is still unknown how fast the microbial community can respond to variations in methane flux. Long-term investigations, including AOM and calcification rate measurements, might help in determination of the response microbial communities have to temporal changes in methane supply. The response time of AOM activity is a crucial factor for the efficiency of the benthic filter in the case of increasing advection of methane.

At active continental margins, subduction of oceanic plate material might cause fluid advection at previously inactive seep locations (Martinelli and Panahi, 2005), which can introduce considerable amounts of methane into the water column until the microbial community has adjusted. Slope failures at continental margins often cause decreased pressure on deeper sediment layers in combination with removal of the upper sediment microbial community (Schwab and Lee, 1988). Consequently, areas of slope failure might emit methane, due to gas hydrate destabilization, for a prolonged time before AOM consortia have re-established in the upper sediment.

The response time of AOM activity might have a considerable effect in the Arctic region, where methane is deposited as gas hydrate in shallow seafloor regions (Kvenvolden, 1988). Due to global warming, substantial amounts of liberated methane might ascend through the sediment into the water column (Biastoch et al., 2011) and into the atmosphere. The response time of methanotrophic microbes and the consequential carbonate formation largely determine the amount of captured methane and carbon storage, before entering the atmosphere.

Recent climate modeling clearly indicated the adverse effects of increasing atmospheric carbon dioxide concentration on global warming (IPCC 2007). The World's ocean is of prime importance for the global carbon budget as it absorbs more than a quarter of the currently emitted carbon dioxide (Cox et al. 2000

Nature). Therefore, the ocean represents the largest carbon sink on Earth (Fig 1.) (Siegenthaler and Sarmiento, 1993).

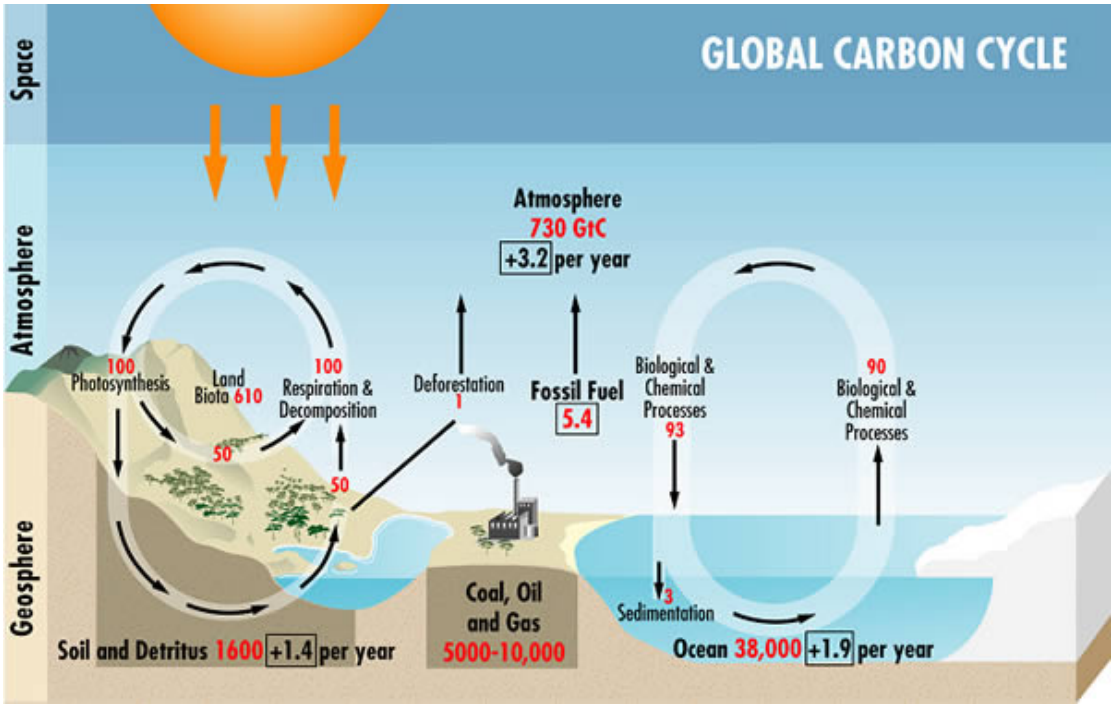

Figure 1. Illustration of the global carbon reservoirs in giga tons of carbon and the annual fluxes and accumulation rates in GtC/year, calculated over the period 1990 to 1999. The values shown are approximate and considerable uncertainties exist as to some of the flow values. Source http://www.bom.gov.au/info/climate/change

However, the calculated annual accumulation rate is only about 1.5 (± 0.9) Gt C (Chuck et al., 2005). Considering the fact that considerable uncertainties exist for the different carbon fluxes (Battle et al. 2000), it is uncertain if the global ocean represents a sink or a source for carbon. To constrain the marine carbon cycle, model approaches need to be supported by measurements that quantify relevant processes creating carbon sources and sinks. Among these processes, authigenic carbonate formation, due to AOM, represents a major carbon sink (Ziebis and Haese, 2005). Numerical modeling indicates that carbonate crusts at fluid venting sites may form within a time period of several centuries (Luff and Wallmann, 2003; Luff et al., 2004, 2005), but these estimates of growth rate and duration have not been confirmed by measurements. In addition, in geochemical models, precipitation is

assumed at a saturation state ≥ 1 (Karaca et al., 2010), while experiments suggest that the onset of calcite precipitation occurs at a saturation state between 18-25 (Morse, 1993). Measurements of calcification rates, such as those presented here in this thesis will help to develop models closely resembling the chemical situation in natural marine sediments.

2. Evaluation of used methods

Microscopy imaging

During the study, carbonate crystals and biofilms were imaged using scanning electron microscopy (SEM). This technique yields information of morphological structures at high spatial resolution. In combination with Energy-dispersive X-ray spectroscopy (EDX) individual features can be characterized for composition of chemical elements. The preparation of biological samples for SEM includes substantial manipulation, including fixation, dehydration and critical point drying. These steps are necessary to allow sample imaging at high vacuum.

A fundamental disadvantage for imaging of biofilms are the involved drying procedures creating artifacts by compromising hydrated structures (Richards and Turner, 1984). Due to the loss of water, hydrated structures are strongly altered, causing substantial deviations from the natural appearance of biofilm components. As a consequence, the natural features of biofilm cannot be visualized with SEM

In addition, SEM is only suitable for surface imaging, while three-dimensional information is limited. The cryo-SEM technology provides an advantage for biofilm imaging as hydrated structures can be preserved to some degree in their natural state by rapid cooling of the sample. Nonetheless, also cryo-SEM causes strong alterations of the three-dimensional biofilm structure.

In contrast, confocal laser scanning microscopy (CLSM) allowed detailed investigations of fully hydrated biofilms, as sample drying was not required. Individual staining allowed discriminating of biofilm components spatial distribution.

An advantage of CLSM was the step-wise imaging of optical sections beneath the biofilm surface, providing three-dimensional information. A principle disadvantage of CLSM is the relative short time study time as the applied staining agents were susceptible to photobleaching.

pH measurements

The experiments carried out during the present study involved the determination of pH in solutions, not in equilibrium with the atmosphere. This included the pressure and gas composition of headspaces. For experiments a conventional pH-meter was used. For pH measurements it was therefore necessary to abstract liquid samples and measure pH under atmospheric conditions. This procedure caused equilibration between atmospheric and sample concentration of carbon dioxide, representing a major error source for pH determination of solutions kept under conditions differing from the atmosphere. Consequently, subsequent calculations based on pH measurements bare the danger of not being representative of physicochemical solution properties. To avoid equilibration between solution and atmospheric carbon dioxide concentration, a pH-measuring device was designed allowing measurements while maintaining experimental conditions (see Appendix). However, additional calibration and refinement of the device is required to allow high accuracy measurement of pH in solutions, which are not in equilibrium with the atmosphere.

Radiotracer experiments

The use of radioisotopes for rate measurements was favored over conventional chemical analysis as they provide the possibility to measure turnover rates in natural samples. Radioanalytical techniques require about 10^5 smaller quantities than

chemical analysis, thus providing a comparatively high sensitivity (Horányi, 2004). Therefore, even very low turnover rates can be measured. In chapter 4 of the present thesis it was demonstrated that ^{45}Ca and ^{14}C radioisotopes were suitable to measure carbonate precipitation rates in marine sediment slurries. The simultaneous incubation of microbially active and sterilized sediment allowed discrimination between gross and microbially-induced carbonate precipitation. A disadvantage of ^{45}Ca is its interaction with organic components of sediments, including intra- and extracellular binding. As a consequence, measurement of residual ^{45}Ca in the sediment might include ^{45}Ca bound to organic molecules in addition to radioisotopes precipitated as carbonate minerals. Microbial alkalinity production during the incubation with ^{14}C-bicarbonate tracer leads to a decreasing ratio between radioactive and non-radioactive carbonate system components. As a linear relationship of $^{14}CO_3^-$ and non-radioactive CO_3^- precipitation is assumed, calculated rates might be too low. Therefore, refinement procedures need to address the described sources of errors to increase the accuracy of the proposed method.

3. Future research questions

Future studies need to address the combined effects of microbial physicochemical changes of seawater and organic substances to determine the mechanism of carbonate precipitation and dissolution. To understand the relationships between microbes and carbonates in the marine realm it is important to address the following questions:

- How are kinetic barriers for carbonate precipitation overcome by microbial organic substances?
- How do microbial organic substances interact with calcium and magnesium ions?

- What role do microbial organic substances play for element and isotope fractionation during the sequestration of dissolved ions into carbonate minerals?
- Are mineral isotopes suitable as paleo-proxies for microbial involvement in carbonate formation?
- How strong is the effect of microbial carbon dioxide production on carbonate dissolution?

Using advances of modern imaging technology, it would also be helpful to perform live microscopy investigations of carbonate mineral nucleation in active biofilms. In addition, mapping of element distribution within biofilms might contribute to the understanding of chemical gradients caused by microbial activity.

REFERENCES CITED

Barnes, D.. J., and Crossland, C.J., 1977, Coral Calcification : Sources of Error in Radioisotope Techniques: Marine Biology, v. 42, p. 119-129.

Battle, M., Bender, M.L., Tans, P.P., White, J.W.C., Ellis, J.T., Conway, T., Francey, R.J., 2000, Global carbon sinks and their variability inferred from atmospheric O2 and d13C, Science, v. 287, p. 2464-2470.

Biastoch, A., Treude, T., Rüpke, L.H., Riebesell, U., Roth, C., Burwicz, E.B., Park, W., Latif, M., Böning, C.W., Madec, G., and Wallmann, K., 2011, Rising Arctic Ocean temperatures cause gas hydrate destabilization and ocean acidification: Geophysical Research Letters, v. 38, no. 8, p. 1-5, doi: 10.1029/2011GL047222.

Bice, K.L., and Marotzke, J., 2002, Could changing ocean circulation have destabilized methane hydrate at the Paleocene/Eocene boundary?: Paleoceanography, v. 17, no. 2, p. 1018-1030.

Bohrmann, G., Greinert, J., Suess, E., and Torres, M., 1998, Authigenic carbonates from the Cascadia subduction zone and their relation to gas hydrate stability: Geology, v. 26, no. 7, p. 647-650, doi: 10.1130/0091-7613(1998)026<0647:ACFTCS>2.3.CO;2.

Böhm, F., Gussone, N., Eisenhauer, A., Dullo, W., Reynaud, S., and Paytan, A., 2006, Calcium isotope fractionation in modern scleractinian corals: Geochimica et Cosmochimica Acta, v. 70, no. 17, p. 4452-4462, doi: 10.1016/j.gca.2006.06.1546.

Chave, K.E., 1965, Carbonates: association with organic matter in surface seawater: Science, v. 148, p. 1723-1724.

Christensen, B.E., 1989, The role of extracellular poly- saccharides in biofilms: J Biotechnol, v. 10, p. 181-202.

Chuck, A., Tyrrell, T., Totterdell, I.J. and Holligan, P.M. 2005. The oceanic response to carbon emissions over the next century: investigation using three ocean carbon cycle models. Tellus 57B, 70–86.

Cox, P.M., Betts, R.A., Jones, C.D., Spall, S.A.,and Totterdell, I.J., 2000, Acceleration of global warming due to carbon-cycle feedbacks in a coupled climate model, Nature, v. 408, p. 184-187.

Daughney, C.J., and Fein, J.B., 1998, The effect of ionic strength on the adsorption of H+, Cd2+, Pb2+ and Cu2+ by Bacillus subtilis and Bacillus licheniformis: a surface complexation model: Journal of Colloid Interface Science, v. 198, p. 53-77.

Davis, K.J., Nealson, K.H., and Lüttge, A., 2007, Calcite and dolomite dissolution rates in the context of microbe-mineral surface interactions: Geobiology, v. 5, no. 2, p. 191-205.

Dillaman, R.M., and Ford, S.E., 1982, Measurement of Calcium Carbonate Deposition in Molluscs by Controlled Etching of Radioactively Labeled Shells: Marine Biology, v. 66, p. 133-143.

Donlan, R.M., 2002, Biofilms: microbial life on surfaces.: Emerging infectious diseases, v. 8, no. 9, p. 881-90.

Dupraz, C., Reid, R.P., Braissant, O., Decho, A.W., Norman, R.S., and Visscher, P.T., 2009, Processes of carbonate precipitation in modern microbial mats: Earth-Science Reviews, v. 96, no. 3, p. 141-162, doi: 10.1016/j.earscirev.2008.10.005.

Flemming, H.-C., Neu, T.R., and Wozniak, D.J., 2007, The EPS matrix: the “house of biofilm cells”.: Journal of bacteriology, v. 189, no. 22, p. 7945-7, doi: 10.1128/JB.00858-07.

Given, R.K., and Wilkinson, B.H., 1987, Dolomite abundance and stratigraphic age: Constraints on rates and mechanisms of Phanerozoic dolostone formation: J. Sediment. Petrol., v. 57, p. 1068-1078.

Greinert, J., Bollwerk, S.M., Derkachev, A., Bohrmann, G., and Suess, E., 2002, Massive barite deposits and carbonate mineralization in the Derugin Basin, Sea of Okhotsk: precipitation processes at cold seep sites: Earth and Planetary Science Letters, v. 203, no. 1, p. 165-180.

Hensen, C., and Wallmann, K., 2005, Methane formation at Costa Rica continental margin—constraints for gas hydrate inventories and cross-décollement fluid flow: Earth and Planetary Science Letters, v. 236, no. 1-2, p. 41-60, doi: 10.1016/j.epsl.2005.06.007.

Himmler, T., Brinkmann, F., Bohrmann, G., and Peckmann, J., 2011, Corrosion patterns of seep-carbonates from the eastern Mediterranean Sea: Terra Nova, v. 23, no. 3, p. 206-212, doi: 10.1111/j.1365-3121.2011.01000.x.

Horányi, G. (Ed.), 2004, Radiotracer Studies of Interfaces: Elsevier.

Intergovernmental Panel on Climate Change (IPCC), 2007, Climate Change 2007: The Physical Science Basis. Contribution of Working Group I to the Fourth Assessment Report of the Intergovernmental Panel on Climate Change, edited by S. Solomon et al., Cambridge Univ. Press, Cambridge, U.K.

Ireland, C., and Scheuer, P.J., 1979, Photosynthetic Marine Molluscks: In vivo 14C Incorporation into Metabolites of the Sarcoglossan Placobranchus ocellatus: Science, v. 205, no. AUGUST, p. 922-923.

Jefferson, K.K., 2004, What drives bacteria to produce a biofilm?: FEMS microbiology letters, v. 236, no. 2, p. 163-73, doi: 10.1016/j.femsle.2004.06.005.

Karaca, D., Hensen, C., and Wallmann, K., 2010, Controls on authigenic carbonate precipitation at cold seeps along the convergent margin off Costa Rica: Geochemistry Geophysics Geosystems, v. 11, no. 8, p. 1-19, doi: 10.1029/2010GC003062.

Knittel, K., and Boetius, A., 2009, Anaerobic Oxidation of Methane: Progress with an Unknown Process: Annual Review of Microbiology, v. 63, p. 311-334.

Kuile, B., and Erez, J., 1987, Uptake of inorganic carbon and internal carbon cycling in symbiont-bearing benthonic foraminifera: Marine Biology, v. 94, p. 499-509, doi: 10.1007/BF00431396.

Kutterolf, S., Liebetrau, V., Mörz, T., Freundt, a., Hammerich, T., and Garbe-Schönberg, D., 2008, Lifetime and cyclicity of fluid venting at forearc mound structures determined by tephrostratigraphy and radiometric dating of authigenic carbonates: Geology, v. 36, no. 9, p. 707, doi: 10.1130/G24806A.1.

Kvenvolden, K.A., 1988, Methane hydrates and global climate: Global Biogeochem. Cycles, v. 2, no. 3, p. 221-229.

Lasaga, A.C., 1989, A new approach to the isotopic modelling of the variation of atmospheric oxygen through the Phanerozoic: American Journal of Science, v. 298, p. 411-435.

Liebetrau, V., Eisenhauer, A., and Linke, P., 2010, Cold seep carbonates and associated cold-water corals at the Hikurangi Margin, New Zealand: New insights into fluid pathways, growth structures and geochronology: Marine Geology, v. 272, no. 1-4, p. 307-318, doi: 10.1016/j.margeo.2010.01.003.

Liu, Z., 2001, Role of Carbonic Anhydrase as an Activator in carbonate Rock Dissolution and Its Implications for Atmosphere CO2 Sink: Acta Geologica Sinica, v. 75, no. 3, p. 275-278.

Ludwig, R., Al-horani, F.A., Beer, D.D., and Jonkers, H.M., 2005, Photosynthesis-controlled calcification in a hypersaline microbial mat: Limnol. Oceanogr., v. 50, no. 6, p. 1836-1843.

Luff, R., and Wallmann, K., 2003, Fluid flow, methane fluxes, carbonate precipitation and biogeochemical turnover in gas hydrate-bearing sediments at Hydrate Ridge, Cascadia Margin: numerical modeling and mass balances: Geochimica Et Cosmochimica Acta, v. - 67, no. - 18, p. - 3421.

Luff, R., Greinert, J., Wallmann, K., Klaucke, I., and Suess, E., 2005, Simulation of long-term feedbacks from authigenic carbonate crust formation at cold vent sites: Chemical Geology, v. 216, no. 1-2, p. 157-174.

Luff, R., Wallmann, K., and Aloisi, G., 2004, Numerical modeling of carbonate crust formation at cold vent sites: significance for fluid and methane budgets and chemosynthetic biological communities: Earth and Planetary Science Letters, v. 221, no. 1-4, p. 337-353, doi: 10.1016/S0012-821X(04)00107-4.

Martinelli, G., and Panahi, B., 2005, Mud volcanoes, geodynamics and seismicity: Springer.

McEnery, M., and Lee, J.J., 1970, Tracer studies on calcium and strontium mineralization and mineral cycling in two species of foraminifera, Rosalina leei and Spiroloculina hyalina: Limnology and Oceanography, v. 15, no. 173-.

Michaelis, W., Seifert, R., Nauhaus, K., Treude, T., Thiel, V., Blumenberg, M., Knittel, K., Gieseke, A., Peterknecht, K., Pape, T., Boetius, A., Amann, R., Jørgensen, B.B., Widdel, F., et al., 2002, Microbial reefs in the Black Sea fueled by anaerobic oxidation of methane.: Science (New York, N.Y.), v. 297, no. 5583, p. 1013-5, doi: 10.1126/science.1072502.

Morita, R., 1980, Calcite precipitation by marine bacteria: Geomicrobiology Journal, v. 2, no. 1, p. 63-82, doi: 10.1080/01490458009377751.

Morse, J., 1993, Influences of T, S and PCO2 on the pseudo-homogeneous precipitation of CaCO3 from seawater: implications for whiting formation: Marine Chemistry, v. 41, no. 4, p. 291-297, doi: 10.1016/0304-4203(93)90261-L.

Niemann, H., Lösekann, T., de Beer, D., Elvert, M., Nadalig, T., Knittel, K., Amann, R., Sauter, E.J., Schlüter, M., Klages, M., Foucher, J.P., and Boetius, A., 2006, Novel microbial communities of the Haakon Mosby mud volcano and their role as a methane sink.: Nature, v. 443, no. 7113, p. 854-8, doi: 10.1038/nature05227.

Peckmann, J., Thiel, V., Michaelis, W., Clari, P., Gaillard, C., Martire, L., and Reitner, J., 1999, Cold seep deposits of Beauvoisin (Oxfordian ; southeastern France) and Marmorito (Miocene ; northern Italy): microbially induced authigenic carbonates: International Journal of Earth Sciences, v. 88, p. 60-75.

Rosso, K.M., Zachara, J.M., Fredrickson, J.K., Gorby, Y.A., and Smith, S.C., 2003, Nonlocal bacterial electron transfer to hematite surfaces: Geochimica Et Cosmochimica Acta, v. 67, no. 5, p. 1081-1087.

Russell, W.A., Papanastassiou, D.A., and Tombrello, T.A., 1978, Ca isotope fractionation on the Earth and other solar system materials: Geochimica et Cosmochimica Acta, v. 42, p. 1075-1090.

Schwab, W.C., and Lee, H.J., 1988, Causes of two slope-failure types in continental-shelf sediment, northeastern Gulf of Alaska: JOURNAL OF SEDIMENTARY RESEARCH, v. 58, no. 1, p. 1-11.

Siegenthaler, U. and Sarmiento, J.L., 1993, Atmospheric carbon dioxide and the ocean, Nature, v. 365, p. 119-125.

Suess, E., 1970, Interaction of organic compounds with calcium carbonate. Association phenomena and geochemical implications, Geochimica et Cosmochimica Acta, v. 34, p. 157-168.

Summer, D.Y., John, P., and Grotzinger, P., 1996, Were kinetics of Archean calcium carbonate precipitation related to oxygen concentration?: Geology, v. 24, no. 2, p. 119-122.

Sutherland, I.W., 2001, Biofilm exopolysaccharides: a strong and sticky framework: Microbiology-Uk, v. 147, p. 3-9.

Sánchez-Román, M., Vasconcelos, C., Schmid, T., Dittrich, M., McKenzie, J.A., Zenobi, R., and Rivadeneyra, M.A., 2008, Aerobic microbial dolomite at the nanometer scale: Implications for the geologic record: Geology, v. 36, no. 11, p. 879-882, doi: 10.1130/g25013a.1.

Wallmann, K., Drews, M., Aloisi, G., and Bohrmann, G., 2006, Methane discharge into the Black Sea and the global ocean via fluid flow through submarine mud volcanoes: Earth and Planetary Science Letters, v. 248, no. 1-2, p. 545-560, doi: 10.1016/j.epsl.2006.06.026.

van der Wal, P., Van Bleijswijk, J.D.L., and Egge, J.K., 1994, Primary productivity and calcification rate in blooms of the coccolithophorid Emiliania huxleyi (Lohmann) Hay et Mohler developing in mesocosms: Sarsia, v. 79, no. 4, p. 401-408.

Zachos, J.C., Rohl, U., Schellenberg, S.A., Sluijs, A., Hodell, D.A., Kelly, D.C., Thomas, E., Nicolo, M., Raffi, I., Lourens, L.J., McCarren, H., and Kroon, D., 2005, Rapid acidification of the ocean during the Paleocene-Eocene thermal maximum: Science, v. 308, no. 5728, p. 1611-1615.

Ziebis, W., and Haese, R.R., 2005, Interactions between fluid flow, geochemistry and biogeochemical processes at methane seeps. In: Kristensen E, Kostka J, Haese RR, editors. Macro and microorganisms in marine sediments: AGU 267–298.

Danksagung

Mein allerherzlichster Dank gilt Tina Treude für die Vergabe dieses hochinteressanten Themas und das Vertrauen, dass sie in mich gesetzt hat. Ich verdanke ihr darüber hinaus jede erdenkliche, hilfreiche Unterstützung und viele anregende Diskussionen. Jede Phase meiner Arbeit wurde von ihr intensiv, professionell und warmherzig begleitet. Besonders bedanken will ich mich auch für die Freiheit, die sie mir gewährte, was maßgeblich zum Gelingen dieser Arbeit beigetragen hat.

Volker Liebetrau möchte ich ebenfalls meinen allerherzlichsten Dank aussprechen. Jederzeit konnte ich bei der Planung, Durchführung und Auswertung der vorliegenden Arbeit auf seine außerordentlich sachkundige, erfahrene und wertvolle Unterstützung zurückgreifen. Seine kreativen Ideen haben meine Arbeit außerordentlich bereichert.

Mein herzlichster Dank gilt Judith A. McKenzie für ihre zahlreichen fachlichen Ratschläge, ihre Einladung in die Schweiz und für ihr herzliches Angagement für meine Arbeit.

Für seine unermüdliche und professionelle Einführung in die Feinheiten des marinen Karbonatsystems möchte ich mich herzlichst bei Giovanni Aloisi bedanken.

Als nächstes möchte ich meinen Kollegen Philip Steeb und Victoria Bertics herzlichst für ihre forwährende Unterstützung, für anregende Diskussionen danken.

Julia Hommer und Julia Farkaś gilt mein herzlicher Dank für ihre technische Unterstützung jeglicher Art im Labor.

Marion Liebtrau danke ich an dieser Stelle herzlich für ihre großartige Unterstützung in allen organisatorischen und administrativen Belangen.

Für ihre technische Unterstützung im Geomar möchte ich mich herzlichst bei Bettina Domeyer, Anke Bleyer, Ana Kolevica, Regina Surberg, Jutta Heinze, Mario Thöner und Armin Freundt bedanken.

Stanislav Gorb, Mónica Sánchez-Román, Joachim Ösert und Anne Greet Bittermann möchte ich herzlich für eine erfolgreiche wissenschaftliche und technische Zusammenarbeit danken.

Ich möchte mich herzlich für die technische Unterstützung und wissenschaftliche Zusammenarbeit auf meinen Seereisen bei den Fahrtleitern Rick Coffin und Christian Hensen, sowie bei Andrew Dale, Kelly Rose, Leila Hamdan, Jens Greinert, Maik Lange und Renate Ebbinghaus bedanken.

Meinen Eltern, Sigrid und Jürgen, sowie Elina und Lillian danke ich für ihre Unterstützung in jeglicher Hinsicht und für ihre unendliche Geduld.

Appendix

Composition of growth media used for cultivation of microbes

Nitrate Mineral Salts (NMS) Medium for cultivation of *Methylosinus trichosporium*

Solution 1, 10 x NMS salts:

KNO_3	10.0 g
$MgSO_4 \cdot 7H_2O$	10.84 g
$CaCl_2 \cdot 2H_2O$	2.65 g

Dilute to 1 liter.

Solution 2, Iron EDTA:

FeEDTA	3.8 g

Made up to 100 ml with ultra purified water.

Solution 3, Sodium molybdate:

$Na_2MoO_4 \cdot 2H_2O$	0.26 g

Solution 4. Trace elements:

$CuCl_2 \cdot 2H_2O$	0.25 g
$FeSO_4 \cdot 7H_2O$	0.625 g
$ZnSO_4 \cdot 7H_2O$	0.5 g
H_3Bo_3	0.0187

$CoCl_2 \cdot 6H_2O$	0.0625 g
EDTA di solium salt	0.3125 g
$MnCl_2 \cdot 2H_2O$	0.025 g
$NiCl_2 \cdot 6H_2O$	0.0125 g

Dissolve the above in the specified order in ultra purified water and dilute to 1 liter.

Solution 5, Phosphate buffer:

$Na_2HPO_4 \cdot 12H_2O$	71.6 g
KH_2PO_4	26.0 g

Dissolve the above in the specified order in 800 ml of ultra purified water. Adjust pH to 6.8 and dilute to 1 liter.

Preparation of NMS Medium :

1. Dilute 100 mls of solution 1 (10x salts) to 1 litre.
2. Add 1 ml of solution 3 (Na molybdate) and 1 ml of solution 4 (trace elements).
3. Add 0.1 ml of solution 2 (Fe EDTA).
4. Add 1.5% agar for plates.
5. Autoclave for 20 minutes at 121°C.
6. Autoclave separately 10 ml of solution 5 (phosphate buffer) for every liter of NMS.
7. When the NMS is cool enough to hold in the hand, aseptically add the phosphate buffer. If this is done too early the phosphate will precipitate out.

Sulfate-reducer medium (Medium 196, DSMZ) for cultivation of *Desulfobulbus mediterraneus*

Solution A:

Na_2SO_4	3.0 g
KH_2PO_4	0.2 g
NH_4Cl	0.3 g
NaCl	21.0 g
$MgCl_2 \cdot 6\ H_2O$	1.3 g
KCl	0.5 g
$CaCl_2 \cdot 2\ H_2O$	0.15 g
Resazurin solution	0.2 ml
Ultra purified water	870 .0 ml

Dissolve the above in the specified salt order in 870 ml of ultra purified water.

Solution B:

Trace element solution SL-10 1.0 ml

Solution C:

$NaHCO_3$ 5.0 g

Ultra purified water 100.0 ml

Solution D:

Na-lactate 2.5 g

Ultra purified water 10.0 ml

Solution E:

Vitamin solution 5 ml

Solution F:

$Na_2S \cdot 9H_2O$ 0.40 g

Ultra purified water 10.0 ml

Solution A is boiled for a few minutes, cooled to room temperature, gassed with 80% N2 + 20% CO2 gas mixture to reach a pH below 6, then autoclaved anaerobically under the same gas mixture. Solutions B, D, E and F are autoclaved separately under nitrogen. Solution C is filter-sterilized and flushed with 80% N2 + 20% CO2 to remove dissolved oxygen. Solution B to F are added to the sterile, cooled solution A in the sequence as indicated. The complete medium is distributed anaerobically under 80% N2 + 20% CO2 into appropriate vessels. Final pH of the medium is 7.1 - 7.4

Modifications of Sulfate-reducer medium 196 (on Medium 196, DSMZ) for cultivation of *Desulfobulbus mediterraneus*

Medium 196 B

Molar Mg/Ca ratio adjusted to 5 (modern seawater)

Use medium 193 but change in solution A the amount of:

$MgCl_2 \cdot 6\ H_2O$ to 3.1 g

$CaCl_2 \cdot 2\ H_2O$ to 0.45 g

Molar Mg/Ca ratio adjusted to 5 and Mg, Ca concentrations adjusted to modern seawater concentrations, carbonat alkalinity adjusted to 2 mEq (modern seawater)

Use medium 193 but change in solution Athe amount of:

$MgCl_2 \cdot 6\ H_2O$ to 10.83 g

$CaCl_2 \cdot 2\ H_2O$ to 1.53 g

Use medium 193 but change in solution C the amount of:

$NaHCO_3$ to 0.17 g

Ultra purified water 100.0 ml

Working procedures

Biofilm growth on glass slide

- Grow the desired in a 30 -50 ml serum vial.
- Transfer the vial into a glove box and opened under 80% N_2, 20% CO_2 atmosphere (for sulfate reducers).
- Place a sterilized microscopy glass slide on the opening of the vial and fix with tape.
- Turn the vial upside and store
- After the biofilm has developed carefully remove the slide.
- Rinse the biofilm carefully with 1x phosphate buffered saline (PBS) and remove excess liquid.

The biofilm is now ready for imaging or further analyses.

Poly l- lysine coating of the glass slide enhances adhesion of cells. Procedure:

- Use acid washed slides
- Store poly l- lysine stock solution (0.1% w/v in water) at room temperature
- Working poly l- lysine solution: dilute stock 1:10 in ultra purified water. Store working solution up to 4 months at 4°C
- Incubate acid washed glass slide with working solution for 5 minutes at room temperature
- Remove the poly l- lysine with suction and leave to dry

Separation of bulk liquid medium, biofilm and crystals for mass spectrometry anylsis

- Transfer medium step wise into acid-washed 50 ml centrifuge vials and centrifuged at 4500x g for 10 minutes.
- The clear supernatant is transferred into acid washed 50 ml centrifuge vials.
- The remaining pellet, containing floating organic material is washed four times in purified water with a pH of 8-9 (adjusted with NH_4^+).

- The supernants of the washing steps were transferred separately into 50 ml acid washed centrifuge vials.
- The biofilm at the bottom is to be resuspended in approx. 10 ml centrifuged medium and transferred into a 50 ml acid washed centrifuge vial.
- Centrifuge the sample at 4000 RPM for 10 minutes and transferred into a 15 ml Teflon beaker.
- Add 8 ml of ultra pure NaClO (1%) bleaching solution and leave to react for 12 hours. Subsequently, the sample is centrifuged at 4000 RPM for 10 minutes and NaClO is exchanged. This procedure should be repeated 3 times.
- After bleaching, the sample is washed 4 times in purified water with adjusted pH (see above) and the supernatants of individual washing steps are transferred separately into 50 ml centrifuge vials.
- Finally, the remaining pellet is transferred into a 6 ml teflon beaker.
- All samples need to dried at 95°C for at least 12 hrs. Organic bearing samples and blanks should be additionally resuspended in 1 ml purified water and 1 ml HNO_3 8N and dried at 95°C, followed by resuspension in 1 ml HNO_3 and 20 µl $HCLO_4$ and left to react for 3 hours at 95°C.
- All applied HCl and HNO_3 based acids refer to 2-step Teflon cascade still (pico trace) purification of initially per analysis quality.
- After drying at 180°C 0.75 ml 8N HNO_3 and 0.25 ml H_2O_2 is added and leave to react for at least 12 hrs, subsequently drying at 80°C.
- Aliquots of up to 3000 ng Ca equivalent might be taken for Ca-isotope preparation and mixed with a $^{43}Ca/^{48}Ca$ double spike. Spiked samples need to dry at 95°C, followed by resuspension in 2.2 N HNO_3,
- Ca might be separated using 600 µl columns (biorad) with MCI-Gel 75-150 µm.
- Prior to filament loading samples need to be dried and transferred into chloride form by evaporation in 2.2 N HCl.
- After uptake with loading solution, aliquots of about 300 ng might be loaded with $TaCl_5$ activator in a sandwich technique on a zone-refined Re filament.

Device for pH measurements of anoxic solutions

A cheap and simple device was manufactured to enable pH measurements of solutions being either anoxic or not in equilibrium with the atmosphere.
Requirements:

10 ml plastic syringe

Silicone hose (10-15 cm)

Aquarium silicone

Teflon tape

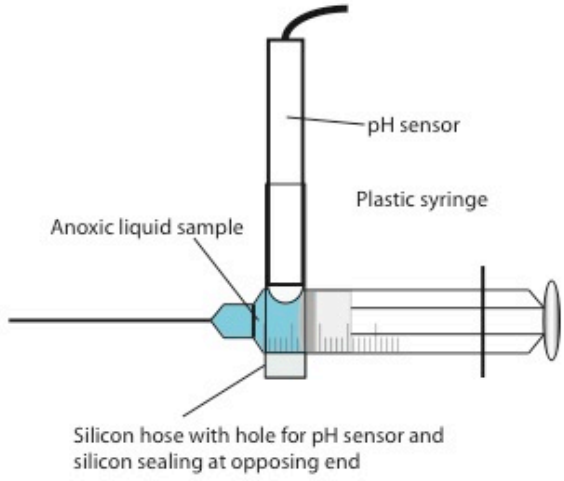

Puncture a hole into the lower part of the syringe, which is big enough for the sensor tip. Cut two opposing holes into the silicone hose, just big enough for the syringe to be squeezed through. Turn syringe until the punctured hole faces longer hose ending. Seal the short hose ending with aquarium silicone. If necessary, wrap some layers of Teflon tape around the pH sensor for tight fitting to the hose. Push sensor tip slightly through the punctured hole of the syringe. For best pH results, flush device repeatedly with N_2 and sterile solution by gently moving the plunger